MOLECULAR MECHANISMS IN THE DEVELOPING AND MATURING BRAIN

Ayumi Nakamura

A dissertation submitted to the faculty at the University of North Carolina at Chapel Hill in partial fulfillment of the requirements for the degree of Doctor of Philosophy in the Curriculum of Neurobiology

Chapel Hill
2016

Approved by:

Mohanish Deshmukh

Eva Anton

Mark Zylka

Timothy Gershon

Norman Sharpless

ABSTRACT

Ayumi Nakamura: Molecular Mechanisms in the Developing and Maturing Brain
(Under the direction of Mohanish Deshmukh)

Neurons, unlike other cell types, persist throughout the entire lifespan of an organism. Additionally, neurons use multiple anti-apoptotic brakes during different stages of their life cycle in order to maintain their long-term survival. This dissertation investigates the role of two well-known anti-apoptotic genes, Bcl-xL and miR-29, which are believed to serve important functions in preventing cell death during embryonic brain development and during the period of postnatal brain maturation, respectively. Using conditional knockout mouse models of Bcl-xL and miR-29, I found that these genes may have additional non-apoptotic roles at different timepoints during the neuron's life cycle, challenging the previously accepted roles of these genes. First, I found that Bcl-xL, which is believed to be critical for brain development during the embryonic stages, was expressed at low levels in the rapidly dividing neuronal progenitor cells and was thus dispensable for the survival of these cells during embryonic development. In contrast, the early differentiated postmitotic neurons acutely rely on Bcl-xL for their survival, the lack of which results in severe consequences in mice including microcephaly and neurobehavioral deficits such as hyperactivity, increased risk-taking and self-injurious behaviors. Second, to probe the role of miR-29, a microRNA that is known to be critical for neuronal maturation by preventing apoptosis in neurons, I generated knockout mice that were conditionally

deleted for miR-29. We and other labs have predicted that the main role of miR-29 is to prevent apoptosis and that deleting miR-29 could lead to widespread neuronal death. Surprisingly, however, miR-29-deficient mice exhibit no signs of cell death in the brain. In contrast, we identified a novel function of miR-29 in governing DNA methylation, an event that has been primarily studied in the context of cancer and whose roles in the brain are just beginning to be uncovered. I have found that miR-29 has an important epigenetic role in the brain *via* its ability to target the 3' untranslated region (3'UTR) of a key DNA methyltransferase known as Dnmt3a. miR-29-deleted brains have increased levels of Dnmt3a, resulting in widespread hypermethylation across the genome. This, in turn, leads to transcriptional repression of multiple neuronal genes in the miR-29 knockout brains, resulting in severe neurobehavioral deficits including hyperactivity, hypersociability, excessive self-grooming and repetitive behaviors. Lastly, using RNAseq and gene association studies, I found that the pathways that are dysregulated in the miR-29-deleted mice are similar to those that are disrupted in the brains of patients with autism spectrum disorder (ASD), suggesting that miR-29 could be tested as a potential therapy in neurodevelopmental disorders in the future.

To my family

ACKNOWLEDGEMENTS

The work I describe here was made possible by the support and encouragement of many people. First, I would like to thank my advisor, Dr. Mohanish Deshmukh for not only mentoring me but for also giving me the freedom to pursue new and exciting research directions during my time in graduate school. I would also like to deeply thank my thesis committee members, Eva Anton, Timothy Gershon, Mark Zylka, and Norman Sharpless, for their sound advice and support. I am grateful for the invaluable perspective that they have all brought to these projects, their guidance and their enthusiasm.

I would also like to thank my funding sources, including the National Institute of Child Health and Human Development (NICHD; 1F30HD081865-01) and the National Institutes of Health (NS042197, T32-GM8719 and T32-NS7431).

Finally, I would like to thank my family and friends and my husband, Vijay, for their unconditional love and support.

PREFACE

Chapter Two of this dissertation was previously published. Permission to include the following article was provided by The Journal of Neuroscience.

Nakamura A, Swahari V, Plestant C, Smith I, McCoy E, Smith S, Moy SS, Anton ES and Deshmukh M. Bcl-xL is essential for the survival and function of differentiated neurons in the cortex that control complex behaviors. The Journal of Neuroscience 2016.

TABLE OF CONTENTS

LIST OF FIGURES

LIST OF ABBREVIATIONS

ASD: Autism spectrum disorder

ASO: Antisense oligonucleotide

BBB: Bcl-xL/Bax/Bak

Bcl-2: B- cell lymphoma 2

Bcl-w: B-cell lymphoma w

Bcl-xL: B- cell lymphoma extra large

Brn1: Brain 1

CA: Cornu ammonis

cC3: Cleaved caspase-3

cDNA: Complementary DNA

CGNP: Cerebellar granule neuron precursor

CGN: Cerebellar granule neuron

CNS: Central nervous system

CNTNAP2: Contactin-associated protein-like 2

CTX: Cortex

Cux1: Cut-like homeobox 1

Cyt *c*: Cytochrome *c*

DAPI: 4',6-diamidino-2-phenylindole

DKO: Double knockout

DNA: Deoxyribonucleic acid

Dnmt1: DNA methyltransferase 1

Dnmt3a: DNA methyltransferase 3a

Dnmt3a: DNA methyltransferase 3b

E: Embryonic day

E/I: Excitatory/Inhibitory

ER: Endoplasmic reticulum

FDR: False discovery rate

GABA: Gamma-Aminobutyric Acid

HC: Hippocampus

H/E: Hematoxylin/Eosin

IHC: Immunohistochemistry

KO: Knockout

LNA: Locked nucleic acid

mCH: Methyl CH

MBP: Methyl-CpG-binding protein

Mcl-1: Myeloid cell leukemia 1

MDS: MeCP2 duplication syndrome

MeCP2: Methyl-CpG binding protein

miR-29: microRNA-29

miRNA: MicroRNA

MOMP: Mitochondrial outer membrane permeabilization

mRNA: Messenger RNA

NeuN: Neuronal nuclei

Nex: Neuronal helix-loop-helix

NGF: Nerve growth factor

NPC: Neural progenitor cell

NPY: Neuropeptide Y

OCD: Obsessive-compulsive disorder

P: Postnatal day

PBS: Phosphate buffered saline

PCNA: Proliferating cell nuclear antigen

PNS: Peripheral nervous system

PPI: Prepulse inhibition

qRT-PCR: quantitative RT-PCR

RFP: Red fluorescent protein

RNA: Ribonucleic acid

RPS6KA3: Ribosomal protein S6 kinase, 90kD, 3

RTT: Rett syndrome

SAM: S-adenosylmethionine

SC: Superior colliculus

Shank3: SH3 and ankyrin repeat protein 3

SVZ: Subventricular zone

Tbr1: T-brain 1

Tet: Ten-eleven translocation

TKO: Triple knockout

TNF: Tumor necrosis factor

UTR: Untranslated region

V1: Primary visual cortex

VZ: Ventricular zone

WT: Wildtype

XCI: X-chromosome inactivation

CHAPTER ONE: INTRODUCTION

1.1 An overview of apoptosis

Roles of the mammalian apoptotic pathway

Apoptosis, a highly regulated pathway in which a cell is programmed to die, is critical for the maintenance of tissue homeostasis and for the maturation of various organs in the developing embryo (Jacobson et al. 1997). Cell death functions to eliminate cells that are no longer needed by the organism (Danial and Korsmeyer 2004). As a result, strict homeostasis is achieved between newly dividing cells and dying cells. If apoptosis becomes dysregulated, various diseases can result including cancer, autoimmune and inflammatory diseases, as well as neurodegeneration and neuronal injury (Elmore 2007; Fuchs and Steller 2011).

While the apoptotic pathway can be classified into different types, the process can also be categorized into pathological and physiological states (*e.g.* developmental apoptosis *versus* cancer and neurodegeneration). Physiological apoptosis plays a crucial role during embryogenesis. Failure to activate apoptosis in the organism results in embryonic lethality and severe central nervous system (CNS) defects, including hyperplasia of cells in the CNS, exencephaly (protrusion of brain matter from the skull), and incomplete neural tube closure (Kuida et al. 1996; Cecconi et al. 1998; Hakem et al. 1998; Kuida et al. 1998; Woo et al. 1998; Yoshida et al. 1998) (Fig. 1.1). Although the apoptotic pathway has been well

characterized in certain mammalian cell lines, exactly how cell death is regulated in the cells of the CNS remains largely unknown.

The extrinsic pathway of apoptosis

In mammalian cells, the two well-known mechanisms of activating apoptosis are *via* the extrinsic or intrinsic pathways (Tait and Green 2010). The extrinsic pathway is engaged in certain cell types including immune cells in order to kill pathogen-infected cells and defective lymphocytes, thereby preventing autoimmunity and the development of tumors (Strasser et al. 2009). The extrinsic pathway involves the binding of ligands (*e.g.* Fas, TNF) to death receptors on the plasma membrane. This process leads to the activation of a protein known as caspase-8 and subsequently activates caspase-3, the major executioner caspase that mediates apoptosis, as discussed below (Tait and Green 2010) (Fig. 1.2). In this pathway, caspase-8 is also able to cleave a pro-apoptotic protein known as Bid into the truncated form of Bid (tBid), which then translocates from the cytosol to the mitochondria to engage the mitochondria to activate apoptosis (Strasser et al. 2009).

The intrinsic pathway of apoptosis

In the vast majority of other cells, various stimuli (*e.g.* growth factor deprivation, DNA damage, reactive oxygen species, and endoplasmic reticulum (ER) stress) activate apoptosis *via* the intrinsic pathway (Tait and Green 2010) (Fig. 1.2). Central to the intrinsic pathway of apoptosis is the permeabilization of the outer mitochondrial membrane, which releases cytochrome *c* (cyt *c*) and other apoptogenic proteins (apoptosis inducing factor, endonuclease G, Smac/Diablo) from the mitochondrial intermembrane space into the

cytosol (Saelens et al. 2004). While, for most of history, the mitochondria was referred to as the powerhouse of the cell, it was only in 1996 when Xiaodong Wang's group made a seminal discovery that cyt *c* is released from the mitochondria during cell death (Liu et al. 1996). Although in health cells, cyt *c* functions as a critical protein in the electron transport chain to carry out mitochondrial respiration to generate ATP *via* oxidative phosphorylation, cyt *c* also plays an essential role in mediating cell death upon its release into the cytosol.

The release of cyt *c* from the mitochondria is strictly regulated by the Bcl-2 family of proteins (Jiang and Wang 2004). This family is composed of pro-apoptotic and anti-apoptotic members, which are further sub-classified according to the number of Bcl-2 homology (BH) domains contained within each protein (Fig. 1.3).

Bax and Bak: The gatekeepers of the mitochondria

Among the pro-apoptotic family members are the effector proteins Bax and Bak, which contain the BH1, BH2 and BH3 domains and are considered to be the gatekeepers of cyt *c* release (Wei et al. 2001). In most healthy cells, Bax and Bak are maintained in a monomeric and inactive state (Walensky and Gavathiotis 2011). Upon an apoptotic stimulus, however, these proteins undergo a conformational change and oligomerize to form pores in the mitochondrial outer membrane and induce permeabilization of the membrane (a process known as mitochondrial outer membrane permeabilization, or MOMP) (Chipuk et al. 2006). MOMP thereby enables the release of cyt *c* from the mitochondria into the cytosol to activate the downstream apoptotic pathway.

BH3-only proteins: Initial responders to apoptotic stimuli

Another group of pro-apoptotic Bcl-2 family members known as the BH3-only proteins are composed of a single BH3 domain. These BH3-only proteins (Bid, Bim, Puma, Bik, Bad, Bmf, Hrk) respond to various apoptotic stimuli and are classified as either 'activators' or 'sensitizers' (Lomonosova and Chinnadurai 2008; Chipuk et al. 2010). Activators (Bim, Bid, Puma) function by directly binding to and activating Bax and Bak, while sensitizers (Bmf, Bik, Hrk, Noxa) indirectly activate apoptosis by inhibiting the action of the anti-apoptotic Bcl-2 proteins (Youle and Strasser 2008; Martinou and Youle 2011).

Anti-apoptotic Bcl-2 family members

Finally, the release of cyt *c* requires not only the activation of the pro-apoptotic proteins Bax and Bak and their activation by the BH3-only proteins but also the inhibition of the anti-apoptotic members (*e.g.* Bcl-2, Bcl-xL, Bcl-w, Mcl-1), thus preventing cell death by inadvertent activation of a single pathway. These anti-apoptotic proteins normally prevent cell death by inhibiting Bax and Bak activity (Ow et al. 2008; Bogner et al. 2010). Anti-apoptotic Bcl-2 members contain four BH domains, BH1-BH4 (Kroemer 1997). This group of proteins has gained widespread attention in the cancer field where researchers have found that multiple tumors upregulate these anti-apoptotic proteins to evade cell death. Indeed, one of the exciting future directions in personalized medicine is to downregulate these proteins for tumor therapy. Interestingly, similar approaches are also being developed for tumors that evade cancer by downregulating pro-apoptotic BH3-only family members (Letai et al. 2002; Deng et al. 2007; Friedman et al. 2015).

Events downstream of the release of cyt c

While the release of cytochrome *c* is a prerequisite for the intrinsic pathway of cell death, it is also considered to be a point of no return by most scientists in the cell death field. However, events after cyt *c* release are equally important, and any perturbations downstream of the mitochondria have significant effects. Using a cell extract assay similar to the one that enabled the discovery of cyt *c* in the cell death pathway, Xiaodong Wang's group identified a protein known as Apaf-1 (apoptotic protease activating factor 1). In fact, the key function of mitochondrially-released cyt *c* is to bind to and activate Apaf-1 (Danial and Korsmeyer 2004). Apaf-1 contains a WD40 repeat domain that keeps the protein in an inactive conformation (Riedl and Salvesen 2007). The binding of cyt *c* to the WD40 domain induces a conformational change in Apaf-1 that exposes its caspase activation and recruitment domain (CARD), resulting in its association with and activation of caspase-9 (Riedl and Salvesen 2007) (Fig. 1.4). The Apaf-1/caspase-9 complex, called the apoptosome complex, activates caspase-3, which then cleaves specific cellular proteins to induce rapid cell death (Danial and Korsmeyer 2004). Indeed, mutants of Apaf-1 that lack the WD40 domain are constitutively active and can activate caspase-3 in the absence of cyt *c* (Hu et al. 1998a; Hu et al. 1998b). In addition, in cell culture models that either inhibit the binding of cyt *c* to Apaf-1 (*e.g.* injecting yeast cyt *c* that cannot bind to Apaf-1) or inhibit/knock down Apaf-1, or inhibit capsase-3 activation (either by siRNA knockdown or by using chemical inhibitors such as QVD or z-VAD), these processes can prevent cell death and extend cell survival even in the presence of apoptosis-inducing drugs.

1.2 The apoptotic pathway is essential for embryonic development and survival

Activation of apoptosis is critical for the development of the embryo, and failure to induce cell death leads to embryonic lethality with significant defects in various organ systems. One organ that critically relies on the cell death program during development is the nervous system (Yuan and Yankner 2000). The striking phenotypes of mutant mice that are defective in apoptosis point to the importance of cell death in the CNS (Kuida et al. 1996; Cecconi et al. 1998; Hakem et al. 1998; Kuida et al. 1998; Woo et al. 1998; Yoshida et al. 1998). Mice that are deficient in Apaf-1, Caspase-9, or Caspase-3 are all embryonic or perinatally lethal and display hyperplasia of CNS tissue that results in exencephaly (Fig. 1.1). In particular, these mice exhibit an enlargement of the mitotic ventricular zone and expansion of the telencephalon (Kuida et al. 1996; Cecconi et al. 1998; Hakem et al. 1998; Kuida et al. 1998; Woo et al. 1998; Yoshida et al. 1998). In addition to these phenotypes in the CNS, mice deficient in the various apoptotic proteins display features such as a delay in the removal of interdigital webs of the forelimbs and hindlimbs that normally occurs in wildtype mice, and thymocytes isolated from these mutant mice also exhibit resistance to various apoptotic stimuli.

1.3 Apoptotic mechanisms in the developing CNS

Apoptosis is especially critical and is tightly regulated in the nervous system of a variety of organisms. Bob Horvitz's group mapped out the cell fate of every cell in *Caenorhabditis elegans* (*C. elegans*) and found that exactly 131 cells undergo apoptosis during normal development. What is astonishing is that, of the 131 cells that are programmed to die, 105 are of neuronal origin (Sulston and Horvitz 1977; Sulston et al.

1983). These pioneering discoveries in *C. elegans* underscore the importance of maintaining the proper number of neurons during normal development.

In mammals, the phenomenon of programmed cell death has historically been extensively investigated in the peripheral nervous system (PNS) where trophic factor deprivation is known to activate the mitochondrial pathway to match the number of innervating neurons with the size of its target tissue (De Zio et al. 2005). The apoptotic pathway has been particularly well studied in the sympathetic nervous system, in which sympathetic neurons rely on nerve growth factor (NGF) for survival. In contrast, very little is known about apoptotic mechanisms in the developing CNS. Unlike the PNS, the neurons of the CNS do not depend on a single trophic factor for their survival (Dekkers and Barde 2013; Dekkers et al. 2013) (Fig. 1.5).

The mechanisms underlying the survival and death of various neuronal subtypes, including the excitatory projection neurons and inhibitory interneurons in the CNS are virtually unknown. Recently, Arturo Alvarez-Buylla's group discovered that inhibitory interneurons in the developing cortex utilize an intrinsic mechanism to undergo cell death independent of external cues (Southwell et al. 2012). Approximately 40% of interneurons in the postnatal brain were shown to die in a Bax-dependent mechanism. In addition, transplantation of embryonic interneuron precursors into the postnatal brain during the period when the endogenous interneurons usually undergo cell death revealed that apoptosis was activated in the transplanted population two weeks after they were generated. Southwell et al. also transplanted varying numbers of embryonic interneuron precursors into the postnatal brain. If the neurons were governed by the neurotrophic theory, in which cells compete for limiting target-derived growth factors for survival,

heterochronic transplantation of larger numbers of precursors would lead to greater numbers of dying interneurons. However, the proportion of cell death was similar across all transplant sizes, challenging the hypothesis that the survival of these CNS interneurons is governed by the neurotrophic theory. These findings have uncovered key features of apoptotic mechanisms that determine how cell death is regulated in the developing mammalian brain.

However, how the apoptotic pathway is controlled in the developing CNS must still be investigated further. In particular, the regulation of cell death by anti-apoptotic proteins raises interesting yet unanswered questions. Although mammalian cells express multiple anti-apoptotic Bcl-2 family proteins, including Bcl-2, Bcl-xL and Mcl-1, whether CNS neurons are acutely dependent on a single anti-apoptotic protein for their survival is currently unknown. In addition, which specific neuronal populations are dependent on Bcl-xL and the consequence of the loss of this anti-apoptotic protein on neurobehavior has been unexplored. The work described in this thesis provides insight into how cell death in CNS neurons is regulated by Bcl-xL and sheds light on the essential function of Bcl-xL for the survival of neurons in the cortex that control complex behaviors.

1.4 DNA methylation: An overview

One of the epigenetic modifications that occurs in the mammalian genome is DNA methylation, which involves the addition of a methyl group on to a cytosine adjacent to a guanine (referred to as mCG) (Suzuki and Bird 2008; Smith and Meissner 2013). DNA methylation is a process that is well conserved in plants, fungi and mammals (Chan et al. 2005; Goll and Bestor 2005; Henderson and Jacobsen 2007; Schubeler 2015) and is mediated by the DNA methyltransferase (DNMT) family of proteins (Denis et al. 2011; Jurkowska et al. 2011). DNA methylation is important for processes such as pluripotency and differentiation, embryonic development, genomic imprinting, X chromosome inactivation, chromatin modification and proper brain maturation (Jones 2012).

DNA methylation is a modification that is generally associated with transcriptional silencing of genes (Suzuki and Bird 2008). At promoter regions, this process promotes transcriptional repression by directly blocking the ability of transcription factors to bind or by indirectly causing transcriptional silencing *via* the recruitment of methyl-binding domain-containing proteins and co-repressors such as histone deacetylases, which induce the formation of heterochromatin (Klose and Bird 2006; Lim and Maher 2010) (Fig. 1.6). In addition to promoter regions, gene bodies across the genome are also quite heavily methylated (Rabinowicz et al. 2003; Eckhardt et al. 2006). What is remarkable is that, unlike the inverse correlation between promoter methylation and gene transcription, the opposite relationship holds true for methylation patterns of gene bodies. Thus, the methylation of gene bodies is correlated with genes that are actively transcribed (Hellman and Chess 2007; Lister et al. 2009; Feng et al. 2010). However, the exact function of gene body methylation remains unknown.

1.5 Mediators of DNA methylation: The writers, readers and erasers

The writers

The DNMTs are known to catalyze the transfer of a methyl group from S-adenosylmethionine (SAM) to the C5 position of a cytosine on the DNA, a major process that underlies the epigenetic modification of DNA (Goll and Bestor 2005). To detect the methylation of cytosines throughout the mammalian genome, the gold standard protocol is to use bisulfite genomic DNA sequencing. Treatment of the DNA with sodium bisulfite leads to the deamination of unmethylated cytosine to uracil, while methylated cytosines are not prone to undergoing this chemical conversion (Li and Tollefsbol 2011) (Fig. 1.7). The information in the epigenome can then be sequenced using standard RNAseq analysis or other methods.

The DNMT proteins are often classified into maintenance and *de novo* DNA methyltransferases. Dnmt1 was the first mammalian DNA methyltransferase discovered in mammals (Gruenbaum et al., 1982). Dnmt1is most highly expressed upon entry into the S phase of cell division in dividing cells and is localized to DNA replication foci (Leonhardt et al. 1992; Chuang et al. 1997). Dnmt1 plays a critical role in the transmission of pre-existing methylation patterns on the parental DNA to the daughter strands. Thus, during mitosis, the cytosines on the nascent DNA of daughter cells are recognized by Dnmt1, and the methylation pattern that is present on the parent strand and that already contains the methyl groups is propagated onto the nascent strand (Chuang et al. 1997; Sharif et al. 2007). As such, Dnmt1 is known as a maintenance DNA methyltransferase. In contrast, Dnmt3a and Dnmt3b are known as the *de novo* DNA methyltransferases, as they add

methyl groups to cytosines on unmethylated DNA strands during development (Okano et al. 1999).

Analyses of the DNMTs have revealed unique expression patterns of these proteins throughout embryonic and postnatal development and in the later stages of adulthood. Dnmt1 is highly expressed in the embryonic CNS (Goto et al. 1994; Trasler et al. 1996; Inano et al. 2000). Dnmt3b is expressed in the ventricular zone (VZ) during a narrow period between E10.5 and E13.5, but its levels decrease to undetectable levels in the CNS after E15.5 (Feng et al. 2005; Lister et al. 2013a). In contrast, Dnmt3a is expressed in the proliferating neural precursors of the VZ and subventricular zone (SVZ) in the embryo. However, after birth, Dnmt3a becomes predominantly expressed by postmitotic neurons. Its expression in these neurons continues to go up until three weeks of postnatal life, after which it declines to low levels in adulthood (Feng et al. 2005; Lister et al. 2013a). Taken together, the unique expression pattern of the DNA methyltransferases suggest non-overlapping roles in the embryonic and postnatal brain.

To determine whether the DNA methyltransferases are required for mammalian development, several labs have generated global and conditional knockout mice of Dnmt1, Dnmt3a and Dnmt3b. Conditional deletion of Dnmt1 using a Emx1-Cre transgene results in extensive cell death in the dorsal forebrain (Hutnick et al. 2009). Interestingly, although the $Dnmt1^{f/f}$ Emx1-Cre mice are viable and exhibit a normal lifespan, these mice display multiple neurobehavioral defects including hyperactivity and impaired fear conditioning and learning and memory (Hutnick et al. 2009). While both $Dnmt3a^{+/-}$ and $Dnmt3b^{+/-}$ mice appear normal and are fertile, $Dnmt3a^{-/-}$ mice exhibit retarded growth after birth and die at approximately three to four weeks of age (Okano et al. 1999) (Fig. 1.8A). On the other hand,

Dnmt3b$^{-/-}$ mice are embryonic lethal and exhibit growth impairment and rostral neural tube defects (Fig. 1.8B). Generation of Dnmt3a$^{-/-}$ Dnmt3b$^{-/-}$ double knockout mice results in a smaller sized embryo that is also embryonic lethal at E11.5 (Okano et al. 1999) (Fig. 1.9). To specifically examine the consequence of Dnmt3a loss in the CNS, Nguyen et al. (2007) generated a conditional knockout mouse in which Dnmt3a was deleted in the CNS using the Nestin-Cre transgene. Dnmt3a$^{f/f}$ Nestin-Cre mice were born at the expected Mendelian ratio and were healthy at birth, but the males later developed growth retardation, and the mutant mice exhibited shortened lifespan. In addition, although there were no major structural or anatomical defects in the CNS of the Dnmt3a$^{f/f}$ Nestin-Cre mice, these mice exhibited various neurobehavioral deficits, including hypoactivity, reduced exploratory behavior, reduced grip strength and gait abnormalities (Nguyen et al. 2007).

In humans, dysregulated expression of the DNA methyltransferases has been extensively studied in the context of various cancers (Subramaniam et al. 2014). For example, overexpression of Dnmt1 has been observed in prostate cancer and endometrioid carcinomas and is also associated with poorer tumor differentiation in gastric cancers. Mutations in Dnmt3a are also commonly found in patients with acute myeloid leukemia (Ley et al. 2010; Yan et al. 2011). In addition to the dysregulation of DNA methyltransferases in cancers, patients with loss of function mutations in Dnmt1 have been found to exhibit hereditary sensory neuropathy with dementia, hearing loss and early lethality (Klein et al. 2011). These patients exhibit both central and peripheral nervous system degeneration. Sensory neuropathy in these patients leads to loss of sensation in the extremities, resulting in infections and thus amputation of their limbs. Mutations in Dnmt3a have also been found in patients. Exome sequencing of patients with an

overgrowth syndrome, intellectual disability and facial dysmorphism revealed two Dnmt3a mutations that interfere with domain-domain interactions and histone binding, which result in reduced methyltransferase activity (Tatton-Brown et al. 2014) (Fig. 1.10). Collectively, these studies in mice and humans point to the essential role that the maintenance and *de novo* DNA methyltransferases play in the survival of the embryo and the proper development of the brain.

The readers

MeCP2 (methyl-CpG binding protein 2) was initially discovered more than 20 years ago by Bird and colleagues in a search for proteins that bound methylated DNA. MeCP2 is an X-linked gene whose gene product binds to a symmetrical pair of mCG across the genome. More recently, MeCP2 was found to bind to methylated cytosines adjacent to a nucleotide other than guanine (CH methylation, discussed below). MeCP2 functions to transcriptionally repress genes through its recruitment of and interaction with its corepressors including histone deacetylases and Sin3A proteins at the promoter of target genes (Nan et al. 1998). MeCP2 binds to methylated cytosines *via* its methyl-CpG-binding domain (MBD) (Nan et al. 1993). The other domain in MeCP2 that is critical for its function is the transcription repression domain (TRD), a region in the protein that has been shown to bind to Sin3A. Sin3A was previously shown to recruit and bind to histone deacetylases HDAC1 and HDAC2 (Hite et al. 2009), which remodel chromatin so that genes are transcriptionally repressed.

MeCP2 is known to be expressed across all tissues; however, it is most highly

expressed in the brain, with its expression being five- to ten-fold higher in neurons than in other cell types. In fact, studies on the timing and distribution of MeCP2 expression revealed that MeCP2 protein expression is highest in the maturing neurons in the CNS. For example, the ontogenetically older structures such as the spinal cord and brainstem neurons express MeCP2 at an earlier stage before the hippocampus and cerebral cortex, which are structures that develop later in the embryo. In addition, deeper layer neurons in the cortex begin to express MeCP2 earlier than upper layer neurons, consistent with when these neurons are born in the cerebral cortex (Shahbazian et al. 2002a).

Proper neurodevelopment relies on strict regulation of MeCP2 levels in the brain. Mutations in MeCP2 have been shown to cause a variety of syndromes. For instance, missense, frameshift and nonsense mutations in MeCP2 lead to the loss of function of MeCP2 and were shown to cause Rett syndrome (RTT). RTT is a neurodevelopmental disorder first described in 1966 by pediatrician Andreas Rett, who noticed progressive dementia, motor loss and stereotypic hand movements in two young girls who had a normal developmental course for the first 1 to 1.5 years after birth (Rett 1966). The disorder did not receive much attention until 1983 when Swedish neurologist Bengt Hagberg and others noted patients with similar features in Europe and published their findings in the Annals of Neurology (Hagberg et al. 1983). This disorder almost exclusively occurs in females and is one of the most common causes of mental retardation in females. RTT is believed to be sporadic in 99% of cases, and the incidence of this disorder is approximately 1 in 10,000 live female births. Patients with RTT appear normal at birth and undergo a normal course of development for the first 6-18 months after birth, but they

progressively fail to meet developmental milestones and exhibit features such as microcephaly, scoliosis, seizures, autistic features, gait abnormalities, gradual loss of expressive language and hand use, and stereotypic hand wringing movements. The spectrum of phenotypes that patients exhibit vary widely from mild mental retardation to the classic features of RTT. In addition to the types of mutations seen in the MeCP2 gene, one explanation for this diversity in clinical features may be attributed to X-chromosome inactivation (XCI). Favorable patterns of XCI or heavily skewed XCI can alleviate the effects of the MeCP2 mutation and thus lead to a milder clinical phenotype in patients (Young and Zoghbi 2004). Mice lacking MeCP2 or those carrying a truncated allele of MeCP2 undergo normal development until 4-6 weeks of age but subsequently develop various neurobehavioral abnormalities including seizures, hypoactivity, stereotypies, and early death (Chen et al. 2001; Guy et al. 2001; Shahbazian et al. 2002b). Furthermore, in-depth characterizations of mice lacking MeCP2 in GABA-releasing neurons demonstrated that these mice recapitulate many of the features seen in patients with RTT, including repetitive behaviors, increased sociability, and impaired motor coordination (Chao et al. 2010). Extensive molecular analyses revealed that these mice exhibited a reduction in presynaptic GABA release and inhibitory neurotransmission, leading to hyperexcitability in the brain. These findings suggest that a strict balance between excitation and inhibition is necessary, the loss of which results in a dysregulation of normal neurodevelopment.

While RTT is caused by the loss of function of the MeCP2 gene, extra copies of the MeCP2 gene in patients can lead to MeCP2 duplication syndrome (MDS), a condition also

known as Lubs X-linked mental retardation syndrome (Ramocki et al. 2010; Van Esch 2012). MDS is known to occur almost exclusively in males (Van Esch 1993; Villard 2007) and accounts for 1% of unexplained X-linked intellectual disability in males (Lugtenberg et al. 2008). Females with a duplication of MeCP2 are rarely reported and are usually asymptomatic, possibly due to highly skewed XCI, in which the X chromosome bearing the extra copy of MeCP2 becomes preferentially inactivated (Ramocki et al. 2010). However, mild to severe cognitive impairment was previously described in a subset of female patients (Grasshoff et al. 2011; Scott Schwoerer et al. 2014). Patients with MDS exhibit features such as moderate to severe intellectual disability, autistic features, delayed development, seizures and premature death (Van Esch 2012). Several labs have generated mouse models that recapitulate the clinical features seen in patients with MDS. Bodda et al. generated a transgenic mouse in which MeCP2 was mildly overexpressed ($MeCP2^{WT\_EGFP}$). These mice displayed increased aggression and were more sensitive to undergoing pentylenetetrazole (PTZ)-induced epileptic seizures (Bodda et al. 2013). Huda Zoghbi's group generated a mouse model in which the human wildtype MeCP2 protein was overexpressed at approximately two-fold levels in transgenic mice ($MeCP2^{Tg}$). These $MeCP2^{Tg}$ mice were developmentally normal until 10 weeks of age but developed a progressive neurological phenotype, including forepaw clasping, aggression (as determined by an increased propensity to bite), and kyphosis. Up until 20 weeks of age, $MeCP2^{Tg}$ mice exhibit increased rearing, which is suggestive of reduced anxiety in these mice, as well as enhanced cerebellar and hippocampal learning and enhanced synaptic plasticity in the hippocampus. After 20 weeks of age, however, these mice underwent clonic seizures, had abnormal electroencephalographic traces and exhibited early lethality

(Collins et al. 2004). Overexpression of MeCP2 specifically in neurons (*Tau-MeCP2*) recapitulates the features of MDS, including ataxia, impairments in learning and memory, a progressive retardation in growth and body weights, and heightened anxiety, along with defects in excitatory synapse function. Zilong Qui's group in China developed a transgenic cynomolgus monkey (*Macaca fascicularis*) overexpressing MeCP2 in the brain. These transgenic monkeys displayed autism-like behaviors with increased repetitive circular motions, increased anxiety and reduced social interaction with both wildtype monkeys and other MeCP2 transgenic monkeys (Liu et al. 2016). Recently, to determine whether the phenotypes in the MeCP2^{Tg} mice are reversible, Sztainberg et al. generated a conditional MeCP2-overexpressing mouse model to correct MeCP2 levels to wildtype levels and showed that the correction rescued many of the behavioral and electrophysiological features seen in the MeCP2^{Tg} mice. In addition, the authors used an antisense oligonucleotide (ASO) against MeCP2 and successfully corrected the phenotype in the MeCP2^{Tg} mice with gradual intracerebroventricular infusion of the ASO (Sztainberg et al. 2015). These findings reveal the promising therapeutic approach in successfully delivering ASOs to patients with MDS and reversing their neurological defects.

Taken together, the studies in patients with RTT and MDS and animal models that recapitulate these disorders suggest that maintaining proper levels of MeCP2, particularly in the brain, is essential for normal brain development and maturation, and that too little or too much MeCP2 can have devastating neurological consequences.

The erasers

Although DNA methylation is a relatively stable epigenetic mark, the erasure of DNA methylation has been shown to occur and was also determined to be a stable DNA modification instead of a transient intermediate. The methylation of cytosines by the DNA methyltransferases generates 5-methylcytosine (5mC), which can further be oxidized by ten-eleven translocation (Tet) proteins into 5-hydroxymethylcytosine (5hmC), 5-formylcytosine (5fC) and 5-carboxylcytosine (5caC) (Wu and Zhang 2011) (Fig. 1.11). These oxidation products are believed to be intermediates involved in DNA demethylation and are thought to contribute to another layer of epigenetic regulation (He et al. 2011; Bender and Weber 2013). Although the existence of hmC was noted more than 40 years ago (Penn et al. 1972), its significance in CNS neurons has only begun to be explored recently. In 2009, Kriaucionis and Heintz revealed the presence of 5hmC in the cerebellar Purkinje neurons of the brain (Kriaucionis and Heintz 2009). Examination of the levels of 5hmC across various stages of development in the cerebellum revealed a progressive increase in 5hmC from the early postnatal period to the adult stage (Song et al. 2011). Using a highly sensitive LC-MS method to detect the levels of hmC across various tissues in mice, Globisch et al. found that, although 5hmC is present across all tissues, the highest levels of 5hmC are detected in the brain and the spinal cord (Globisch et al. 2010). 5hmC levels were also found to inversely correlate with proliferation, as 5hmC levels were high in differentiated cells that exhibited low levels of proliferation (*e.g.* brain, liver, intestinal villi) and were low in actively proliferating cells of the germ centers in the spleen and the intestinal crypts (Bachman et al. 2014).

The three mammalian Tet proteins, Tet1, Tet2 and Tet3, are dioxygenases that have all been shown to catalyze the oxidation of 5mC into 5hmC and its subsequent oxidation products. However, the consequence of Tet deficiency in the brain is still unclear. The Tet1 transcript is expressed in hippocampal neurons, and its transcript levels were found to be downregulated by neuronal activity upon KCl-induced cell depolarization *in vitro* and upon flurothyl-induced seizures *in vivo* (Kaas et al. 2013). Similarly, Tet3 mRNA was also found to be responsive to neuronal activity in cortical neurons (Li et al. 2014b), suggesting that the activity that helps to shape circuits in the brain leads to increases in hmC levels. To determine the consequence of Tet1 deletion in the brain *in vivo*, Zhang et al. generated Tet1 knockout mice and found that the mice were viable and fertile and had no growth or anatomical abnormalities during the early stages of development. However, the Tet1 knockout mice displayed reduced neurogenesis in the adult brain and resulted in a smaller neural progenitor pool in the dentate gyrus of the hippocampus, which was suggested to contribute to their impaired spatial learning and memory.

Although hmC and the subsequent oxidation products are largely believed to be intermediates in DNA demethylation, their exact roles are unknown. Their function in the CNS has also been largely unexplored. In fact, the Tet proteins are known to preferentially bind to and oxidize CG compared with CH, and most of the hmC in the brain occurs in a CG context (Lister et al. 2013b). These findings may thus explain the low levels of hmCH in the brain (Hu et al. 2013).

1.6 MicroRNAs and DNA methylation: Focus on miR-29

MicroRNAs are small non-coding RNAs that are evolutionarily conserved. MicroRNAs were only very recently discovered (the first microRNA was described in 1993) (Lee et al. 1993), but they have gained rapid attention due to their ability to modulate the expression of more than half of the mammalian genome (Bartel 2004). They function by binding to the 3'UTR of target mRNAs and by preventing either the transcription or translation of these mRNAs . MicroRNAs are 18-22 nucleotides in length and can be present both in intergenic regions as well as in the introns of genes. They are first produced in the cell as primary microRNA transcripts (or pri-miRNAs), which are cleaved by an enzyme known as Drosha into the precursors of microRNAs (pre-miRNAs) (Guo et al. 2010). The pre-miRNAs are then exported into the cytoplasm by the protein exportin. The exported pre-miRNAs are cleaved by the protein Dicer, giving rise to mature microRNAs. The mature miRNAs are then loaded onto a multiprotein complex called RISC (RNA-induced silencing complex), eventually allowing the microRNA to regulate mRNA levels either by the degradation or translational repression of the mRNA.

Recent work has revealed that microRNAs could play a role in DNA methylation. For example, miR-148 has been shown to target Dnmt3b and Dnmt1 in HeLa cells and in cholangiocarcinoma cell lines. miR-126 and miR-152 were also previously shown to target the 3'UTR of Dnmt1. Several of these microRNAs have also been shown to be dysregulated in various human cancers. Recently, the miR-29 family members were shown to directly target Dnmt3a and Dnmt3b, and overexpression of this microRNA family in lung cancer cell lines and acute myeloid leukemia cell lines led to reduced global DNA methylation (Denis et al. 2011).

The miR-29 family consists of three family members, miR-29a, miR-29b and miR-29c (Kriegel et al. 2012). These three members are expressed from two distinct loci as miR-29ab1 and miR-29cb2. Many of the targets as well as the target sites are broadly conserved across different species. According to *targetscan.org*, miR-29b has at least 2777 transcript sites. Due to its ability to modulate multiple genes and pathways, this microRNA has been widely studied in a variety of contexts including cancer, neurodegeneration, diabetes, and aging (Hebert et al. 2008; Ugalde et al. 2011; Xu et al. 2015). Interestingly, miR-29 has the ability to target two genes that have opposite functions in the same pathway. For example, in certain cancer cell lines, miR-29 is known to target Mcl-1, an anti-apoptotic gene (Mott et al. 2007), thus making this microRNA an attractive molecule for tumor therapy. In contrast, in peripheral neurons, miR-29 is known to target pro-apoptotic BH3-only proteins, thereby preventing cell death (Kole et al. 2011). These findings underscore the contextual and spatial differences of miR-29 function in different cell types.

The role of miR-29 is especially important in the nervous system, as the neurons in the brain engage miR-29 to inhibit the apoptotic pathway. Inhibition of apoptosis is crucial in neurons, which are postmitotic and cannot afford to remain susceptible to apoptosis after the nervous system has developed. Upon screening for microRNAs that were induced upon neuronal maturation, Kole et al. discovered that miR-29 was markedly induced in mature neurons and that this microRNA promoted survival by regulating the expression of multiple pro-apoptotic BH3-only proteins (Kole et al. 2011). However, the role of miR-29 in the context of DNA methylation and brain maturation in the CNS is still poorly understood and remains to be investigated.

1.7 Non-canonical CH methylation

Although the role of the DNA methyltransferases and MeCP2 in CG methylation had been known for some time, the recently discovery of non-canonical DNA methylation has paved the path for understanding the molecular mechanisms behind the development and maturation of the brain under both physiological conditions and in the context of neurodevelopmental disorders. While canonical CG methylation (mCG) involves the methylation of a cytosine that is adjacent to a guanine nucleotide, non-canonical cytosine methylation results in the methylation of a cytosine that is adjacent to a non-guanine nucleotide (referred to as mCH, where H = adenine (A), cytosine (C), or thymine (T)) (Xie et al. 2012; Lister et al. 2013b; Shin et al. 2014a; He and Ecker 2015; Kinde et al. 2015), with mCA being the most predominantly methylated residue in mCH methylation.

Non-CH methylation in pluripotent stem cells

While mCH methylation has been found to occur in various tissue types throughout the human body (Schultz et al. 2015), the highest levels of mCH methylation have been found in human embryonic stem cells (ESCs) (Ramsahoye et al. 2000; Laurent et al. 2010; Lister et al. 2013a) and in the mammalian brain (Xie et al. 2012; Zeng et al. 2012; Lister et al. 2013a). The presence of non-CG methylation in ESCs was first described in 2000 by Rudolf Jaenisch's lab in which they used bisulfite sequencing methods to show that ESCs have higher levels of non-CG methylation compared to various somatic tissues including the liver, kidney, spleen and lung. These sites of non-CG methylation were shown to occur primarily at CA and CT sites. Expression of Dnmt3a in Drosophila led to the methylation of both CG and non-CG sites, suggesting that non-CG methylation in ESCs was mediated by

Dnmt3a (Ramsahoye et al. 2000). Lister et al. found that, compared to the IMR90 fetal lung fibroblasts in which 0.02% of the genome was methylated in the non-CG context, the DNA of male-derived human ESCs (H1) was found to have high levels of mCH, with nearly a quarter of all methylated sites being non-CG methylated (Lister et al. 2009). In addition to ESCs, induced pluripotent stem cells (iPSCs) are also known to display high levels of mCH. Interestingly, Lister et al. found that iPSCs derived from the IMR90 cells underwent a restoration of non-CG methylation, suggesting that non-CG methylation in the epigenome is reconfigured during the process of differentiation and de-differentiation (Lister et al. 2009).

Non-CH methylation in the maturing brain

Non-CG methylation occurs at very low levels and is virtually undetectable in the embryonic and early postnatal frontal cortex, but its levels gradually increase between birth and the adolescent period and plateaus as the brain undergoes maturation (Fig. 1.12). Similar patterns of mCH accumulation have been found in the dentate gyrus of the hippocampus in mice (Guo et al. 2014). Consistent with this accumulation of mCH during brain maturation, the levels of Dnmt3a peak at approximately ten days after birth in the mouse frontal cortex and are markedly reduced by postnatal day 20 (Lister et al. 2013b). In fact, this period during which mCH accumulates coincides with the stage of synaptogenesis and synaptic refinement (Lister et al. 2013a).

In addition to recognizing and binding to mCG across the mammalian genome, MeCP2 was recently found to bind to mCH sites and repress gene expression (Guo et al. 2014; Chen et al. 2015; Gabel et al. 2015). Gabel et al. found that MeCP2 normally binds to

mCA sites within long genes, many of which are associated with neuronal function, and represses their transcription. In both MeCP2 mutant mouse models and postmortem human RTT brains a length-dependent increase in gene expression was observed. Furthermore, Chen et al. found that genes that acquire non-CG methyl marks after birth tend to become dysregulated in mouse models of RTT, suggesting that regulation of mCH by MeCP2 is critical in the postnatal brain. These findings suggest that one of the mechanisms underlying the pathogenesis in RTT could be the dysregulated expression of long genes in the developing and maturing brain.

These observations and the recent interest in non-CG methylation in the brain raise several fascinating questions. What controls the expression of the DNA methyltransferases and thereby regulates noncanonical DNA methylation in the maturing brain? Are there microRNAs that govern the critical period during which non-canonical DNA methylation occurs? What are the anatomical and behavioral consequences of upregulating the expression of DNA methyltransferases in the maturing brain? Several of these points are addressed in this thesis and remain under intense investigation as studies on the role of non-CG methylation in the brain continue to grow.

1.8 Figures and Legends

Figure 1.1: Apoptosis is essential for proper embryonic development.

Gross morphology of caspase-9 heterozygous (**A**) and homozygous (**B**) embryos isolated at embryonic day 16.5 (E16.5). By this time point, a severe malformation (excencephaly) of the brain in the caspase-9 homozygous knockout mice can be seen.

Figure 1.1

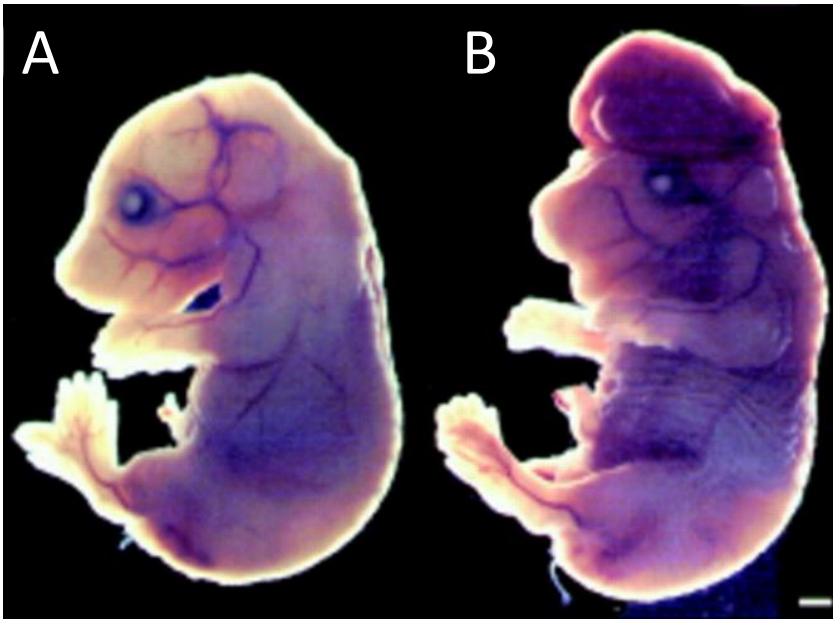

Figure adapted from Kuida et al., *Cell* (1998)

Figure 1.2: The intrinsic and extrinsic pathways of apoptosis.

(**A**) The intrinsic pathway of apoptosis. Following apoptotic stimuli, the pro-apoptotic proteins Bax and Bak are activated and lead to the release of cytochrome *c* from the mitochondria into the cytosol. Cytochrome *c* then binds to Apaf-1, inducing the formation of the apoptosome that activates downstream caspases to induce the death of the cell. (**B**) The extrinsic pathway of apoptosis. After a ligand binds to the death receptor, downstream adaptor molecules are recruited and results in the dimerization and activation of caspase-8. Caspase-8 can either directly activate caspase-3 and caspase-7 without the involvement of mitochondria, or it can activate and cleave Bid into tBid, which engages Bax and Bak to mediate the mitochondrial-dependent pathway of apoptosis.

Figure 1.2

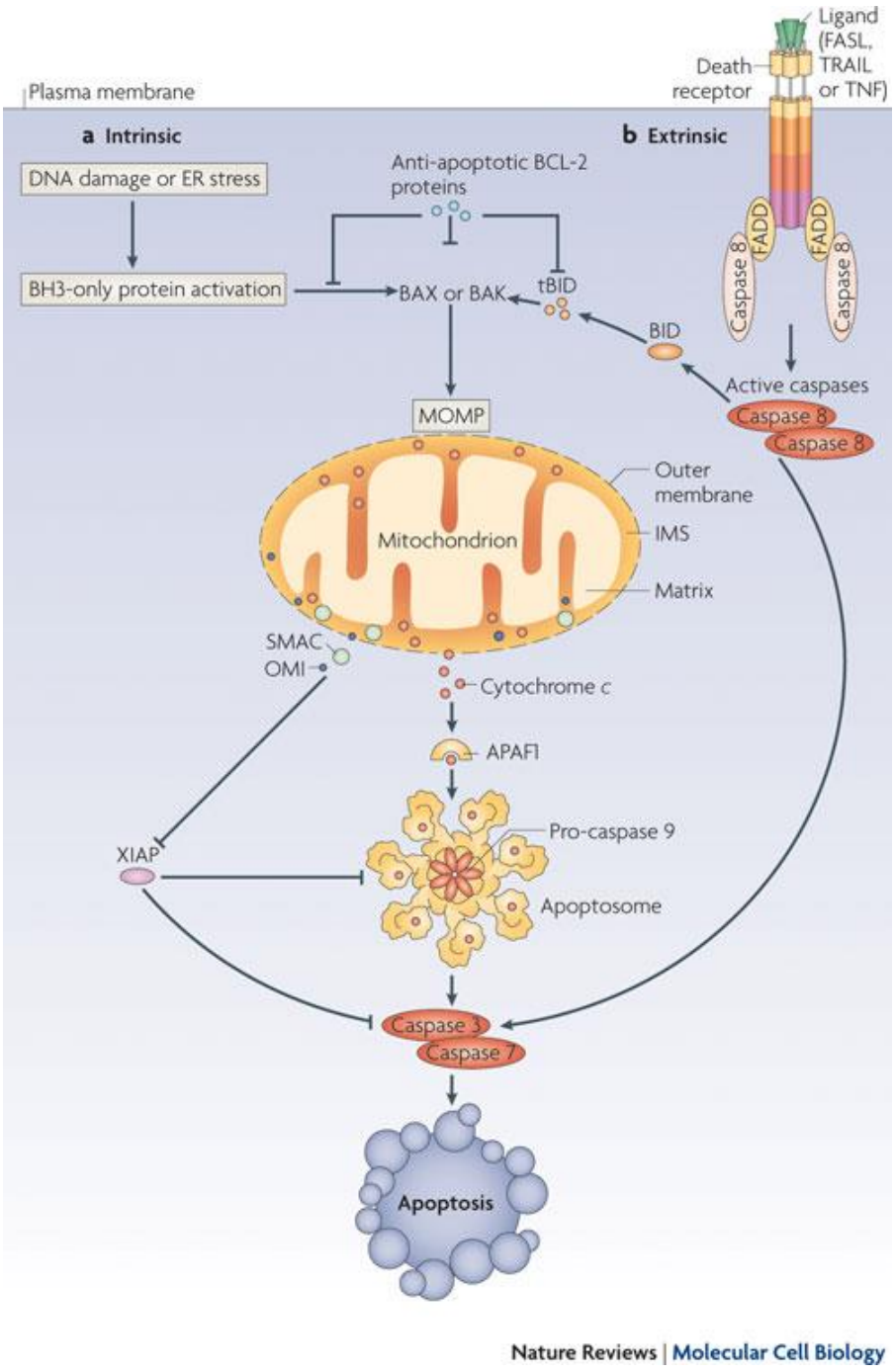

From Tait and Green, *Nature Reviews Molecular Biology* (2010)

Figure 1.3: Members of the Bcl-2 family of proteins.

The Bcl-2 family of proteins is composed of pro-apoptotic and anti-apoptotic members. These proteins are classified according to the number of Bcl-2 homology (BH) domains present within the proteins. The anti-apoptotic family members, which include Bcl-2, Bcl-xL, Bcl-w, A1, and Mcl-1, contain a total of four BH domains (BH1-BH4). The pro-apoptotic proteins Bax, Bak and Bok contain three BH domains (BH1-BH3), while the other group of pro-apoptotic proteins, the BH3-only family members, contains only the BH3 domain.

Figure 1.3

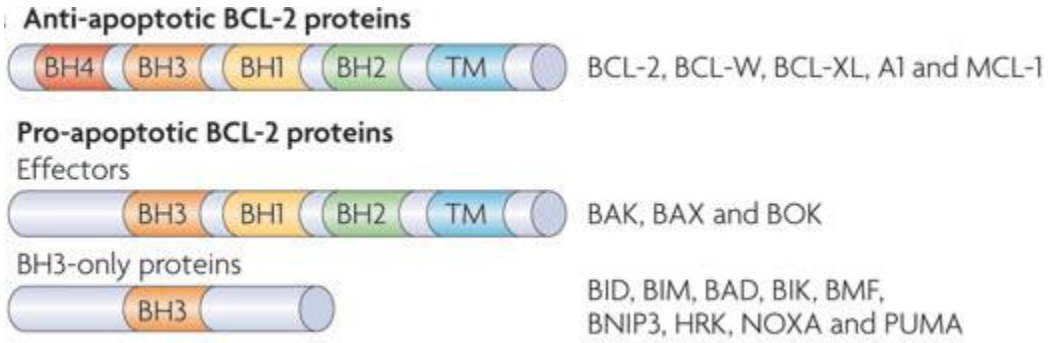

From Tait and Green, *Nature Reviews Molecular Biology* (2010)

Figure 1.4: Formation of the mammalian apoptosome complex.

Normally, in healthy cells that have not released cyt *c* from the mitochondria, Apaf-1 exists in a monomeric state in which the WD40 repeats fold back to prevent dATP and caspase-9 from binding to the protein domains in Apaf-1. Upon mitochondrial release of cyt *c*, cyt *c* binds to the WD40 repeats of Apaf-1, exposing the ATPase domain. Apaf-1 subsequently undergoes a conformational change that allows the binding of dATP and caspase-9, resulting in the formation of the apoptosome.

Figure 1.4

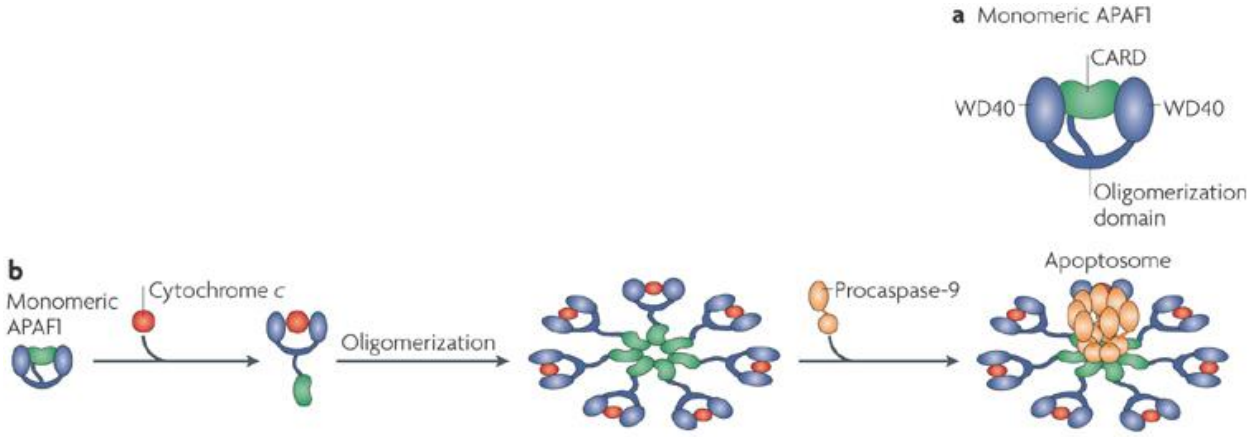

Adapted from Ow et al., *Nature Reviews Molecular Biology* (2008)

Figure 1.5: Programmed cell death in the peripheral and central nervous systems.

While the apoptotic pathway in the peripheral nervous system is governed by the neurotrophic theory (*i.e.* the number of neurons innervating the tissue must match the size of the target tissue), the developing neurons in the CNS do not appear to rely on a single trophic factor for survival, and the mechanisms underlying apoptosis in the CNS are still poorly understood.

Figure 1.5

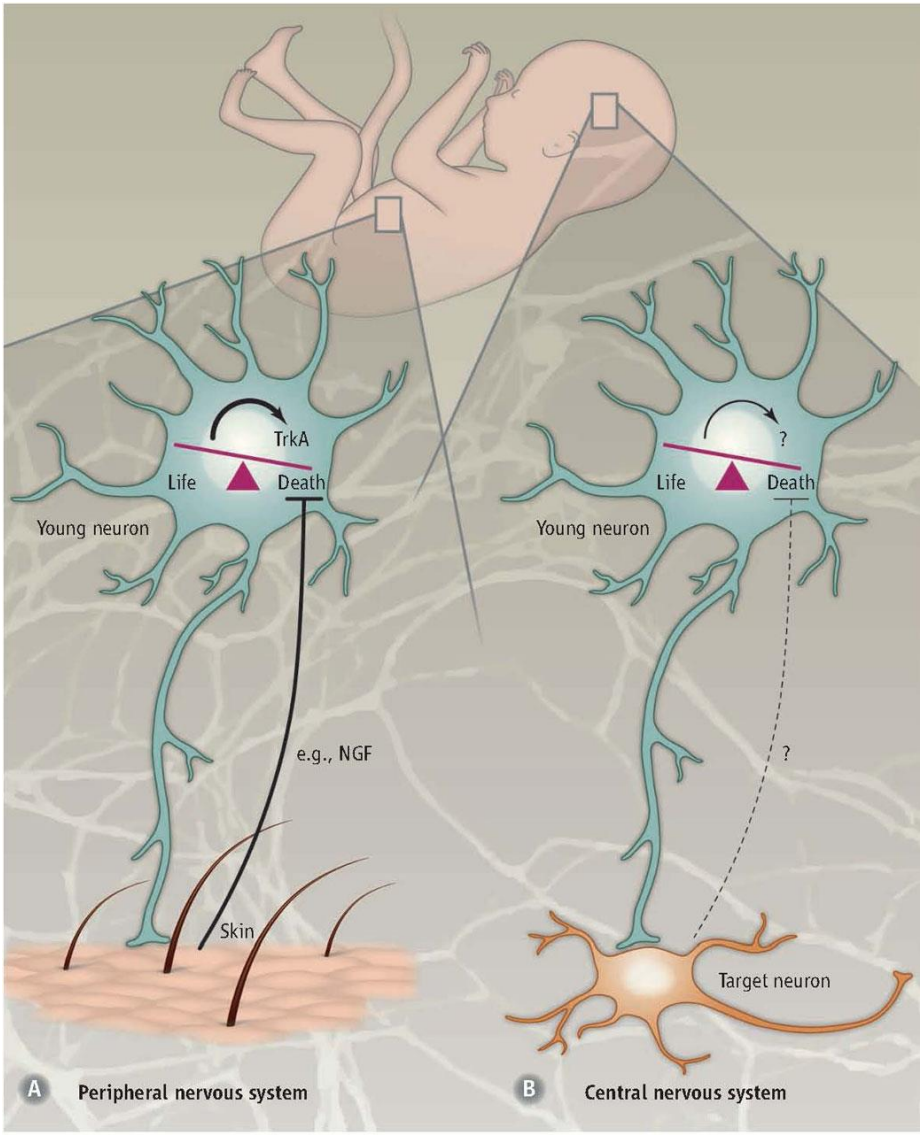

From Dekkers and Barde, *Science* (2013)

Figure 1.6: Mechanisms by which DNA methylation induces transcriptional repression.

(**A**) The presence of DNA methylation in the DNA binding sequences of the promoter region prevents the binding of transcription factors and thus mediates gene silencing. (**B**) Methylated DNA is recognized by the methyl-CpG-binding proteins (MBPs), which function to recruit corepressor proteins to mediate gene silencing.

Figure 1.6

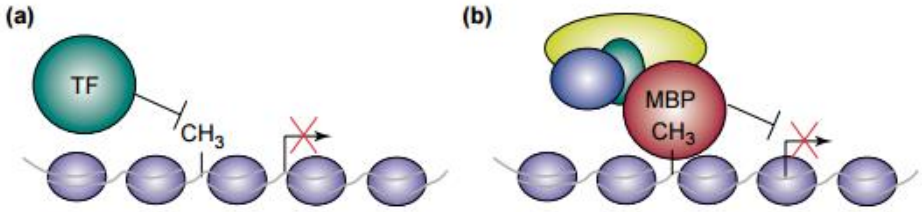

Adapted from Klose and Bird, *Trends in Biochemical Sciences* (2006)

Figure 1.7: Bisulfite genomic sequencing.

After genomic DNA is isolated from cells or tissues, the DNA is treated with sodium bisulfite. Sodium bisulfite treatment converts non-methylated cytosines into uracils, while methylated cytosines are protected from sodium bisulfite conversion and are still read as cytosines. The DNA is then prepared for sequencing.

Figure 1.7

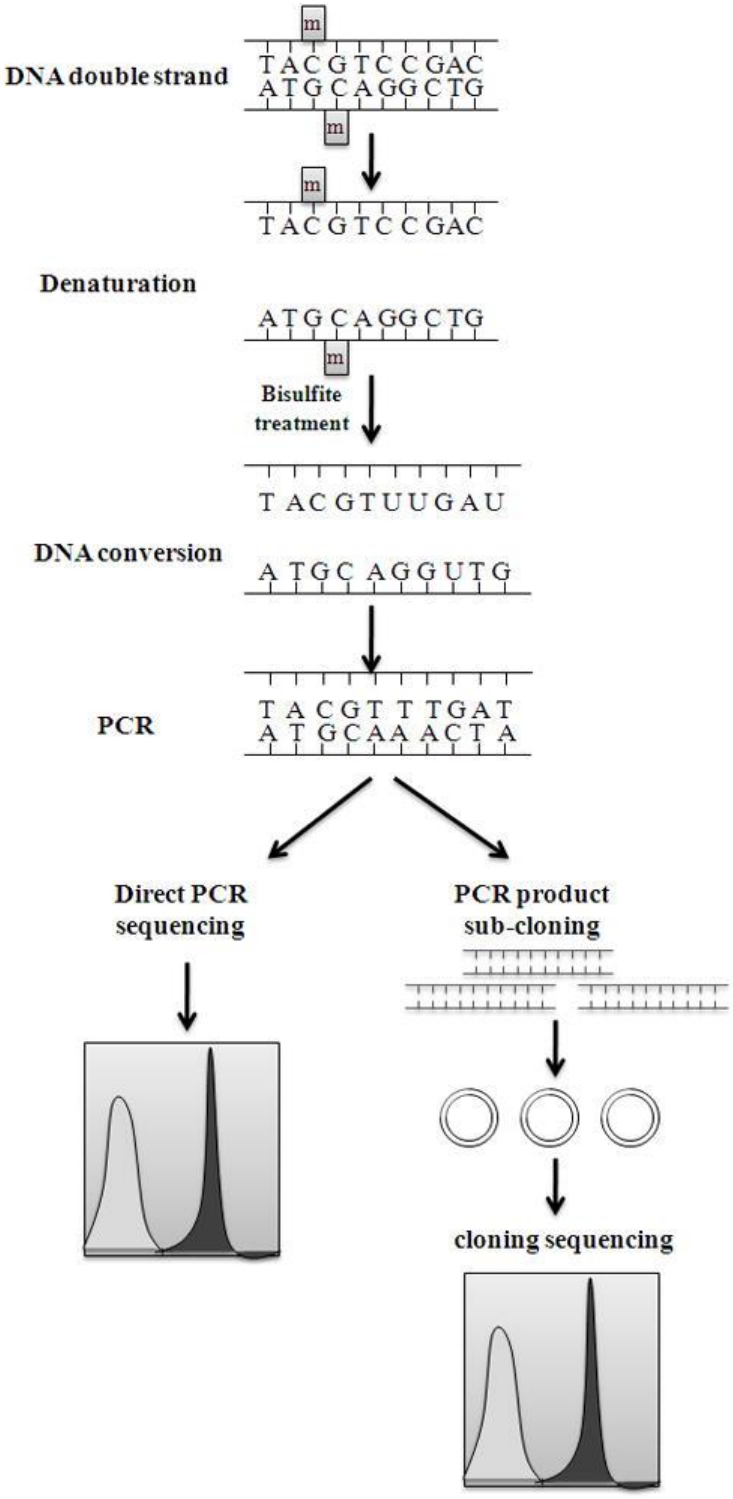

From Li and Tollefsbol, *Methods in Molecular Biology* (2011)

Figure 1.8: Phenotypes of the Dnmt3a and Dnmt3b knockout mice.

(**A**) An image of wildtype and Dnmt3a-deficient mice at postnatal day 18. Although Dnmt3a$^{-/-}$ mice are born at the expected Mendelian ratio and appear normal at birth, they undergo growth retardation and die at approximately four weeks of age. (**B**) An image of wildtype and Dnmt3b-deficient embryos at embryonic day 11.5. The image shows an enlarged head region in the Dnmt3b$^{-/-}$ mice indicative of a rostral neural tube defect.

Figure 1.8

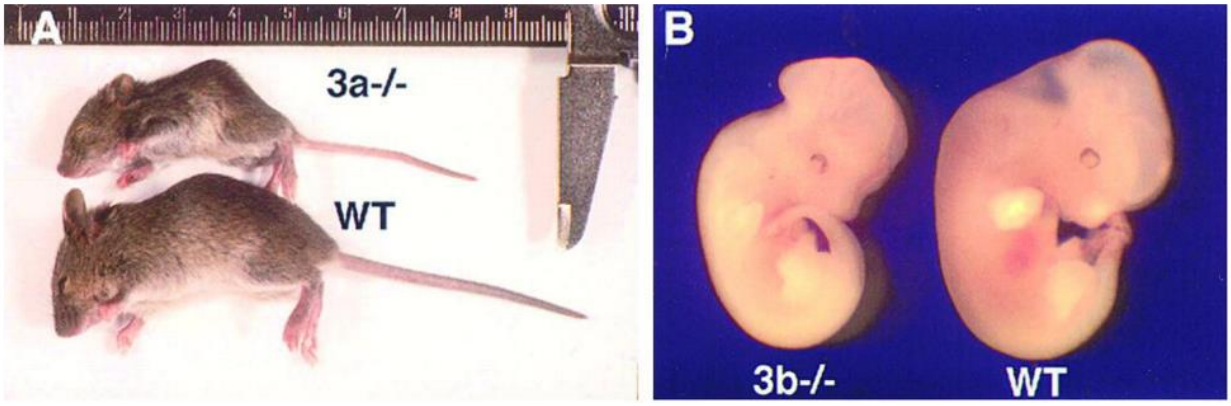

Adapted from Okano et al., *Cell* (1999)

Figure 1.9: Mice deficient in both Dnmt3a and Dnmt3b are embryonic lethal.

(**A**) Wildtype and (**B**) Dnmt3a/Dnmt3b double homozygous embryos at embryonic day 9.5. These mice deficient in both Dnmt3a and Dnmt3b have smaller body size, fail to form somites and die before embryonic day 11.5.

Figure 1.9

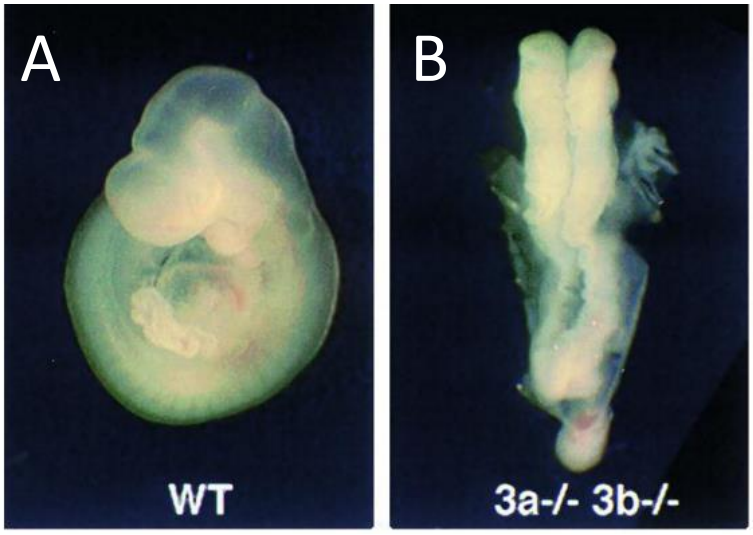

Adapted from Okano et al., *Cell* (1999)

Figure 1.10: Facial dysmorphic features in patients with DNMT3A overgrowth syndrome.

(**A-H**) Photographs of patients with DNMT3A overgrowth syndrome, which is characterized by greater height, intellectual disability and facial dysmorphism.

Figure 1.10

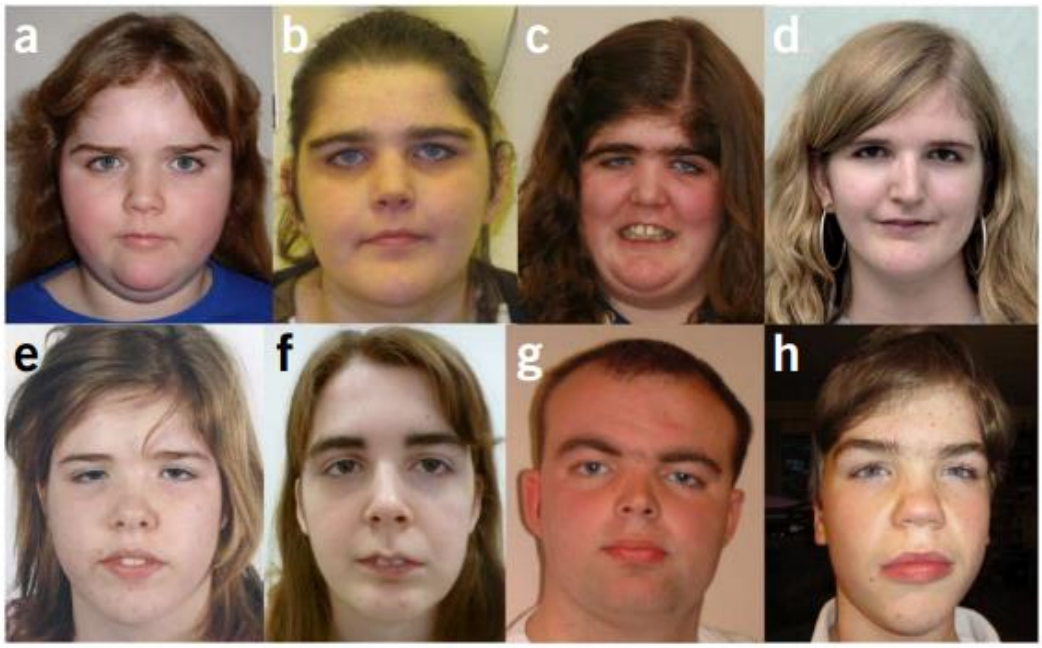

From Tatton-Brown et al., *Nature Genetics* (1999)

Figure 1.11: Cytosine methylation and hydroxymethylation are mediated by the DNA methyltransferases and ten-eleven translocation proteins, respectively.

While the five-position carbon on cytosines in the mammalian genome are methylated by the DNA methyltransferases Dnmt1, Dnmt3a and Dnmt3b, the methylcytosines can be further oxidized to hydroxymethylcytosines by the Tet enzymes, Tet1-3.

Figure 1.11

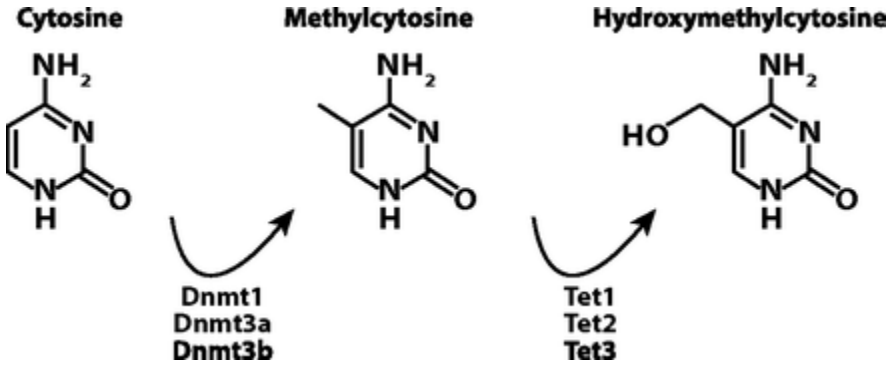

From Kinde et al., *Proceedings of the National Academy of Sciences* (2015)

Figure 1.12: Levels of mCG and mCH in the mouse and human frontal cortex across age.

MethylC-seq analysis on mouse and human frontal cortex reveal the pattern of mCG and mCH levels across age. mCH levels accumulate during the early postnatal stages, and this increase coincides with the period of synaptogenesis and continues to increase during the period of synaptic pruning in the postnatal brain.

Figure 1.12

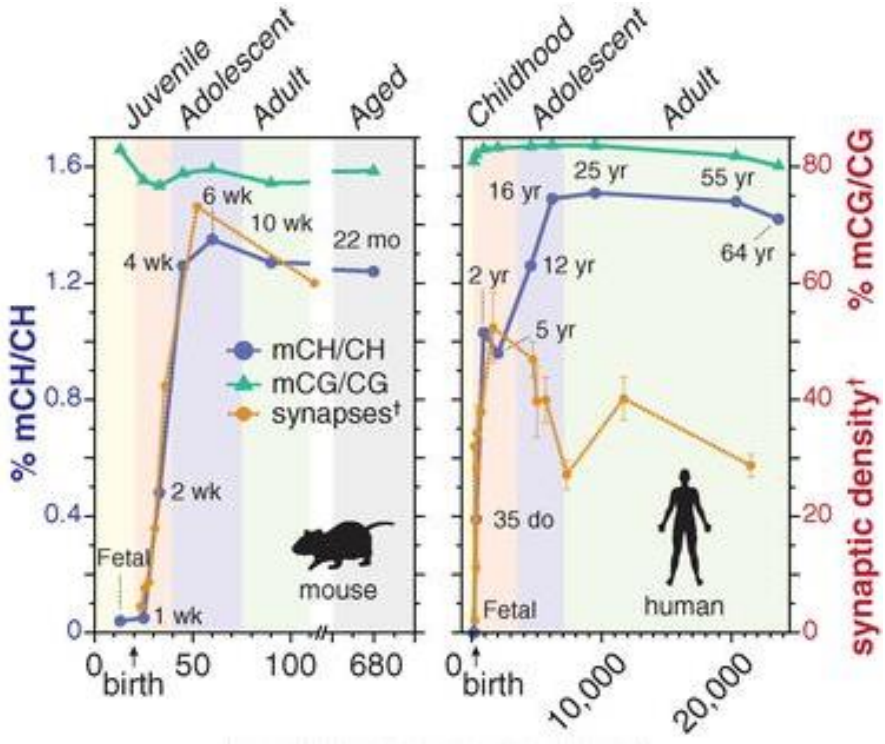

Adapted from Lister et al., *Science* (2013)

CHAPTER TWO: BCL-XL IS ESSENTIAL FOR THE SURVIVAL AND FUNCTION OF DIFFERENTIATED NEURONS IN THE CORTEX THAT CONTROL COMPLEX BEHAVIORS

2.1 Overview

Apoptosis plays an essential role during brain development, yet the precise mechanism by which this pathway is regulated in the brain remains unknown. In particular, mammalian cells are known to express multiple anti-apoptotic Bcl-2 family proteins. However, the cells of the developing brain could also exist in a primed state where the loss of a single anti-apoptotic Bcl-2 family protein is sufficient to trigger apoptosis. Here, we examined the critical role of Bcl-xL, an anti-apoptotic protein, during brain development. Using conditional knockout mice in which Bcl-xL is deleted in neural progenitor cells (Bcl-xL$^{Emx1\text{-}Cre}$), we show that the loss of Bcl-xL is not sufficient to trigger apoptosis in these proliferating progenitors. In contrast, specific populations of postmitotic neurons derived from these progenitors, including upper layer cortical neurons and the CA1-CA3 regions of the hippocampus, were acutely dependent on Bcl-xL. Consistent with this finding, deletion of Bcl-xL selectively in the postmitotic neurons in the brain (Bcl-xL$^{Nex\text{-}Cre}$) also resulted in similar patterns of apoptosis. This Bcl-xL deficiency-induced neuronal death was a consequence of activation of the apoptotic pathway, as the cell death was rescued with co-deletion of the pro-apoptotic proteins Bax and Bak. Importantly, the loss of these Bcl-xL-dependent neurons led to severe neurobehavioral abnormalities including

deficits in motor learning, hyperactivity, and increased risk-taking and self-injurious behaviors. Together, our results identify a population of neurons in the developing brain that are acutely dependent on Bcl-xL during the peak period of synaptic connectivity that are important for the establishment of higher order complex behaviors.

2.2 Introduction

Regulation of apoptosis is critical for proper embryonic and early postnatal brain development (Raff et al. 1993). The apoptotic pathway in the peripheral nervous system (PNS) is well known to be regulated by target-derived trophic factors that maintain the survival of neurons that are properly innervated at their distal targets (Oppenheim 1991). In contrast, while neurons in the central nervous system (CNS) are known to undergo apoptosis during development (Kuida et al. 1996; Cecconi et al. 1998; Hakem et al. 1998; Yoshida et al. 1998), exactly how apoptosis is regulated in the developing CNS remains unclear. For example, in contrast to PNS neurons, neurons in the developing CNS do not rely on a single trophic factor for their survival (Dekkers et al. 2013). However, increasing evidence indicates that CNS neurons rely more on neuronal activity and proper wiring of synaptic connections to maintain their survival (Dekkers and Barde 2013).

The key regulators of apoptosis are the Bcl-2 family proteins, which contain multiple pro-apoptotic (*e.g.* Bax, Bak) and anti-apoptotic (*e.g.* Bcl-2, Bcl-xL, Mcl-1, Bcl-w) proteins (Youle and Strasser 2008; Chipuk et al. 2010). While these pro- or anti-apoptotic proteins are generally thought to have redundant functions, the emerging data points to a level of functional specificity for individual proteins that had not been previously appreciated. For example, deletion of Bax alone is sufficient to inhibit apoptosis in postmitotic neurons (Deckwerth et al. 1996; Besirli et al. 2003). In addition, while loss of Mcl-1 results in peri-implantation embryonic lethality (Rinkenberger et al. 2000), Bcl-xL$^{-/-}$ global knockouts survive longer but are still embryonic lethal, with most knockouts dying at gestational day 13.5 (E13.5) (Motoyama et al. 1995). The cause of death in Bcl-xL-deficient mice is postulated to be the extensive cell death that occurs in the liver

hematopoietic cells, subsequently leading to anemia in these animals; however, another major organ system affected by loss of Bcl-xL is the brain (Motoyama et al. 1995; Roth et al. 1996).

Bcl-xL is known to be expressed in both the embryonic and adult brain (Gonzalez-Garcia et al. 1994; Gonzalez-Garcia et al. 1995). Telencephalic neurons deficient in Bcl-xL are more sensitive to apoptosis both *in vivo* and *in vitro* (Motoyama et al. 1995; Roth et al. 1996). Moreover, in recent years, there has been increasing attention on the role of Bcl-xL in regulating processes beyond neuronal apoptosis, including neurite outgrowth (Kretz et al. 2004; Park et al. 2015), synaptic plasticity (Jonas et al. 2003; Li et al. 2008; Li et al. 2013) and mitochondrial bioenergetics (Vander Heiden et al. 2001; Chen et al. 2011). Although there has been focus on both the apoptotic and non-apoptotic roles of Bcl-xL in the nervous system, a systematic examination of the consequence of Bcl-xL deficiency in the brain has not been conducted to date.

Here, we generated conditional knockout mice in which Bcl-xL is specifically deleted in the neural progenitor cells (NPCs) of the telencephalon and in the postmitotic cells of the brain. We show that, while loss of Bcl-xL appears to be dispensable for the survival of NPCs, specific populations of postmitotic neurons in the brain critically rely on Bcl-xL for their survival and function. The brains of Bcl-xL-deficient mice displayed severe microcephaly as a result of increased apoptotic cell death in the neurons of the cortex and hippocampus during the early postnatal stages, a phenomenon that is rescued with deletion of Bax and Bak. *In vivo* imaging for visually evoked neural activity in mice deleted for Bcl-xL revealed an abnormally small retinotopic map in the visual cortex that, surprisingly, remained topographically intact and functional. Importantly, Bcl-xL deficiency

led to severe consequences in the animal, including deficits in motor learning, self-injurious behavior, overt hyperactivity, and increased risk-taking behavior. Together, these results point to the critical role of Bcl-xL in the survival of specific postmitotic neurons in the developing mammalian brain, the loss of which results in neurobehavioral deficits.

2.3 Results and Discussion

Bcl-xL deletion leads to cell death of newly differentiated neurons

Mice globally deleted for Bcl-xL are embryonic lethal at E13.5 (Motoyama et al. 1995). While Bcl-xL is known to regulate apoptosis in neurons, its essential role in the survival of hematopoietic cells precluded studies that could identify the precise function of Bcl-xL in the nervous system. To critically examine the role of Bcl-xL in the developing brain, we generated conditional knockouts by crossing mice floxed for Bcl-xL with Emx1-Cre mice (Bcl-xL$^{loxP/loxP}$; Emx1-Cre, hereafter referred to as Bcl-xL$^{Emx1\text{-}Cre}$). To confirm that Emx1-Cre induces recombination in the NPCs of the dorsal telencephalon (Gorski et al. 2002), we also generated Emx1-Cre; rosa26reporter-tdTomato mice. As expected, there is robust expression of tdTomato in the dorsal telencephalon at E12.5 (Fig. 2.1A). Our results show that Bcl-xL expression is lost throughout all layers of the cortex in the Bcl-xL$^{Emx1\text{-}Cre}$ mice (Fig. 2.1B). A few neurons, including excitatory projection neurons and interneurons, continue to exhibit Bcl-xL immunoreactivity, as Emx1-Cre is known to induce recombination at an efficiency of ~88% in the cortex and does not induce recombination in interneurons (Gorski et al. 2002) (Fig. 2.1B).

In contrast to mice globally deleted for Bcl-xL, Bcl-xL$^{Emx1\text{-}Cre}$ mice were born at the expected Mendelian ratio and appeared normal at postnatal day 1 (P1) (Fig. 2.1C). At P1, the brains of Bcl-xL$^{Emx1\text{-}Cre}$ mice also appeared similar to those of wildtype mice, and there was no difference in the brain weights between the two genotypes (Fig. 2.1D, E). By P25, however, although Bcl-xL$^{Emx1\text{-}Cre}$ mice remained grossly normal, examination of their brains revealed profound microcephaly (Fig. 2.1F-H). From P1 to P30, Bcl-xL$^{Emx1\text{-}Cre}$ mice also exhibited a significant reduction in the cortical thickness, and the number of NeuN-positive

cells throughout the cortex at P30 was markedly reduced in the Bcl-xL$^{Emx1\text{-}Cre}$ mice (Fig. 2.2A-G).

The fact that the deletion of Bcl-xL in the developing brain did not result in embryonic lethality prompted us to examine Bcl-xL expression in the developing brain. Contrary to our expectation that Bcl-xL is expressed throughout the brain, we found that the expression of Bcl-xL was significantly higher in the non-proliferating cells of the cortex compared to the proliferating progenitors in the subventricular zone (Fig. 2.3A-C). To determine whether the microcephaly observed in Bcl-xL$^{Emx1\text{-}Cre}$ mice postnatally was due to increased apoptosis, we probed the brains for cleaved caspase-3 at multiple time points (E16, P1). Consistent with the expression patterns of Bcl-xL throughout the brain, cell death in the Bcl-xL-deficient embryonic brain occurred primarily in the NeuN-positive differentiated neurons while the proliferating (PCNA-positive) progenitors were largely spared (Fig. 2.3D-H). Even more striking, we found that deletion of Bcl-xL induces cell death and formation of pyknotic nuclei predominantly at P1 in the cortex of the postnatal brain (Fig. 2.4A-D). Analysis of the hippocampus also showed extensive cell death in the CA1-CA3 regions of Bcl-xL$^{Emx1\text{-}Cre}$ mice at P1 (Fig. 2.4E, F). Thus, consistent with its pattern of expression, deletion of Bcl-xL selectively affects the postmitotic neurons rather than their proliferating progenitors.

Bcl-xL deficiency induces cell death predominantly in upper layer cortical neurons and results in a significantly smaller but functional visual cortex

As the majority of cells that are undergoing apoptosis in Bcl-xL$^{Emx1\text{-}Cre}$ mice at P1 are located in the upper regions of the cortex, we investigated the specific neuronal layers that

are affected most by Bcl-xL deficiency. By P30, the Bcl-xL$^{Emx1\text{-}Cre}$ mice had a significant reduction in the number of Cux1^{+} cells in layers II/III and Brn1^{+} cells in layers II-IV of the cortex (Fig. 2.4G-J). While deeper layer Tbr1^{+} neurons also underwent cell death in Bcl-xL$^{Emx1\text{-}Cre}$ mice (Fig. 2.4K, L), cell death was more prominent in the upper layer cortical neurons.

To examine the physiological relevance of loss of Bcl-xL in the brain, we focused on the primary visual cortex (V1) as a marker for structural and functional organization of the cortex (Fig. 2.5A). Surprisingly, despite the significant reduction in layers II-IV of the cortex, *in vivo* imaging of visual responses to a white bar moving either in a horizontal or vertical direction revealed a functional and retinotopically organized visual cortex in Bcl-xL$^{Emx1\text{-}Cre}$ mice (Fig. 2.5B). Further tests using a vertical grating patch found that, although the neurons appeared to be wired in a topographically correct manner, the size of the visual cortex as measured by the whole V1 area as well as the area representing a 50-degree diameter portion of visual space were both significantly smaller in Bcl-xL$^{Emx1\text{-}Cre}$ mice compared to their wildtype littermates (Fig. 2.5B-D). In fact, as a consequence of the reduced size of the visual cortex, the underlying superior colliculus was fully exposed (Fig. 2.5A). Thus, we were able to image the retinotopic organization of the superior colliculus within the same field-of-view that contained the visual cortex in the Bcl-xL$^{Emx1\text{-}Cre}$ mice (Fig. 2.5B). Together, these results highlight the importance of Bcl-xL in maintaining the survival of upper layer neurons, the loss of which led to markedly smaller, yet functional, areas of cortical retinotopy.

Neuronal death induced by Bcl-xL deficiency is rescued with co-deletion of Bax and Bak

The key effectors of apoptosis are the pro-apoptotic proteins Bax and Bak, which can be activated either directly or indirectly by the loss of their binding to the anti-apoptotic proteins such as Bcl-xL (Cheng et al. 2001; Kim et al. 2006; Westphal et al. 2014). Thus, we examined whether the cell death caused by Bcl-xL deficiency is mediated *via* a Bax- and Bak-dependent apoptotic pathway. To test this, we crossed Bcl-xL$^{Emx1\text{-}Cre}$ mice with Bax$^{loxP/loxP}$; Bak$^{-/-}$ mice to generate Bax$^{loxP/loxP}$; Bcl-xL$^{loxP/loxP}$; Emx1-Cre; Bak$^{-/-}$ triple knockout mice (triple knockouts hereafter referred to as BBB TKO). First we confirmed that Bcl-xL and Bax underwent recombination in these mice (Fig. 2.6A, B). Bak, which is known to be minimally expressed in postmitotic neurons in the brain (Krajewski et al. 1996), is globally deleted in the BBB TKO mice (Fig. 2.6C). BBB TKO knockouts were born at the expected Mendelian ratio and appeared normal at birth (data not shown). More importantly, the apoptotic cell death observed in Bcl-xL$^{Emx1\text{-}Cre}$ mice was completely rescued in P1 BBB TKO mice (Fig. 2.6D, E). As a result, the cortical thickness and neuronal numbers at P30 were completely restored in these triple knockout mice (Fig. 2.6F-J). Together, these findings show that the neuronal death observed in the brains of Bcl-xL$^{Emx1\text{-}Cre}$ mice can be rescued with deletion of Bax and Bak.

Deletion of Bcl-xL in postmitotic neurons leads to selective neuronal death in the upper layers of the cortex

Our results show that inducing deletion of Bcl-xL in the NPCs of the dorsal telencephalon leads to the death of mainly postmitotic neurons in the early postnatal

animal. To specifically investigate the role of Bcl-xL deletion in postmitotic neurons throughout the brain, we utilized the Nex-Cre mouse model. Nex-Cre directs recombination in the postmitotic neurons at embryonic day E13.5 and spares recombination in neuronal progenitors (Goebbels et al. 2006). Bcl-xL$^{loxP/loxP}$; Nex-Cre mice (Bcl-xL$^{Nex\text{-}Cre}$), similar to Bcl-xL$^{Emx1\text{-}Cre}$ mice, were born at the expected Mendelian ratio. Interestingly, Bcl-xL$^{Nex\text{-}Cre}$ mice displayed smaller body weights at P30 (Fig. 2.7A, B). The brains of Bcl-xL$^{Nex\text{-}Cre}$ mice were also smaller compared to their wildtype littermate controls (Fig. 2.7C, D). Importantly, deletion of Bcl-xL in postmitotic neurons in Bcl-xL$^{Nex\text{-}Cre}$ mice still resulted in a cell death phenotype in the brain that was similar to what was observed in the Bcl-xL$^{Emx1\text{-}Cre}$ mice, with significantly increased cleaved caspase-3 staining in the upper cortical layers at P1 (Fig. 2.7E, F). Taken together, our results from both the Bcl-xL$^{Emx1\text{-}Cre}$ and Bcl-xL$^{Nex\text{-}Cre}$ mice show that the loss of Bcl-xL does not cause widespread apoptosis in the developing brain but instead results in the loss of postmitotic neurons in the upper regions of the cortex during the early postnatal stages.

Loss of Bcl-xL-dependent neurons results in deficits in motor learning, hyperactivity, and increased risk-taking and self-injurious behaviors

To determine the functional consequence of Bcl-xL deletion in postmitotic neurons, we conducted neurobehavioral assessments of wildtype and Bcl-xL$^{Nex\text{-}Cre}$ mice starting at P30. A three-minute tail suspension test revealed that, while wildtype mice exhibited the characteristic flailing of their hindlimbs, Bcl-xL$^{Nex\text{-}Cre}$ mice displayed hindlimb clasping, an indicator of generalized neurological dysfunction (Fig. 2.8A, B). The Bcl-xL$^{Nex\text{-}Cre}$ mice also displayed self-injurious behavior. Persistent skin lesions in their hindlimbs, chest, neck, and other areas began to appear approximately one month after birth and were observed

in approximately 50% of these mice (Fig. 2.8C). These lesions were not a result of fighting with cage mates, as Bcl-xL$^{Nex\text{-}Cre}$ mice housed alone also developed these lesions. Analysis of grooming behavior revealed that male Bcl-xL$^{Nex\text{-}Cre}$ mice spent significantly more time grooming compared to wildtype controls (Fig. 2.8D). Male Bcl-xL$^{Nex\text{-}Cre}$ mice also displayed an altered sensation to pain, as they were significantly more insensitive to noxious heat stimuli on the Hargreaves test (Fig. 2.8E).

In a multi-test behavioral regimen, both male and female Bcl-xL$^{Nex\text{-}Cre}$ mice displayed increased locomotor activity in the open field test without changes in rearing movements or time spent in the center region (Fig. 2.9A-C). Interestingly, male Bcl-xL$^{Nex\text{-}Cre}$ mice also displayed significantly increased risk-taking behavior as they spent more time in the open arms of the elevated plus maze, suggesting a loss of typical cautionary avoidance of the open areas (Fig. 2.9D, E). The total number of entries in the elevated plus maze was not altered in the knockout mice, indicating that the increased risk-taking behavior in the male Bcl-xL$^{Nex\text{-}Cre}$ mice could not be attributed to general hyperactivity during the test (Fig. 2.9F).

In contrast to the intact ability for locomotion and rearing movements, the Bcl-xL$^{Nex\text{-}Cre}$ knockout mice had profound deficits in motor coordination on an accelerating rotarod. The Bcl-xL$^{Nex\text{-}Cre}$ mice failed to show improvement across repeated trials, indicating impaired motor learning in the rotarod test (Fig. 2.9G). A subset of Bcl-xL-deficient mice without skin lesions (8/16) was further evaluated in the Morris water maze task to determine the ability of mice to locate a visible escape platform. While all of the wildtype mice demonstrated proficient learning in the visible platform test, Bcl-xL$^{Nex\text{-}Cre}$ knockout mice had an overt impairment in reaching the escape platform, with only two Bcl-xL$^{Nex\text{-}Cre}$ mice meeting the 15-second criterion for learning across three days of testing (Fig. 2.9H, I).

Taken together, these results show that Bcl-xL plays a critical role in postmitotic neuronal survival and that the Bcl-xL-dependent neurons control a variety of complex behaviors, the loss of which results in severe neurobehavioral abnormalities.

2.4 Materials and Methods

Mice. Bcl-xL$^{loxP/loxP}$ mice were generously provided by Dr. You-Wen He (Duke University). To induce conditional deletion of Bcl-xL, Bcl-xL$^{loxP/loxP}$ mice were crossed with two different Cre lines, Emx1-Cre and Nex-Cre. Emx1-Cre and tdTomato mice were a kind gift from Dr. William Snider (UNC-Chapel Hill) and Dr. Timothy Gershon, respectively (UNC-Chapel Hill). All other mice were obtained from Jackson Laboratory. Mice were maintained in a 12 hr light, 12 hr dark cycle (lights on at 7AM, lights off at 7 PM). All animal handling and protocols were carried out in accordance with established practices as described in the National Institutes of Health Guide for Care and Use of Laboratory Animals and as approved by the Animal Care and Use Committee at UNC-Chapel Hill.

Surgeries

For intrinsic signal optical imaging, craniotomy was performed on a total of 6 mice at age P29 – 34 (n = 3 wildtype, n = 3 Bcl-xL$^{Emx1\text{-}Cre}$ mice). Mice were anesthetized with isoflurane (5% for induction, 1-2% for surgery, 0.5% for imaging) augmented with chlorprothixene (2.5mg/kg, i.p.). Skull overlaying right visual cortex was exposed, and a custom head-fixing imaging chamber with a 5-mm diameter opening was mounted and secured with cyanoacrylate glue (Oasis Medical) and dental acrylic (Lang Dental). A 4-mm diameter craniotomy was made within the chamber to expose the visual cortex for imaging. The imaging chamber was then filled with a saline solution containing (in mM) 150 NaCl, 2.5 KCl, 10 HEPES, 2 $CaCl_2$, and 1$MgCl_2$. Physically-activated heat packs (SpaceGel, Braintree Scientific) and a feedback-controlled electric heat pad system (custom-built; 37°C) were used for maintaining body temperature during surgery and imaging, respectively.

Intrinsic signal optical imaging

Custom instrumentation adapted from previous reports (Kalatsky and Stryker 2003; Smith and Trachtenberg 2007) was used. Briefly, two F-mount lenses were used to form a tandem lens macroscope (respective focal lengths of 135 and 50mm; Nikon) which was connected to a Dalsa 1M30 CCD camera (Teledyne DALSA), providing a 4.6mm x 4.6mm field of view. The pial vasculature illuminated (Asahi Spectra low noise halogen source) with green light (550 ± 50nm, Edmund Optics) and imaged through a green emission filter (560 ± 5nm) served as a landmark for depth. From the vasculature, the imaging was focused 600 μm deep into the neocortex where hemodynamic intrinsic signals were imaged with red light (700 ± 38nm, Chroma). Reflected light was then captured through a second red filter (700 ± 5nm, Edmund Optics) at 30 frames/s with custom image acquisition software (code kindly provided by D. Ferster, Northwestern University; with adaptations by J. Stirman, University of North Carolina). Fourier analysis was performed on each pixel column to measure the magnitude and phase of stimulus-evoked signals at the frequency of the periodic visual stimuli (0.125Hz). Area and vertical and horizontal diameters of the entire V1 and a portion of V1 representing 50-degree visual space were measured using ImageJ software (Schindelin et al. 2012).

Visual stimuli

Head-fixed mice were positioned 20cm from an LCD monitor (60cm x 34cm) that was tilted 17.5° from vertical towards the mouse. The nose of the animal was pointed to the right edge of the monitor such that the stimulus covered 110° by 75° of visual space and was

viewed by the contralateral eye. A 3° thick drifting white bar sweeping across the monitor once every 8 seconds on a black background (horizontal or vertical) was used for retinotopic mapping, and a vertical grating patch (50° diameter displayed at the center of the monitor, 2 cycles/s, 0.04 cycle/°) drifting for the last two seconds of an eight-second period was used to measure basic cortical representation of a 50-degree visual space. The periodic motion cycle for both of these stimuli was at 0.125Hz and repeated 50 cycles. The stimulus movies were produced and presented using MATLAB (Pelli 1997) and the Psychophysics Toolbox (Brainard 1997) and were corrected for three dimensional distortion due to the flatness of the monitor using a custom MATLAB code (code is available online, http://labrigger.com/blog/2012/03/06/mouse-visual-stim/).

Behavioral regimen

Subjects were 16 Bcl-xL$^{Nex\text{-}Cre}$ (10 males and 6 females) and 19 wildtype controls (10 males and 9 females). Testing began when mice were approximately 6-7 weeks of age. For each procedure, measures were taken by an observer blind to mouse genotype. Mice were tested in the following assays, with one or two tests per week: elevated plus maze, open field, rotarod, and Morris water maze.

Elevated plus maze. This test was used to assess anxiety–like behavior, based on a natural tendency of mice to actively explore a new environment, versus a fear of being in an open area. Mice were given one 5-min trial on the plus maze, which had two walled arms (the closed arms, 20 cm in height) and two open arms. The maze was elevated 50 cm from the floor, and the arms were 30 cm long. Mice were placed on the center section (8 cm x 8

cm), and allowed to freely explore the maze. Measures were taken of percent time spent in the open arms and percent entries into the open arms. Total number of entries was used as an index for activity during the test.

Open field test. Exploratory activity in a novel environment was assessed by a 60-min trial in an open field chamber (41 cm x 41 cm x 30 cm) crossed by a grid of photobeams (VersaMax system, AccuScan Instruments). Counts were taken of the number of photobeams broken during the trial in 5-min intervals, with measures for total distance traveled, rearing movements, and time spent in the center region.

Rotarod. Subjects were tested for motor coordination and learning on an accelerating rotarod (Ugo Basile, Stoelting Co., Wood Dale, IL). For the first test session, animals were given 3 trials, with 45 seconds between each trial. Two additional trials were given 48 hours later. Rpm (revolutions per minute) was set at an initial value of 3, with a progressive increase to a maximum of 30 rpm across 5 min (the maximum trial length). Measures were taken for latency to fall from the top of the rotating barrel.

Morris water maze. The visible platform task was used to assess swimming ability and visual function. The water maze consisted of a large circular pool (diameter = 122 cm) partially filled with water (45 cm deep, 24-26^{o} C), located in a room with numerous visual cues. Each mouse was given 4 trials per day, across 3 days, to swim to an escape platform cued by a patterned cylinder extending above the surface of the water. For each trial, the mouse was placed in the pool at 1 of 4 possible locations (randomly ordered), and then

given 60 seconds to find the visible platform. If the mouse found the platform, the trial ended, and the animal was allowed to remain 10 seconds on the platform before the next trial began. If the platform was not found, the mouse was placed on the platform for 10 seconds, and then given the next trial. Measures were taken of latency to find the platform, swimming speed, and swimming distance via an automated tracking system (Noldus Ethovision).

Hargreaves assay. Heat sensitivity was measured by heating each hindpaw once per day using the Plantar Test apparatus (IITC) with a cut-off time of 20 seconds.

Immunohistochemistry. For immunohistochemistry experiments, mice were anesthetized using isoflurane and transcardially perfused with 4% paraformaldehyde. The mice were then decapitated, and the brains were post-fixed in 4% paraformaldehyde overnight. All of the stained sections were obtained from identical regions of the brain that were carefully selected based on structural and anatomical landmarks. Paraffin-embedded sections were used for hematoxylin-eosin (H/E), cleaved caspase-3, NeuN, Bcl-xL, and PCNA, and RFP stains. Briefly, IHC was carried out in the Bond Autostainer (Leica Microsystems Inc. Norwell, MA 02061). Slides were dewaxed in Bond Dewax solution (Leica, part #AR9222) and hydrated in Bond Wash solution (Leica, catalog #AR9590). Antigen retrieval was performed for 30 min at 100ºC in Bond-Epitope Retrieval solution 1 pH-6.0 (AR9961). Slides were incubated with the RFP, Bcl-xL, PCNA, cleaved caspase-3, NeuN, Bax, and Bak primary antibodies for 1 hour. DAPI or hematoxylin was used as a nuclear stain. Antibody detection was performed using the Bond Polymer Refine Detection

System (DS9800). Stained slides were dehydrated and coverslipped. Representative images are obtained from independent experiments, done at least in triplicate.

For all other stains, wildtype and Bcl-xL-deficient brains were embedded in 4% low-melting-point agarose in 1x PBS and were sectioned coronally (50 μm) on a vibratome (Leica VT 1200S). The following antibodies were used for immunohistochemistry on vibratome sections: cleaved caspase-3 (catalog #9664, Cell Signaling), Cux1 (catalog #sc-13024, Santa Cruz Biotechnology), Brn1 (kind gift from A. Ryan, McGill University), Tbr1 (catalog # ab31940, Abcam), NeuN (catalog #MAB377, Millipore). Appropriate anti-mouse, anti-rabbit, anti-rat, or anti-guinea pig secondary antibodies were used to detect primary antibody binding. DAPI was used as a nuclear stain. Representative images are obtained from independent experiments, done at least in triplicate.

Statistics. Statistical analyses were performed using GraphPad Prism 5 or Statview 5.0.1 (SAS) software. *Ex vivo* data are obtained from at least three independent experiments and expressed as mean ± s.e.m. unless otherwise specified. The Student's *t*-test (unpaired, two-tailed) for parametric data was used for analysis of two groups. Behavioral data were analyzed using 1-way, 2-way, or repeated measures ANOVAs, with the factors genotype and sex. Fisher's protected least-significant difference (PLSD) tests were used for comparing group means only when a significant F value was determined. No statistical methods were used to predetermine sample sizes, but our sample sizes are consistent with those reported in previous publications.

2.6 Figures and Legends

Figure 2.1: Loss of Bcl-xL in the dorsal telencephalon results in microcephaly.

(**A**) tdTomato+/Cre- (rosa26reporter-tdTomato; no Cre control) and tdTomato+/Cre+ (Emx1-Cre; rosa26reporter-tdTomato) brains at E12.5 stained with RFP show the recombination pattern of the Emx1-Cre line. Scale bar denotes 100 μm. (**B**) Wildtype and Bcl-xL$^{Emx1\text{-}Cre}$ mouse cortices stained with Bcl-xL at postnatal day 1 (P1). Samples were counterstained with hematoxylin. Scale bar denotes 50 μm. (**C**) Wildtype and Bcl-xL$^{Emx1\text{-}Cre}$ mice at P1. (**D**) Images of brains and (**E**) brain weights of P1 wildtype and Bcl-xL$^{Emx1\text{-}Cre}$ mice. (**F**) Wildtype and Bcl-xL$^{Emx1\text{-}Cre}$ mice at P25. (**G**) Images of brains and (**H**) brain weights of P25 wildtype and Bcl-xL$^{Emx1\text{-}Cre}$ mice. Data shown are means ± s.e.m. for each group. ** $P<0.01$; n.s. = not significant.

Figure 2.1

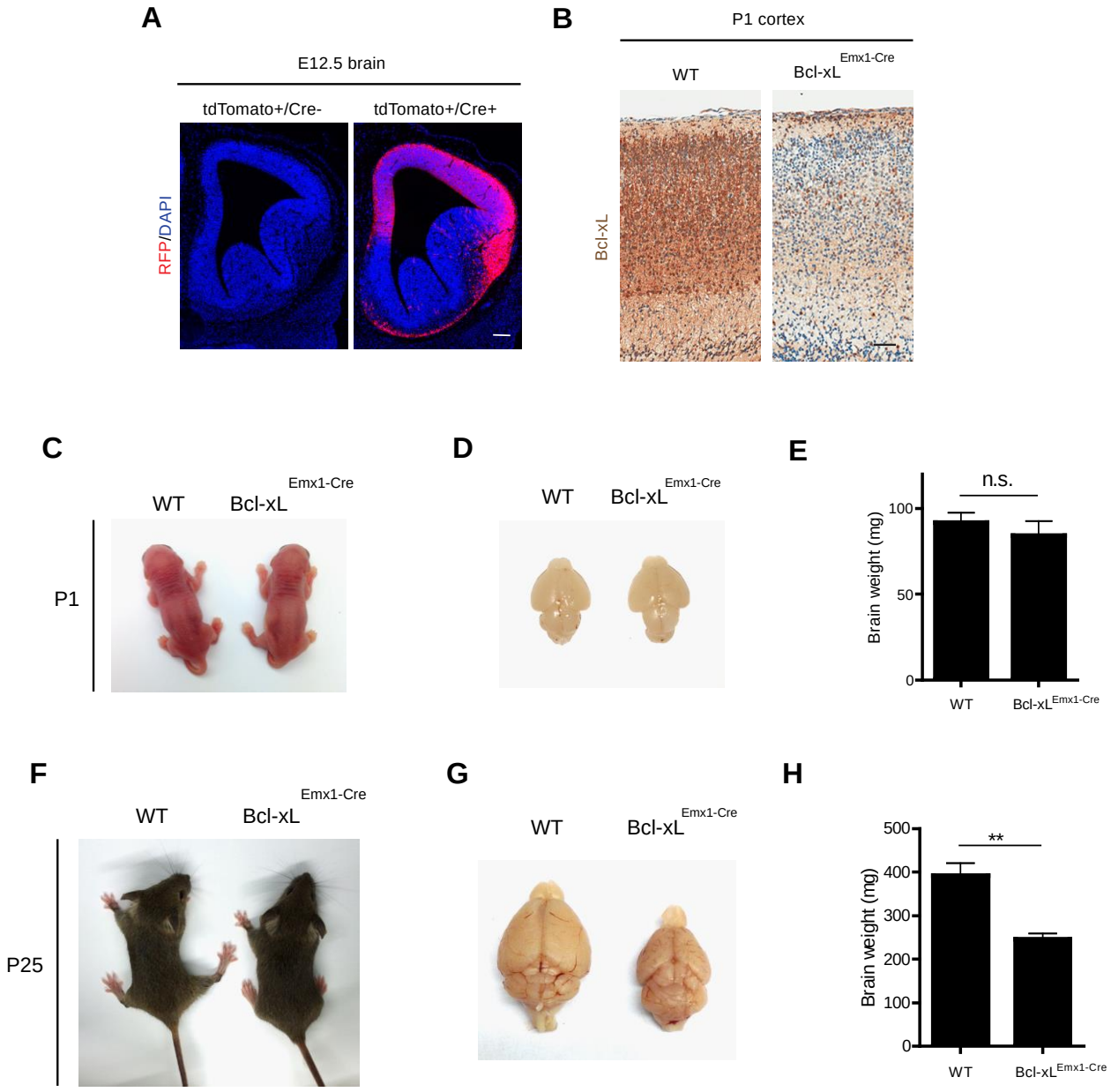
A
E12.5 brain
tdTomato+/Cre-
tdTomato+/Cre+
RFP/DAPI
B
P1 cortex
WT
Bcl-xL Emx1-Cre
Bcl-xL
C
WT
Bcl-xL Emx1-Cre
P1
D
WT
Bcl-xL Emx1-Cre
E
n.s.
Brain weight (mg)
100
50
0
WT
Bcl-xL Emx1-Cre
F
WT
Bcl-xL Emx1-Cre
P25
G
WT
Bcl-xL Emx1-Cre
H
**
Brain weight (mg)
500
400
300
200
100
0
WT
Bcl-xL Emx1-Cre

Figure 2.2: Bcl-xL deletion in the brain causes a reduction in cortical thickness by P30.

(**A**) Wildtype and Bcl-xL$^{Emx1\text{-}Cre}$ mouse brains stained with DAPI at P1. Quantification of the cortical thickness is shown in (**B**). (**C**) Wildtype and Bcl-xL$^{Emx1\text{-}Cre}$ mouse brains stained with DAPI at P7. Quantification of the cortical thickness is shown in (**D**). (**E**) Wildtype and Bcl-xL$^{Emx1\text{-}Cre}$ mouse brains stained with DAPI at P30. Quantification of the cortical thickness is shown in (**F**). (**G**) Wildtype and Bcl-xL$^{Emx1\text{-}Cre}$ mouse brains stained with NeuN ((neuronal marker) at P30. CTX = cortex; HC = hippocampus. Scale bars in *A*, *C* and *E* denote 50 μm. Data shown are means ± s.e.m. for each group. ** P<0.01; *** P<0.0001; n.s. = not significant.

Figure 2.2

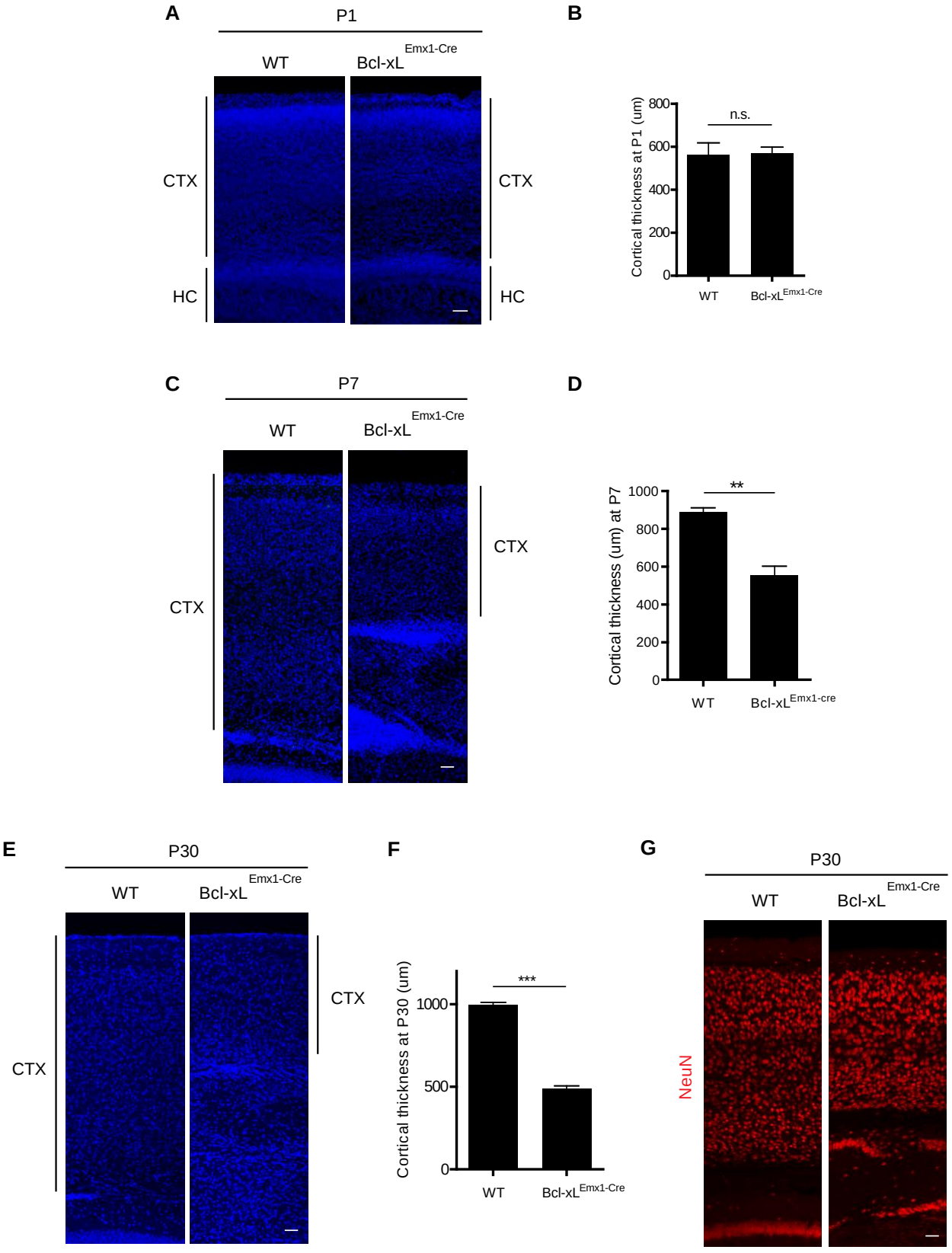
A
P1
WT
Bcl-xL
Emx1-Cre
CTX
HC
B
Cortical thickness at P1 (um)
n.s.
WT
Bcl-xL Emx1-Cre
C
P7
D
Cortical thickness (um) at P7
**
E
P30
F
Cortical thickness at P30 (um)
***
G
NeuN

Figure 2.3: Bcl-xL deletion leads to cell death in postmitotic neurons.

(**A**) Brains of wildtype and Bcl-xL$^{Emx1\text{-}Cre}$ mice at gestational day 16 (E16) stained with Bcl-xL. (**B**) Cortex of wildtype mice at E16 stained with a marker of proliferation, PCNA (red), and Bcl-xL (green). Scale bar denotes 50 μm. (**C**) Quantification of Bcl-xL in PCNA-positive and PCNA-negative cells shown in *B*. (**D**) Brains of wildtype and Bcl-xL$^{Emx1\text{-}Cre}$ mice at E16 co-stained with NeuN (green), cleaved caspase-3 (red), and DAPI. (**E**) Quantification of the number of cleaved caspase-3-positive cells in the NeuN-negative and NeuN-positive populations in the Bcl-xL$^{Emx1\text{-}Cre}$ cortex. Scale bar denotes 25 μm. (**F**) Cortices of wildtype and Bcl-xL$^{Emx1\text{-}Cre}$ mice at E16 stained with cleaved caspase-3, PCNA, and DAPI. The image on the right is a magnified image of the cortex (dotted white box). Scale bar denotes 300 μm. (**G**) Quantification of the number of cleaved caspase-3-positive and PCNA-positive cells shown in (G). (**H**) Quantification of the number of cleaved caspase-3-positive and PCNA-negative cells shown in (F). Data shown are means ± s.e.m. for each group. * $P<0.05$, ** $P<0.01$, *** $P<0.001$; n.s. = not significant.

Figure 2.3

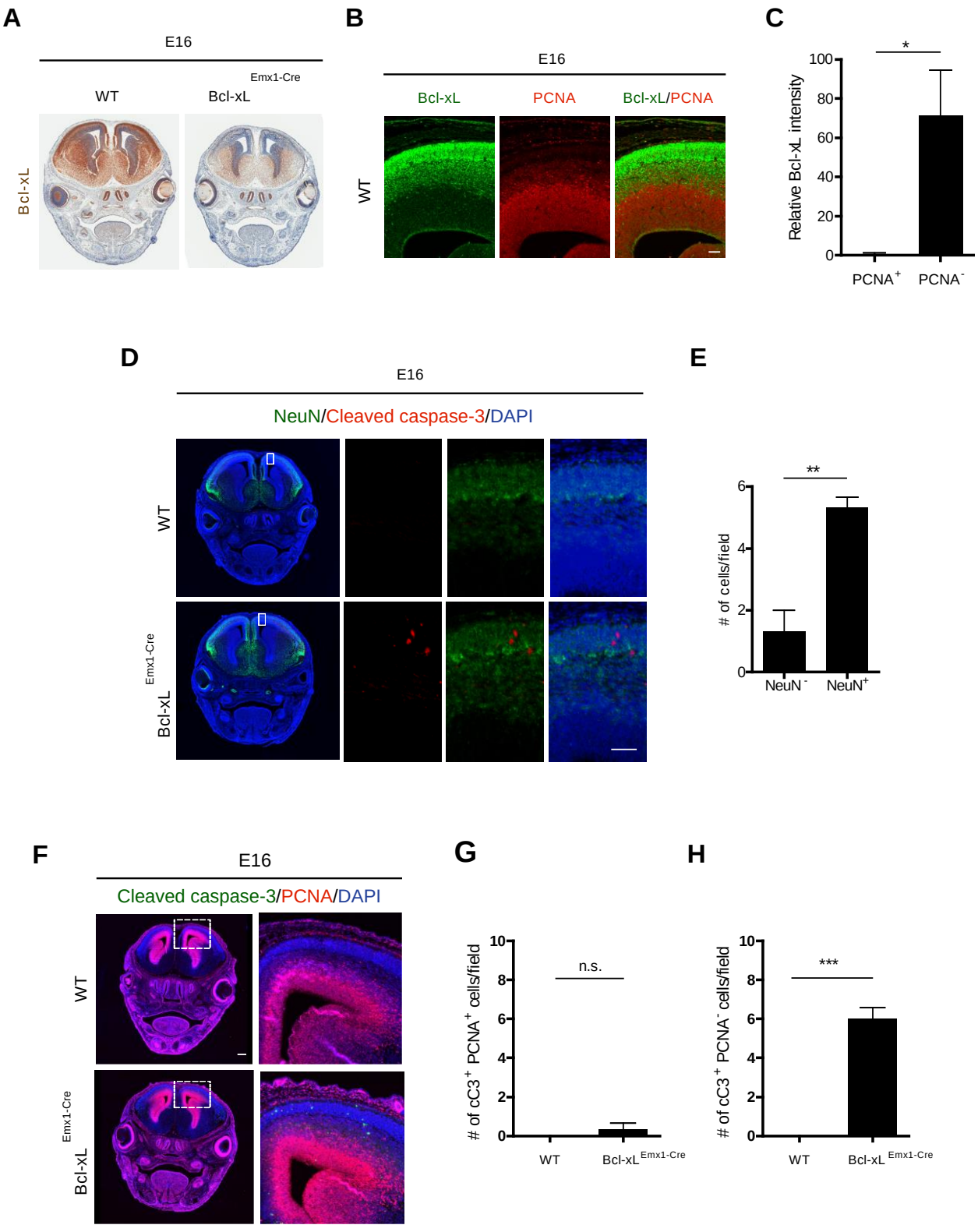
A
E16
Emx1-Cre
WT
Bcl-xL
Bcl-xL
B
E16
Bcl-xL
PCNA
Bcl-xL/PCNA
WT
C
*
100
80
60
40
20
0
Relative Bcl-xL intensity
PCNA+
PCNA-
D
E16
NeuN/Cleaved caspase-3/DAPI
WT
Emx1-Cre
Bcl-xL
E
**
6
4
2
0
# of cells/field
NeuN-
NeuN+
F
E16
Cleaved caspase-3/PCNA/DAPI
WT
Emx1-Cre
Bcl-xL
G
n.s.
10
8
6
4
2
0
# of cC3+ PCNA+ cells/field
WT
Bcl-xL Emx1-Cre
H
***
10
8
6
4
2
0
# of cC3+ PCNA- cells/field
WT
Bcl-xL Emx1-Cre

Figure 2.4: Bcl-xL is critical for the survival of specific populations of cortical neurons.

(**A**) Cortices of P1 wildtype and Bcl-xL$^{Emx1\text{-}Cre}$ mice stained with cleaved caspase-3, a marker of apoptosis. (**B**) Quantification of the number of cleaved caspase-3-positive cells shown in (A). (**C**) Presence of pyknotic nuclei in the cortex of Bcl-xL$^{Emx1\text{-}Cre}$ mice. Inset, magnified image of the white box in the cortex. White arrows denote pyknotic nuclei. (**D**) Quantification of the number of pyknotic nuclei shown in (C). (**E**) Hippocampus of P1 wildtype and Bcl-xL$^{Emx1\text{-}Cre}$ mice stained with cleaved caspase-3. (**F**) Hippocampus of P1 wildtype and Bcl-xL$^{Emx1\text{-}Cre}$ mice stained with DAPI reveal the presence of pyknotic nuclei. Inset, magnified image of the white box in the hippocampus. White arrows denote pyknotic nuclei. Cortices of P30 wildtype and Bcl-xL$^{Emx1\text{-}Cre}$ mice co-stained with DAPI and (**G**) Cux1; (**I**), Brn1; and (**K**), Tbr1. Quantification of the number of (**H**) Cux1-positive cells; (**J**), Brn1-positive cells; and (**L**), Tbr1-positive cells. Data shown are means ± s.e.m. for each group. CTX = cortex; HC = hippocampus. The wildtype image in (G) shows the cortex and the top region of the hippocampus in the wildtype and Bcl-xL$^{Emx1\text{-}Cre}$ mice. Scale bars in (A), (C), (E), (F), (G), (I), *and* (K) denote 50 μm. * $P<0.05$ and ** $P<0.01$.

Figure 2.4

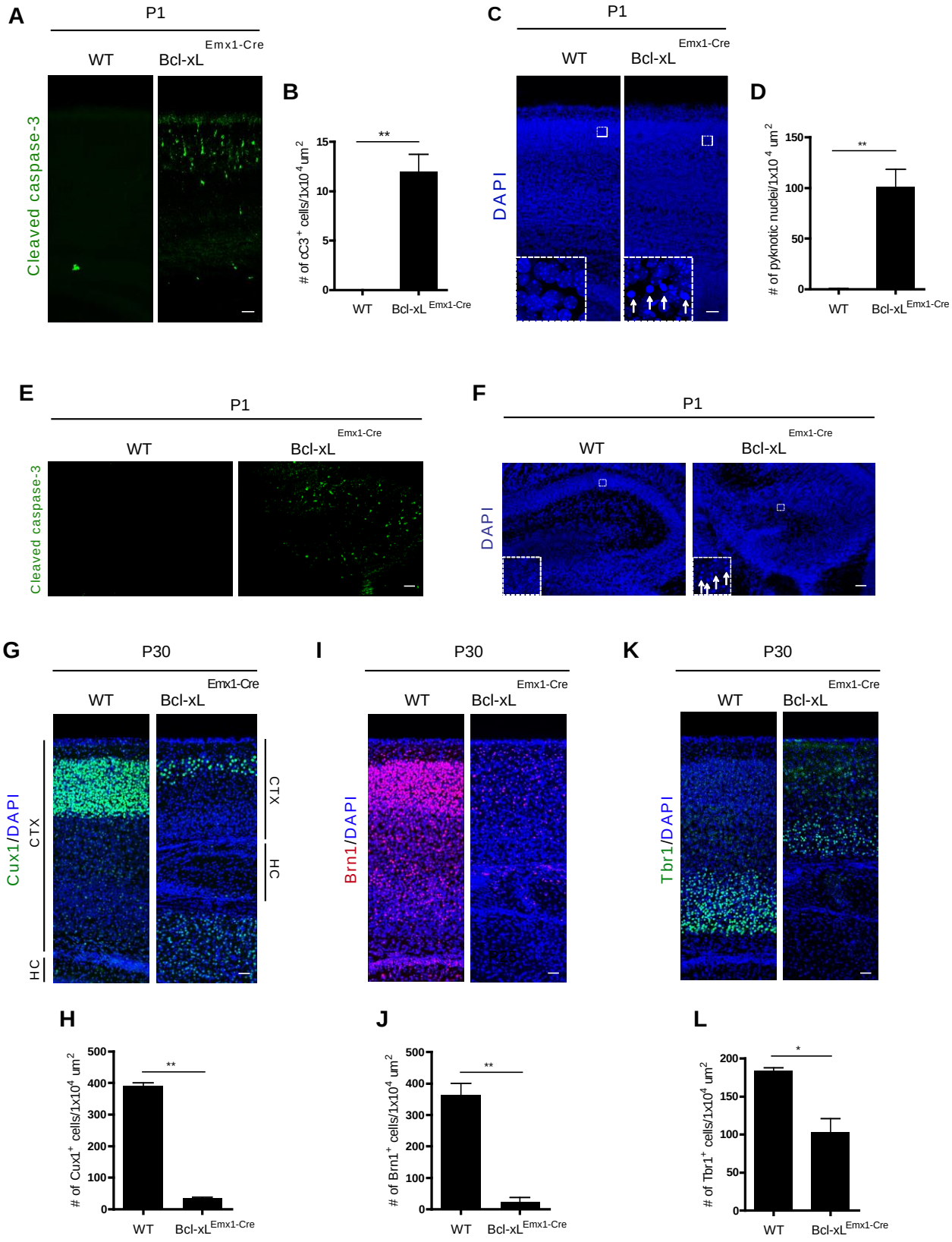
A
P1
Emx1-Cre
WT
Bcl-xL
Cleaved caspase-3
B
**
# of cC3+ cells/1x10^4 um^2
WT
Bcl-xL Emx1-Cre
C
P1
Emx1-Cre
WT
Bcl-xL
DAPI
D
**
# of pyknotic nuclei/1x10^4 um^2
WT
Bcl-xL Emx1-Cre
E
P1
Emx1-Cre
WT
Bcl-xL
Cleaved caspase-3
F
P1
Emx1-Cre
WT
Bcl-xL
DAPI
G
P30
Emx1-Cre
WT
Bcl-xL
Cux1/DAPI
CTX
HC
I
P30
Emx1-Cre
WT
Bcl-xL
Brn1/DAPI
K
P30
Emx1-Cre
WT
Bcl-xL
Tbr1/DAPI
H
**
# of Cux1+ cells/1x10^4 um^2
WT
Bcl-xL Emx1-Cre
J
**
# of Brn1+ cells/1x10^4 um^2
WT
Bcl-xL Emx1-Cre
L
*
# of Tbr1+ cells/1x10^4 um^2
WT
Bcl-xL Emx1-Cre

Figure 2.5: Loss of Bcl-xL leads to a smaller but functional retinotopic map in the visual cortex.

(**A**) Microcephaly in Bcl-xL$^{Emx1\text{-}Cre}$ mice. Tilted rectangles depict the *in vivo* imaging field-of-view. V1 = primary visual cortex, SC = superior colliculus. (**B**) Retinotopic maps acquired with *in vivo* imaging of visually-evoked responses to horizontal (left) and vertical (right) bars in wildtype and Bcl-xL$^{Emx1\text{-}Cre}$ mice. (**C**, **D**) Quantification of the entire V1 area and the area within it that represents a 50-degree space in visual field in wildtype and Bcl-xL$^{Emx1\text{-}Cre}$ mice. Data shown are means ± s.e.m. for each group. * P<0.05, ** P<0.01, *** P<0.001.

Figure 2.5

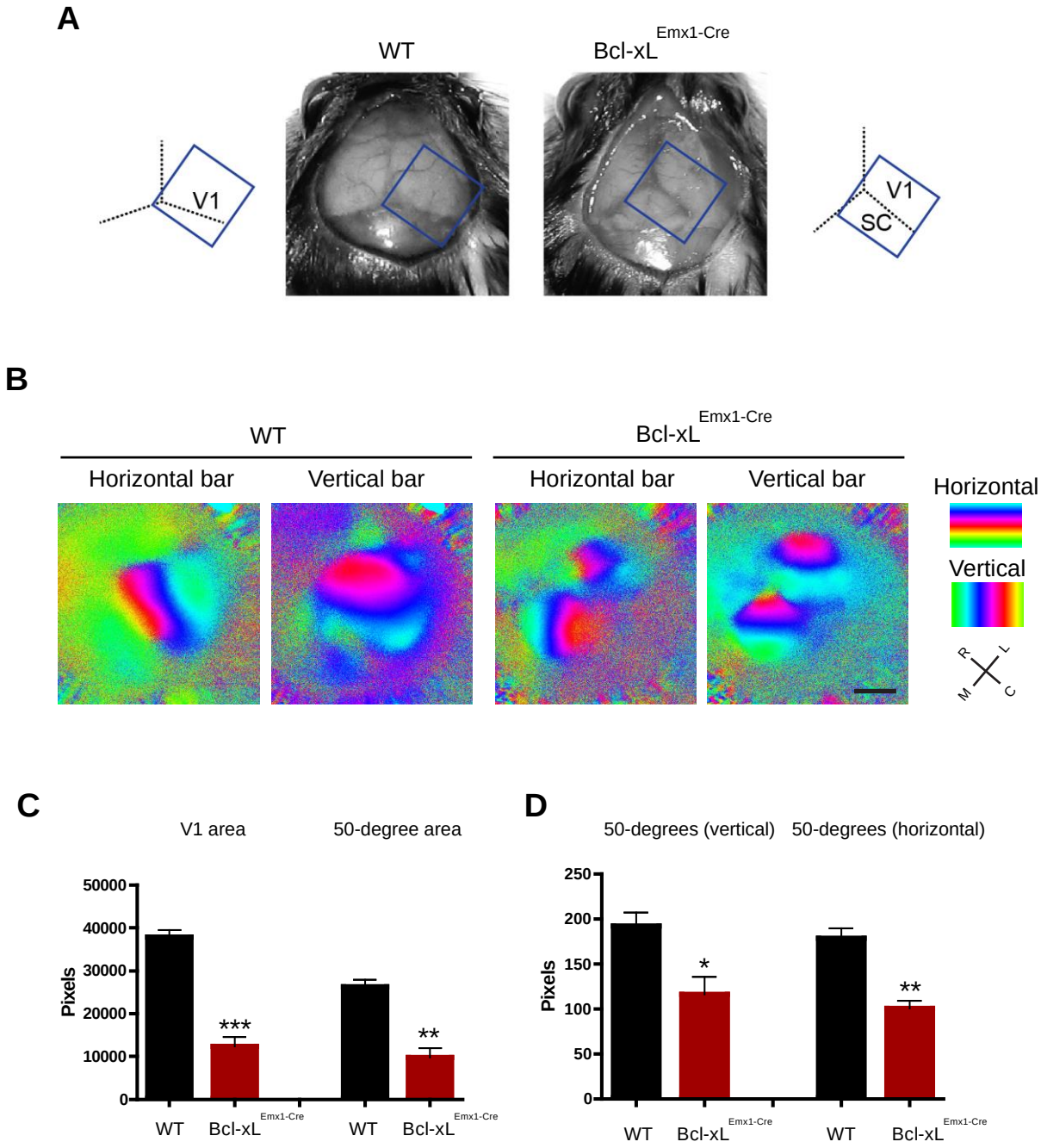
A
WT
Bcl-xL Emx1-Cre
V1
V1
SC
B
WT
Bcl-xL Emx1-Cre
Horizontal bar
Vertical bar
Horizontal bar
Vertical bar
Horizontal
Vertical
R
L
M
C
C
V1 area
50-degree area
Pixels
50000
40000
30000
20000
10000
0
***
**
WT
Bcl-xL Emx1-Cre
WT
Bcl-xL Emx1-Cre
D
50-degrees (vertical)
50-degrees (horizontal)
Pixels
250
200
150
100
50
0
*
**
WT
Bcl-xL Emx1-Cre
WT
Bcl-xL Emx1-Cre

Figure 2.6: The apoptotic cell death and microcephaly in Bcl-xL$^{Emx1\text{-}Cre}$ mice can be rescued with co-deletion of Bax and Bak.

Cortices of P1 wildtype and Bcl-xL$^{loxP/loxP}$ Bax$^{loxP/loxP}$ Emx1-Cre Bak$^{-/-}$ triple knockout (BBB TKO) mice stained with (**A**) Bcl-xL; (**B**) Bax; and (**C**) Bak. Scale bars in (A), (B) and (C) denote 50 μm. (**D**) Cortices from P1 wildtype, Bcl-xL$^{Emx1\text{-}Cre}$ (Bcl-xL KO), and BBB TKO mice stained with cleaved caspase-3 and DAPI. Quantification of the number of cleaved caspase-3-positive cells is shown in (**E**). (**F**) Wildtype, Bcl-xL KO, and BBB TKO brains co-stained with NeuN and DAPI. (**G**) Cortical thickness in P30 wildtype, Bcl-xL KO, and BBB TKO brains. Quantification of the number of NeuN-positive cells is shown in (**H**). (**I**) Cortices from P30 wildtype, Bcl-xL KO, and BBB TKO mice stained with Cux1 and DAPI. (**J**) Quantification of the number of Cux1-positive cells is shown. Data shown are means ± s.e.m. for each group. Scale bars in (D), (F) and (I) denote 50 μm. ** $P<0.01$, *** $P<0.001$.

Figure 2.6

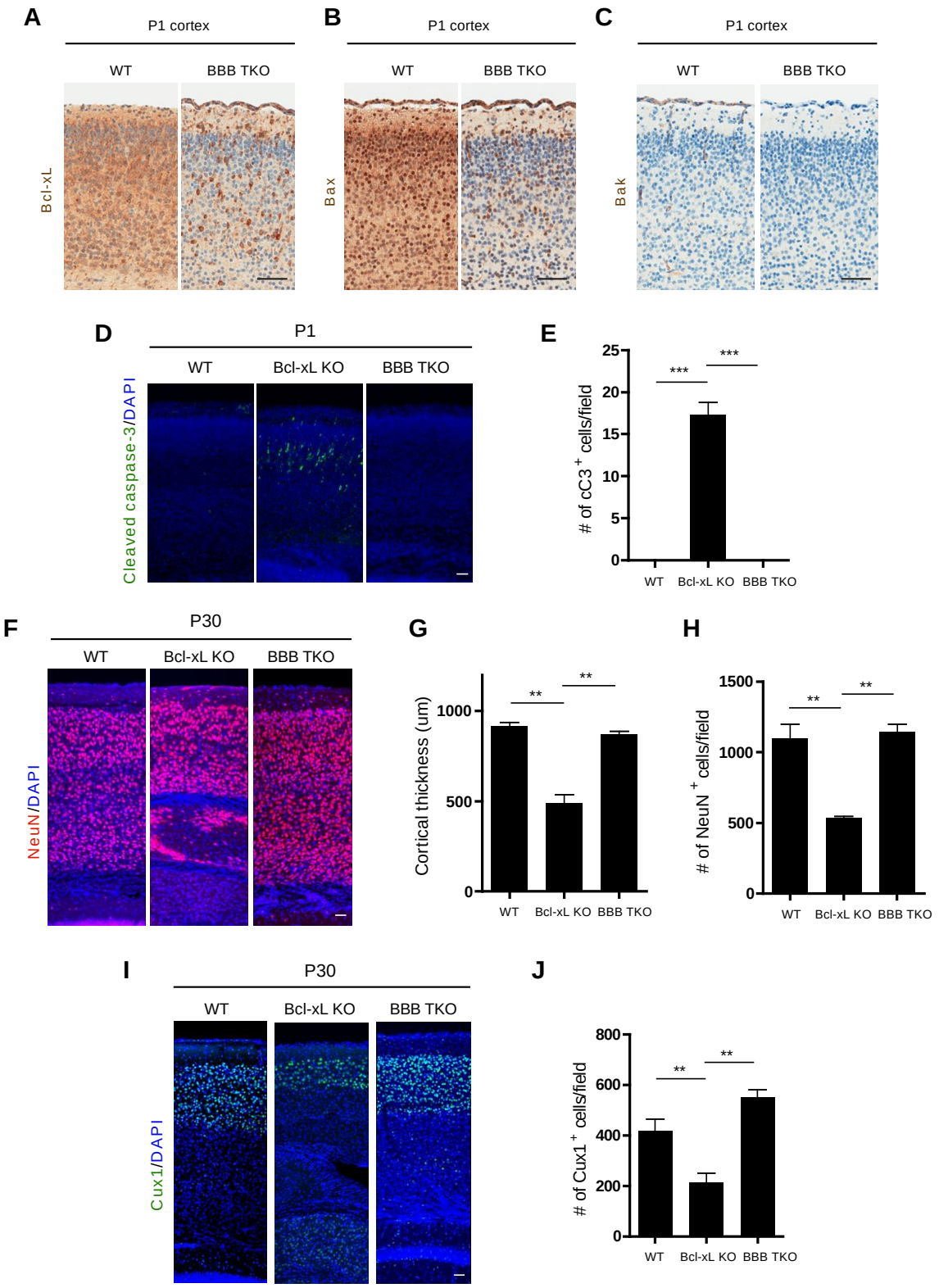
A
P1 cortex
WT
BBB TKO
Bcl-xL
B
P1 cortex
WT
BBB TKO
Bax
C
P1 cortex
WT
BBB TKO
Bak
D
P1
WT
Bcl-xL KO
BBB TKO
Cleaved caspase-3/DAPI
E
# of cC3+ cells/field
25
20
15
10
5
0
***
***
WT
Bcl-xL KO
BBB TKO
F
P30
WT
Bcl-xL KO
BBB TKO
NeuN/DAPI
G
Cortical thickness (um)
1000
500
0
**
**
WT
Bcl-xL KO
BBB TKO
H
# of NeuN+ cells/field
1500
1000
500
0
**
**
WT
Bcl-xL KO
BBB TKO
I
P30
WT
Bcl-xL KO
BBB TKO
Cux1/DAPI
J
# of Cux1+ cells/field
800
600
400
200
0
**
**
WT
Bcl-xL KO
BBB TKO

Figure 2.7: Loss of Bcl-xL selectively in postmitotic neurons results in reduced body and brain weights and cell death in the upper regions of the cortex.

(**A**) Photos of wildtype and Bcl-xL$^{Nex\text{-}Cre}$ mice at P30. (**B**) Body weights of wildtype and Bcl-xL$^{Nex\text{-}Cre}$ male mice at P30. (**C**) Images of brains isolated from wildtype and Bcl-xL$^{Nex\text{-}Cre}$ mice at P30. (**D**) Brain weights of wildtype and Bcl-xL$^{Nex\text{-}Cre}$ male mice at P30. (**E**) Cortices of P1 wildtype and Bcl-xL$^{Nex\text{-}Cre}$ mice stained with cleaved caspase-3. (**F**) Quantification of the number of cleaved caspase-3-positive cells shown in (E). Scale bar in (E) denotes 25 μm. * $P<0.05$; *** $P<0.0001$.

Figure 2.7

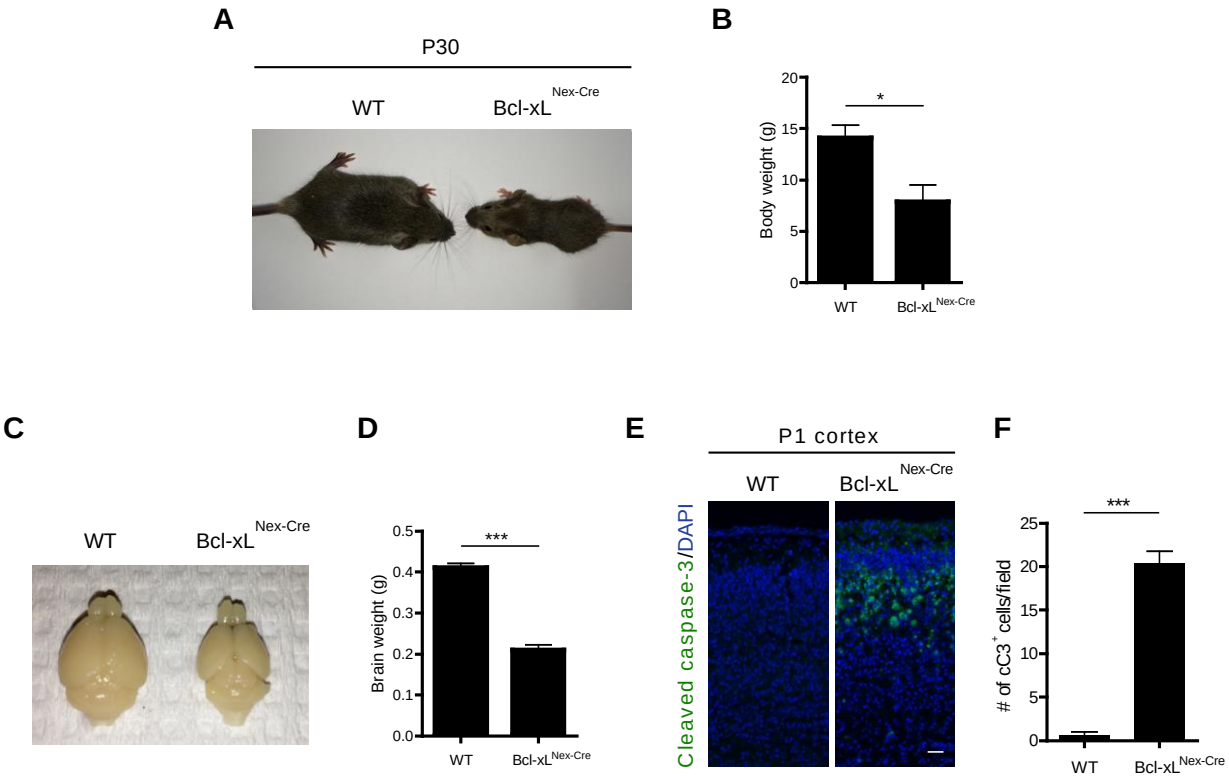
A
P30
WT
Bcl-xL Nex-Cre
B
Body weight (g)
20
15
10
5
0
*
WT
Bcl-xL Nex-Cre
C
WT
Bcl-xL Nex-Cre
D
Brain weight (g)
0.5
0.4
0.3
0.2
0.1
0.0
***
WT
Bcl-xL Nex-Cre
E
P1 cortex
WT
Bcl-xL Nex-Cre
Cleaved caspase-3/DAPI
F
# of cC3+ cells/field
25
20
15
10
5
0
***
WT
Bcl-xL Nex-Cre

Figure 2.8: Bcl-xL$^{Nex\text{-}Cre}$ mice display self-inflicted skin lesions.

(**A**) Bcl-xL$^{Nex\text{-}Cre}$ mice spend significantly greater periods of time undergoing hindlimb clasping. Analyses were conducted on P30 wildtype and Bcl-xL$^{Nex\text{-}Cre}$ mice. (**B**) Quantification of the number of seconds P30 wildtype and Bcl-xL$^{Nex\text{-}Cre}$ mice display hindlimb clasping over a three-minute period. Hindlimb clasping was examined in n = 3 wildtype and n = 3 Bcl-xL$^{Nex\text{-}Cre}$ mice. (**C**) Severe skin lesions observed in the hindlimb of Bcl-xL$^{Nex\text{-}Cre}$ mice. Lesions began to appear at approximately one month of age. (**D**) Percentage of time spent grooming in wildtype and Bcl-xL$^{Nex\text{-}Cre}$ mice. (**E**) Withdrawal latency (seconds) in wildtype and Bcl-xL$^{Nex\text{-}Cre}$ mice on the Hargreaves apparatus. Data shown are means ± s.e.m. for each group. * $P<0.05$; ** $P<0.01$; *** $P<0.0001$; n.s. = not significant.

Figure 2.8

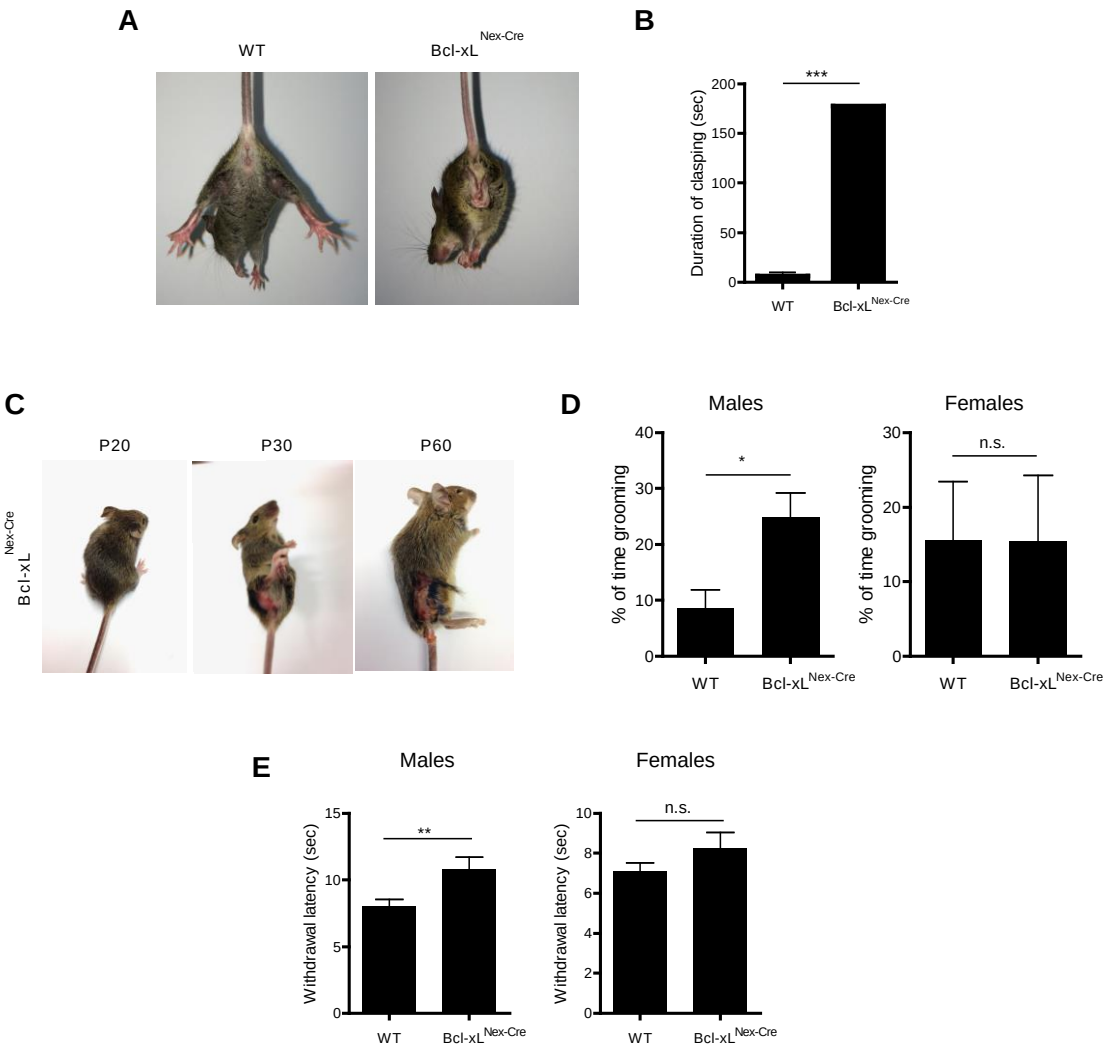
A
WT
Bcl-xL Nex-Cre
B
Duration of clasping (sec)
200
150
100
50
0
***
WT
Bcl-xL Nex-Cre
C
P20
P30
P60
Bcl-xL Nex-Cre
D
Males
Females
% of time grooming
40
30
20
10
0
*
n.s.
WT
Bcl-xL Nex-Cre
E
Males
Females
Withdrawal latency (sec)
15
10
5
0
**
10
8
6
4
2
0
n.s.
WT
Bcl-xL Nex-Cre

Figure 2.9: Bcl-xL$^{Nex\text{-}Cre}$ mice exhibit numerous neurobehavioral deficits.

(**A**) 60-minute open field analyses reveal that both male and female Bcl-xL$^{Nex\text{-}Cre}$ mice travel significantly greater distances compared to wildtype animals. Both male and female Bcl-xL$^{Nex\text{-}Cre}$ mice exhibit similar number of rears (**B**) and spend similar amounts of time in the center of the open field as compared to wildtype mice (**C**). (**D**) Percentage of time spent in the open arms of the elevated plus maze by wildtype and Bcl-xL$^{Nex\text{-}Cre}$ mice. (**E**) Percentage of entries into the open arms of the elevated plus maze by wildtype and Bcl-xL$^{Nex\text{-}Cre}$ mice. (**F**) Total number of entries into the open arms of the elevated plus maze by wildtype and Bcl-xL$^{Nex\text{-}Cre}$ mice. ***G***, Latency to fall from an accelerating rotarod. Latency (**H**) and speed (**I**) in reaching the visible platform in the Morris water maze task in wildtype and Bcl-xL$^{Nex\text{-}Cre}$ mice. Data shown are means ± s.e.m. for each group. * $P<0.05$.

Figure 2.9

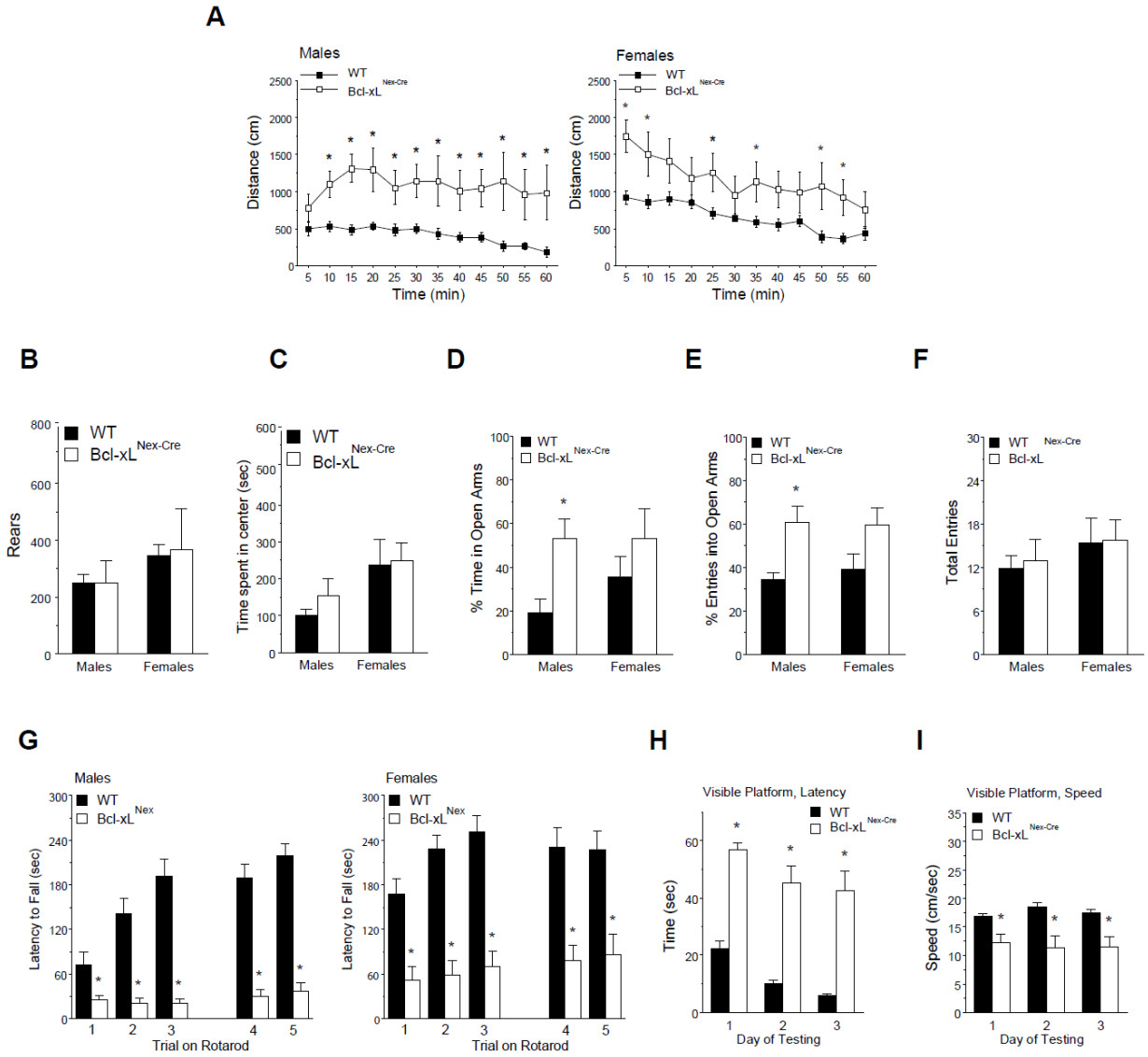
A
Males
Females
WT
Bcl-xL Nex-Cre
Distance (cm)
Time (min)
B
Rears
C
Time spent in center (sec)
D
% Time in Open Arms
E
% Entries into Open Arms
F
Total Entries
Bcl-xL
Males
Females
G
Latency to Fall (sec)
Trial on Rotarod
H
Visible Platform, Latency
Time (sec)
Day of Testing
I
Visible Platform, Speed
Speed (cm/sec)

CHAPTER THREE: MICRORNA-29 IS AN ESSENTIAL REGULATOR OF DNA METHYLATION DURING BRAIN MATURATION

3.1 Overview

While early brain development and neurodegeneration have been examined extensively, the events that govern brain maturation are less understood. During postnatal development, the number of neurons remains relatively constant (Bandeira et al. 2009; Fu et al. 2013), but widespread changes in synaptic connectivity are evident (Stiles and Jernigan 2010). Importantly, perturbations of synaptic development or maturation during this period can have severe neurobehavioral consequences as seen in autism spectrum disorders (ASD), obsessive-compulsive disorders and schizophrenia (Blakemore 2008). Recent studies have led to the unexpected discovery that marked increases in noncanonical (non-CG) DNA methylation occur during brain maturation (Xie et al. 2012; Lister et al. 2013a; Guo et al. 2014; Chen et al. 2015; Gabel et al. 2015; Mo et al. 2015). This *de novo* CH methylation (where H= A, C, T), which occurs 1-4 weeks postnatally in mice and 1-15 years in humans (Lister et al. 2013a), is important as binding of MeCP2 to CH-methylated DNA mediates the repression of many neuronal genes (Chen et al. 2015; Gabel et al. 2015); consequently, loss or duplication of MeCP2 leads to intellectual and behavioral disabilities (Lombardi et al. 2015). Thus, the levels of CH methylation need to be strictly balanced in the maturing brain. The critical period of CH methylation appears to be mediated by Dnmt3a, the DNA methyltransferase that catalyzes CH methylation (Guo et al.

2014; Gabel et al. 2015). During brain maturation, Dnmt3a levels are elevated and then sharply decline (Feng et al. 2005; Lister et al. 2013a). Here we identify miR-29 as an essential regulator of Dnmt3a and CH methylation during brain maturation. Mice deficient in miR-29 exhibit enhanced levels of Dnmt3a, global CH hypermethylation, and an increased repression of neuronal genes in the mature brain. As a consequence, the miR-29-deficient mice appear normal at birth, but subsequently displayed excitatory-inhibitory (E/I) imbalance and an increased susceptibility to seizures. These mice also exhibit severe neurological deficits including hyperactivity and compulsive overgrooming as well as early lethality. Together, these results identify an essential function of miR-29 in defining the critical period of DNA methylation during brain maturation, the absence of which results in multiple neurobehavioral deficits.

3.3 Results

Several recent studies have identified a critical period during postnatal mammalian brain development during which there is a dramatic increase in the methylation of the neuronal genome at CH sequences (Xie et al. 2012; Lister et al. 2013a; Guo et al. 2014; Chen et al. 2015; Gabel et al. 2015; Mo et al. 2015). These methylCH (mCH) marks have been hypothesized to control the generation of neuronal diversity by regulating gene transcription across the genome. In the mouse, mCH is catalyzed by the enzyme Dnmt3a, and the deposition of mCH marks peak during the first few weeks of life (Guo et al. 2014; Gabel et al. 2015). The time course of mCH deposition in postnatal neurons is tightly controlled such that the level of Dnmt3a begins to decrease significantly several weeks after birth (Feng et al. 2005; Lister et al. 2013b). This decrease in Dnmt3a results in a cessation in the deposition of additional mCH marks, and may be important for proper brain maturation as mutations in Dnmt3a, as well as the methyl binding protein MeCP2 that binds to mCH, are associated with devastating disorders of postnatal brain development (Gabel et al. 2015; Lombardi et al. 2015). However, the mechanisms that regulate the activation and subsequent repression of Dnmt3a expression, and the proper deposition of mCH marks during postnatal brain development have not yet been identified.

MicroRNAs (miRNAs), which have the potential to post-transcriptionally silence hundreds of genes, are known to modulate neurodevelopment (Petri et al. 2014) and neurodegeneration (Abe and Bonini 2013). To determine if Dnmt3a expression during brain maturation and, in particular, the decrease in Dnmt3a expression that occurs at the closure of the critical period of CH methylation, is mediated by a miRNA(s) we examined the 3' untranslated (UTR) region of the mouse Dnmt3a gene for consensus binding sites for

miRNAs (Fig. 3.1). To focus on the specific miRNA(s) that could be important for inhibiting Dnmt3a expression in the mature brain, we conducted an unbiased small RNA sequencing analysis to identify miRNAs that are induced during brain maturation. For this analysis we employed the mouse cerebellum, as the timeline for cerebellar postnatal development is well defined. Cerebellar granule neuron precursors (CGNPs) undergo rapid proliferation and complete their differentiation into cerebellar granule neurons (CGNs) by postnatal day 18 (P18) (Hatten and Roussel 2011) (Fig. 3.2). Thus, we probed for miRNAs that are differentially expressed between young (P18) and adult (P250) cerebella. The most upregulated miRNAs during this period all belonged to the miRNA-29 (miR-29) family, which were strikingly increased approximately 80 fold (Fig. 3.3A). The miR-29 family consists of three members—miR-29a, miR-29b and miR-29c—that are expressed from two genomic loci: miR-29ab1 and miR-29b2c (Kriegel et al. 2012). Quantitative PCR analysis for miR-29b, which is expressed from both of these loci, confirmed that the marked increase in miR-29 was most evident during cerebellar maturation (Fig. 3.3B). This increase in miR-29b expression is even more evident in the cortex where the expression of miR-29 is very low during the embryonic period but increases significantly postnatally (Li et al. 2014a) during the period of brain maturity (Fig. 3.3C). The observation that miR-29 expression increases significantly in the postnatal period was of particular interest given that Dnmt3a has multiple evolutionarily conserved binding sites in its 3' UTR (Fig. 3.1) and has previously been shown to be regulated by miR-29 (Fabbri et al. 2007; Pandi et al. 2013). Consistent with this idea, the marked increase in miR-29 beyond P20 is coincident with the sharp decrease in Dnmt3a expression that occurs during this period (Feng et al. 2005; Lister et al. 2013a).

To determine if miR-29 regulates Dmnt3a expression and function during brain maturation *in vivo*, we generated mice that were floxed for both alleles of miR-29. Specifically, miR-29a/b1$^{f/f}$ and miR-29b2/c$^{f/f}$ mice were crossed together to generate mice where all three members of the miR-29 family could be deleted in the presence of a Cre driver. To globally delete miR-29, we crossed these mice with CMV-Cre-expressing mice (hereafter referred to as miR-29^{CMV}) (Fig. 3.4A, B). These mice were born at the expected Mendelian ratio, appeared normal at birth and were indistinguishable from wildtype littermate controls at postnatal day 10. However, starting at 10 days, the miR-29 knockouts begin to exhibit retarded growth, become ataxic, and die by 30 days of age (Fig. 3.3D-F). To specifically examine the importance of miR-29 in the brain, we used the Nestin-Cre mice to conditionally delete miR-29 in the brain (hereafter referred to as miR-29^{Nestin}) (Fig. 3.4C-E). The miR-29^{Nestin} mice were also born normally and exhibited the same growth retardation and ataxia as miR-29^{CMV} mice, with most mice dying by 40 days (Fig. 3.3G-I). The lethality seen with miR-29 deletion was dose-dependent as mice with partial deletion of miR-29 survived longer (Fig. 3.5). Ataxia and motor dysfunction have previously been observed when only a subset of the miR-29 family was targeted, either with miR-29a- and miR-29b-specific locked nucleic acids (LNAs) or deletion of only the miR-29ab1 cluster (Roshan et al. 2014; Papadopoulou et al. 2015). Moreover, consistent with the finding that miR-29 is not expressed during the stages of early brain development, miR-29^{Nestin} mice did not exhibit any gross developmental brain abnormalities (Fig. 3.6, 3.7). We also found no defects in intrinsic cell parameters such as resting membrane potential or the ability to generate action potentials in miR-29-deficient neurons (Fig. 3.8). Thus, fundamental aspects of early brain development were not affected by the absence of miR-29. The fact that the brain-

specific deletion of miR-29 recapitulates the ataxia, growth retardation and lethality seen with global deletion of miR-29 suggests that the essential function of miR-29 is in the maturing brain.

To determine if miR-29 is required for the downregulation of Dnmt3a expression in the maturing brain, we examined Dnmt3a levels in miR-29-deficient brains. Dnmt3a, both at the transcript and protein levels, were markedly elevated in miR-29^{Nestin} mice at P40 (Fig. 3.9A, B, 3.10). A potential consequence of sustained Dnmt3a levels in the brains of miR-29-deficient animals is persistent DNA methylation. To investigate whether DNA is hypermethylated in the brains of miR-29^{Nestin} mice, we conducted whole-genome bisulfite sequencing analysis on P40 wildtype and miR-29^{Nestin} mice. Strikingly, loss of miR-29 in the brain led to significantly greater levels of CH methylation during brain maturation (Fig. 3.9C). CH methylation in the mature brain is predominantly known to occur at CA sites (Xie et al. 2012; Lister et al. 2013a; Guo et al. 2014; Kinde et al. 2015), a pattern consistent with the finding in miR-29-deficient brains. We did not detect any increases in CG methylation in miR-29-deficient brains (Fig. 3.11). Importantly, the increase in CH methylation in the miR-29-deficient mice occurred at sites normally methylated in the maturing brain (Fig. 3.9D).

CH methylation, which mediates gene repression in neurons, is important for fine tuning neuronal gene expression during brain maturation. To gain insight into the specific pathways affected in the miR-29-deficient mice, we conducted a gene array analysis of cortical samples from wildtype and miR-29^{Nestin} mice and found 444 annotated genes to be differentially expressed (226 upregulated genes, 218 downregulated genes, FDR < 0.1) (Fig. 3.9E). As expected, an unbiased query identified miR-29 as the miRNA predicted to target

the largest number of upregulated genes in this gene set (*e.g.* of the 226 upregulated genes, 31 genes are predicted direct targets of miR-29, including Dnmt3a and the Wnt/β-catenin pathway (Shin et al. 2014b)) (Fig. 3.9F, Fig. 3.10). Importantly, consistent with our observation that miR-29-deficient brains have hypermethylated DNA, a large number of key neuronal genes associated with defects in synaptic neurotransmission, OCD, autism-spectrum disorders, and susceptibility to seizures were markedly downregulated in miR-29-deficient brains (Fig. 3.9G). These include multiple GABA receptor subunits, Shank3 and Cntnap2. Also downregulated was RPS6KA3 (RSK2), mutations of which are associated with Coffin-Lowry syndrome, in which patients exhibit OCD and autism-related deficits (Trivier et al. 1996). Further analysis revealed that these repressed neuronal genes were indeed hypermethylated in the miR-29 deficient brains (Fig. 3.9H).

Many of the genes we found to be hypermethylated in the miR-29-deficient brain are also linked to diseases associated with excitatory-inhibitory (E/I) imbalance (Rubenstein and Merzenich 2003; Penagarikano et al. 2011). Thus, we examined whether miR-29 deficiency induced an E/I imbalance in the brain. Indeed, we found that the number of inhibitory interneurons (GABA-, NPY-, calretinin-, and calbindin-positive cells) was globally decreased throughout the cortex in miR-29^{Nestin} mice (Fig. 3.12A-D). Interestingly, miR-29^{Nestin} mice also displayed an increase in the number of Cux1-positive excitatory projection neurons throughout layers II/III of the cortex as compared to brains from wildtype mice (Fig. 3.12E). Thus, miR-29 expression is important for maintaining the excitatory/inhibitory balance in the cortex which, with miR-29 deficiency, shifts the brain towards an excitatory phenotype.

To probe the consequences of this increased excitatory phenotype, we examined whether the miR-29-deficient mice were more susceptible to seizures. Kainic acid, a structural analog of glutamate, is known to induce an epileptiform state in the brain by disrupting the E/I balance of neurons. All miR-29^{Nestin} mice displayed Racine seizure scale characteristics and underwent tonic-clonic seizures within 15 minutes of kainic acid injection (30mg/kg, intraperitoneal), while no wildtype animals exhibited tonic-clonic seizures during this time frame (Fig. 3.12F, G). Importantly, following tonic-clonic seizures, all miR-29^{Nestin} mice, but none of the wildtype mice, died within 20 minutes of kainic acid injection (Fig. 3.12G).

Lastly, to examine whether the disruption of miR-29 expression, the prolonged expression of Dnmt3a, and/or the enhanced methylation of CH sequences during brain maturation might lead to behavioral abnormalities, we conducted a variety of assessments in miR-29-deficient mice. Upon tail suspension, while wildtype mice displayed flailing hindlimb movements, miR-29^{Nestin} mice exhibited hindlimb clasping—a common sign of a neurological defect (Fig. 3.13A). In a two-minute test, miR-29^{Nestin} mice spent significantly longer periods of time clasping their hindlimbs compared to wildtype controls (Fig. 3.13B). Importantly, both miR-29^{Nestin} and miR-29^{CMV} mice demonstrated repetitive, excessive self-grooming behavior by 20 days of age, leading to facial hair loss and self-inflicted ulcerative skin lesions (Fig. 3.13C, 3.14A). These lesions were first observed 10-15 days after the onset of over-grooming in the miR-29 knockout mice and appeared primarily in the facial area, with a subset of mice grooming extensively around the eyes such that the orbital area became inflamed and bled. The self-inflicted lesions were paradoxically more severe in mice with partial deletion of miR-29 as these mice lived longer and, thus, sustained longer

periods of excessive grooming (Fig. 3.13D, 3.14B). The abnormal repetitive grooming was often exacerbated upon animal handling and after transferring the animals to a novel environment. In this context, miR-29^{Nestin} mice spent 40% of the time grooming, compared to 10% for wildtype controls (Fig. 3.13E).

Upon further assessing for hyperkinetic behavior, open field analyses revealed that deletion of miR-29 leads to overt hyperactivity with increases in the total distance traveled as well as greater numbers of fine movements, a measure of stereotypic behavior (Fig. 3.13F, G). miR-29^{Nestin} mice also spend significantly more time in the center region compared to wildtype controls, suggesting a loss of typical cautionary avoidance of a novel open area (Fig. 3.13H). Clinical studies have found that patients with autism spectrum disorders have impaired sensorimotor gating (Perry et al. 2007). Therefore, we evaluated wildtype and miR-29^{Nestin} mice for prepulse inhibition (PPI) in an acoustic startle test. In line with findings from the human studies, the miR-29^{Nestin} mice exhibited profound PPI deficits at almost every decibel level (Fig. 3.13I). Additionally, both grip strength and motor coordination were impaired in the miR-29^{Nestin} mice, the latter of which is consistent with the progressive ataxia observed in these mice (Fig. 3.13J, K). These findings show that loss of miR-29 leads to numerous neurobehavioral abnormalities including a striking hyperkinetic phenotype.

3.4 Discussion

While brain maturation is recognized as a period during which experience can fine tune neuronal activity, the epigenetic mechanisms by which this is achieved are just starting to become uncovered. A major clue has come from recent studies that found marked increases in Dnmt3a-dependent noncanonical (CH) DNA methylation in the maturing brain (Xie et al. 2012; Lister et al. 2013a; Guo et al. 2014; Chen et al. 2015; Gabel et al. 2015; Mo et al. 2015). Our results reveal that miR-29 regulates a critical period during which neuronal genes are epigenetically methylated in the maturing brain. In the absence of miR-29, Dnmt3a levels remain elevated and DNA is hypermethylated at CH sequences in the mature brain.

mCH (predominantly mCA) in DNA is recognized by MeCP2, a protein that functions to mediate transcriptional repression of neuronal genes. As a consequence, genes that are methylated at CH sites during brain maturation are preferentially reduced with MeCP2 duplication (Chen et al. 2015; Gabel et al. 2015), a phenomenon that we also observe with hypermethylated DNA in the miR-29-deficient brains. Interestingly, mice overexpressing MeCP2 develop multiple neurological abnormalities that are also strikingly similar to the defects observed in our miR-29-deficient mice, including hyperactivity, decreased anxiety, seizures, as well as premature death (Lombardi et al. 2015). The fact that both MeCP2-overexpressing mice and miR-29-deficient mice appear normal at birth but then progressively deteriorate illustrates the essential role that these molecules play selectively during brain maturation. The relevance of regulating CH methylation and fine-tuning neuronal gene expression in humans is underscored by the fact that both the loss or duplication of MeCP2 result in Rett syndrome or intellectual disability,

respectively(Lombardi et al. 2015). Likewise, dysregulation of miR-29 is associated with psychiatric disorders such as schizophrenia and bipolar disorder (Geaghan and Cairns 2015).

The complex phenotype of the miR-29-deficient mice could be attributed to a number of key neuronal genes that are epigenetically hypermethylated and repressed in the absence of miR-29. For example, loss of GABA receptor activity is associated with numerous neurodevelopmental disorders including autism, Angelman Syndrome, schizophrenia, Fragile X syndrome and epilepsy (Braat and Kooy 2015). In addition, Shank3 and Cntnap2, both of which are downregulated in the miR-29-deficient brain, are associated with autism (Peca et al. 2011; Penagarikano et al. 2011). Mice deficient in Shank3 exhibit repetitive grooming and OCD-like behavior (Peca et al. 2011), whereas mice deficient in Cntnap2 have ectopic Cux1-positive cells in the cortex and exhibit spontaneous epileptic seizures (Penagarikano et al. 2011). The fact that both of these phenotypes are manifested in the miR-29-deficient mice highlights the central importance of this single miRNA family in modulating these diverse pathways in the brain.

Together, these results not only identify an essential function of miR-29 as a key driver that regulates DNA methylation during brain maturation, but they also highlight why restricting DNA methylation during a critical window is important for sustaining a functional, mature brain.

3.4 Materials and Methods

Mice. The miR-29ab1 floxed allele was generated by homologous recombination and genomic targeting. A 827 bp gene segment containing miR-29a and miR-29b1 was cloned from genomic DNA of 129/SvEv mice. To amplify the long arm (LA) and short arm (SA), a BAC clone (RP24-248C11) was used as the PCR template. LA, SA and the miR-29ab1 gene segment were cloned into the PGKneoF2L2DTA backbone. The targeting vector was sequenced and confirmed to have no sequence mutation compared with the genomic DNA sequence listed in NCBI database. Targeting vectors were linearized by SacII (New England BioLabs) restriction enzyme digestion and were used for microinjection. ES cells from 129/SvEv-B6 mice were microinjected and positively selected in neomycin-containing medium, and successful genomic targeting was confirmed by PCR. The transgenic procedure was performed by the Duke Transgenic Mouse Facility. Animals were bred and maintained in the SPF facility managed by Duke University Division of Laboratory Animal Research. All animal procedures were approved by the Duke University Institutional Animal Care and Use Committee. Similar procedures were used to generate miR-29b2c conditional knockout mice as described above. In brief, a 817 bp gene fragment containing miR-29b2 and miR-29c was cloned from genomic DNA of 129/SvEv mice. LA and SA were PCR amplified from a BAC clone (RP23-465H4), and were cloned into the PGKneoF2L2DTA targeting vector.

The above mice were bred to generate mice floxed at both genomic loci (miR-29ab$^{loxP/loxP}$; miR-29 bc$^{loxP/loxP}$ mice). Conditional deletion of miR-29 was carried out by crossing the above mice with various Cre lines. Two different Cre lines—Nestin-Cre and CMV-Cre—were used to inactivate miR-29. Nestin-Cre and CMV-Cre were obtained from

Jackson Laboratories. Mice were maintained in a 12 hr light, 12 hr dark cycle (lights on at 7AM, lights off at 7 PM). All animal handling and protocols were carried out in accordance with established practices as described in the National Institutes of Health Guide for Care and Use of Laboratory Animals and as approved by the Animal Care and Use Committee of the University of North Carolina (UNC).

Small RNA sequencing and analysis. Libraries for Illumina sequencing were prepared using a modification of the TruSeq protocol. Briefly, 1 ug total RNA was ligated to 3 pmol of the 3' linker using T4 RNA ligase 2. RNA size fractions corresponding to 35- 70 nucleotides (insert plus linker) were gel isolated and ligated to 3 pmol 5' linker. Products were reverse transcribed, PCR amplified to mid-log phase, and size isolated. Libraries were barcoded using indexed 5' linkers. Libraries were sequenced on an Illumina HiSeq 2000 to ~20 million reads per barcode. Small RNA libraries are aligned to mm9 genome. microRNA annotations were downloaded from miRBase r18.

Bisulfite sequencing. Genomic DNA was extracted with the Blood and Tissue DNeasy kit and sonicated with a covaris to 200 bp. Unmethylated lambda DNA was spiked in (0.5% (w/w)). Whole genome bisulfite sequencing was performed similarly as described(Mo et al. 2015) except that the EZ DNA methylation-gold kit (Zymo) was used for bisulfite conversion. Libraries were sequenced on a Miseq by performing a 75x2 cycle run. BSmap(Xi and Li 2009) was used to map reads and only uniquely mapping reads were retained for analyses. Methylation levels were determined by calculating #C/(#C+#T).

Affymetrix gene array. RNA was extracted from cerebella and cortices using the Qiagen miRNeasy kit (catalog #217004) using the manufacturer's instructions. Total RNA (250 ng) was used to synthesize fragmented and labeled sense-strand cDNA and hybridize onto Affymetrix arrays. The Affymetrix GeneChip® WT PLUS Reagent Kit Manual was followed to prepare the samples. Briefly, the GeneChip® WT PLUS Reagent Kit (Affymetrix) was used to generate sense-strand cDNA from total RNA. Following synthesis of sense-strand cDNA, the cDNA was fragmented and labeled with the kit. Fragmented and labeled cDNA was used to prepare a hybridization cocktail with the Affymetrix GeneTitan Hybridization Wash and Stain Kit for WT Arrays. Hybridization, washing, staining and scanning of the Affymatrix peg plate arrays was carried out using the Affymetrin GeneTitan MC Instrument. GeneChip Command Console Software (AGCC) was used for GeneTitan Instrument control. Affymetrix Expression Console Software was used for basic data analysis and quality control.

miRHub analysis. First, we used the seed-based target prediction algorithm TargetScanS 5.2(Grimson et al. 2007) to determine for each miRNA the number of predicted conserved targets among the genes in our gene sets. Each predicted miRNA-gene interaction was assigned a score based on the strength of the seed match, the level of conservation of the target site, and the clustering of target sites within that gene's 3′-UTR. Additionally, the score for each gene was weighted according to the number of high-confidence protein-protein interactions reported in the STRING 9.0 database(Szklarczyk et al. 2011). Finally, for each miRNA, the final targeting score was calculated by summing the scores across all

genes and dividing by the number of genes. We repeated this procedure 10,000 times, with a new set of randomly selected mouse genes each time, in order to generate a background distribution of the predicted targeting scores for each miRNA (genes and corresponding 3′-UTR sequences were downloaded from http://www.targetscan.org). These score distributions were then used to calculate an empirical p-value of the targeting score for each miRNA in our gene set. Genes were selected at random from a pool with similar overall connectivity to the genes in our gene set, and to account for differences in the average 3′ UTR length between the genes of interest and the randomly selected genes in each simulation, the targeting score was normalized by 3′ UTR length.

Bioinformatics. 3' UTRs of significantly up- and down-regulated genes were analyzed for enrichment of predicted miRNA target sites as previously described(Baran-Gale et al. 2013).

Mouse Behavioral Analysis

Open field test**.** Exploratory activity in a novel environment was assessed by a 60-minute trial in an open field chamber (41 cm x 41 cm x 30 cm) crossed by a grid of photobeams (VersaMax system, AccuScan Instruments). Counts were taken of the number of photobeams broken during the trial in five-minute intervals, with separate measures for total distance traveled and fine movements (the repeated breaking of the same set of photobeams). Time spent in the center region of the open field was measured as an index of anxiety-like and risk-taking behavior.

Acoustic startle test**.** This procedure is based on the reflexive whole-body flinch, or startle response, that follows exposure to a sudden noise. Measures are taken of prepulse inhibition, which occurs when a weak prestimulus leads to a reduced startle in response to a subsequent louder noise. Subjects were tested with a San Diego Instruments SR-Lab system. Briefly, mice were placed in a small Plexiglas cylinder within a larger, sound-attenuating chamber. The cylinder was seated upon a piezoelectric transducer, which allowed vibrations to be quantified and displayed on a computer. The chamber included a ceiling light, fan, and a loudspeaker for the acoustic stimuli. Background sound levels (70 dB) and calibration of the acoustic stimuli were confirmed with a digital sound level meter (San Diego Instruments).

The test began with a 5-min habituation period, followed by 42 trials. There were 7 different types of trials: the no-stimulus trials, trials with the acoustic startle stimulus (40 msec; 120 dB) alone, and trials in which a prepulse stimulus (20 msec; either 74, 78, 82, 86, or 90 dB) occurred 100 ms before the onset of the startle stimulus. An overall analysis was performed for each subject's data for levels of prepulse inhibition at each prepulse sound level (calculated as 100 - [(response amplitude for prepulse stimulus and startle stimulus together / response amplitude for startle stimulus alone) x 100].

Wire-hang test for grip strength. At the start of the test, the mouse was placed on a large metal cage lid. The lid was gently shaken to induce the mouse to grip onto the metal grid. The cage top was then flipped over, and latency for the mouse to fall from the lid was recorded during the 60-sec test. Measures were also taken for coordination of movement

on the wire grid, using the scoring system adapted from a screen developed by William Wetsel, Ph.D., and Ramona Rodriguez, Ph.D., Duke University, Durham, NC.

Rotarod test**.** Subjects were tested for motor coordination and learning on an accelerating rotarod (Ugo Basile, Stoelting Co., Wood Dale, IL). For the first test session, animals were given three trials, with 45 seconds between each trial. An additional trial was given 48 hours later. Rpm (revolutions per minute) was set at an initial value of 3, with a progressive increase to a maximum of 30 rpm across 5 minutes (the maximum trial length). Measures were taken for latency to fall from the top of the rotating barrel.

Kainic acid treatment. P30-P40 wildtype and miR-29^{Nestin} animals were injected intraperitoneally with 30 mg/kg of kainic acid (Sigma, catalog # K0250) in order to induce seizures. Seizures were scored according to Racine's seizure activities score(Morimoto et al. 2004).

microRNA qRT-PCR analysis. RNA was extracted from cerebella and cortices using the Qiagen miRNeasy kit (catalog #217004) using the manufacturer's instructions. Mature miR-29 expression was assayed using TaqMan MicroRNA Assays (Applied Biosystems). Briefly, 10 ng of RNA was reverse transcribed using Superscript III reverse transcriptase (Invitrogen) and specific RT primers for miR-29a, miR-29b, miR-29c and U6 RNA (Applied Biosystems). Reactions were amplified in an ABI7500 system and relative quantification was carried out using the delta delta Ct method. Sample variability was corrected by normalizing to U6 RNA levels.

cDNA synthesis and qRT-PCR analysis. For analysis of Dnmt3a mRNA, cDNA library was prepared synthesized using 500 ng RNA. RNA samples were first treated with RQ1 DNase (Promega) for 30 min at 37C followed by a 10 min incubation at 65C with DNase Stop Solution (Promega). DNase-treated RNA was mixed with 0.25 μg random hexamer primers (Invitrogen) and reverse transcribed using Superscript III reverse transcriptase (Invitrogen) according to the manufacturer's instructions. Each 25 μL PCR reaction contained 1 μL cDNA, each primer at a final concentration of 400 nM, and Power SYBR Green PCR Master Mix (Applied Biosystems). Reactions were amplified in an ABI7500 system and relative quantification was carried out using the delta delta Ct method. Sample variability was corrected by normalizing to GAPDH levels.

Western blotting. Whole cortices were lysed by homogenization in RIPA buffer. Protein concentrations were quantified using the Bicinchoninic acid method (Thermo Scientific), and equal concentrations of protein were resolved on SDS-polyacrylamide gels and transferred onto PVDF membranes. The Dnmt3a (Abcam) and β-actin (Sigma) primary antibodies were used. Antibody conjugates were visualized by chemiluminescence (ECL; Amersham Life Science). Images were quantified using ImageJ software.

Immunohistochemistry. For immunohistochemistry experiments, mice were anesthetized using isoflurane and transcardially perfused with 4% paraformaldehyde. The mice were then decapitated, and the brains were post-fixed in 4% paraformaldehyde overnight. Paraffin-embedded sections were used for hematoxylin-eosin (H/E), cleaved

caspase-3 and NeuN stains. Briefly, IHC was carried out in the Bond Autostainer (Leica Microsystems Inc. Norwell, MA 02061). Slides were dewaxed in Bond Dewax solution (Leica, part #AR9222) and hydrated in Bond Wash solution (Leica, catalog #AR9590). Antigen retrieval was performed for 30 min at 100ºC in Bond-Epitope Retrieval solution 1 pH-6.0 (AR9961). Slides were incubated with the cleaved caspase-3 and NeuN primary antibodies for 1 hour. DAPI was used as a nuclear stain. Antibody detection was performed using the Bond Polymer Refine Detection System (DS9800). Stained slides were dehydrated and coverslipped. Representative images are obtained from independent experiments, done at least in triplicate.

For all other stains, P40 wildtype and miR-29-deficient brains were embedded in 4% low-melting-point agarose in 1x PBS and were sectioned coronally (50 μm) on a vibratome (Leica VT 1200S). The following antibodies were used for immunohistochemistry: NeuN (catalog #MAB377, Millipore), Cux-1 (catalog #SC13024, Santa Cruz Biotechnology), calretinin (catalog #ab702, Abcam), calbindin (catalog #2173, Cell Signaling), GABA (catalog #A2052, Sigma). Appropriate anti-mouse, anti-rabbit, anti-rat, or anti-guinea pig secondary antibodies were used to detect primary antibody binding. DAPI was used as a nuclear stain. Representative images are obtained from independent experiments, done at least in triplicate.

Slice electrophysiology. Slice electrophysiology experiments were conducted and analyzed similarly to those published previously(Sparrow et al. 2012). Briefly, mice were rapidly decapitated under isoflurane anesthesia, and 300uM coronal slices containing the

dorsolateral striatum (DLS) were prepared on a vibratome (Leica VT1200). Extracted brains were placed in ice-cold modified high sucrose artificial cerebrospinal fluid (aCSF) containing the following (in mM): 194 sucrose, 20 NaCl, 4.4 KCl, 2 $CaCl_2$, 1 $MgCl_2$, 1.2 NaH_2PO_4, 10.0 glucose, and 26.0 $NaHCO_3$. Slices were then transferred to normal aCSF maintained at approximately 30 degrees (Warner Instruments, Hamden, Connecticut) containing the following (in mM): 124 NaCl, 4.4 KCl, 2 $CaCl_2$, 1.2 $MgSO_4$, 1 NaH_2PO_4, 10.0 glucose, and 26.0 $NaHCO_3$. Slices were placed in a holding chamber (Warner Instruments, Hamden, CT), and were allowed to rest for one hour, and remained there until used. Slices were continuously bubbled with a 95% O_2 / 5% CO_2 mixture throughout slicing and experiments. Thin-walled borosilicate glass capillary recording electrodes (3–6 MΩ) were pulled on a Flaming-Brown Micropipette Puller (Sutter Instruments). Following rupture of the cell membrane, cells were allowed to rest and equilibrate to the intracellular recording solutions (below). Input resistance was monitored continuously throughout the experiment, and when input resistance deviated by more than 20% the experiment was discarded. Current clamp experiments were conducted to assess intrinsic neuronal excitability and current-injected firing of OFC pyramidal neurons, identical to those published previously(Pleil et al.). Experiments were conducted using a potassium-gluconate based internal containing the following (in mM): K-gluc, 5 NaCl, 2 MgCl2, 10 HEPES, 0.6 EGTA, 4 Na2ATP, 0.4 Na2GTP. Experiments were conducted both at resting membrane potential (RMP) and -70mV. The experimenter was blinded to mouse genotype until after data analysis.

Statistics. Statistical analyses were performed using GraphPad Prism 5 software. Data are obtained from at least three independent experiments and expressed as mean ± s.e.m. unless otherwise specified. The Student's *t*-test (unpaired, two-tailed) for parametric data was used for analysis of two groups. No statistical methods were used to predetermine sample sizes, but our sample sizes are consistent with those reported in previous publications.

3.6 Figures and Legends

Figure 3.1: Potential microRNA binding sites in the 3' UTR of mouse Dnmt3a.

Analysis of the 3' UTR of mouse Dnmt3a for potential miRNA binding sites (www.targetscan.org). Asterisk denotes miRNAs with more than one binding site. miR-29 is highlighted in red.

Figure 3.1

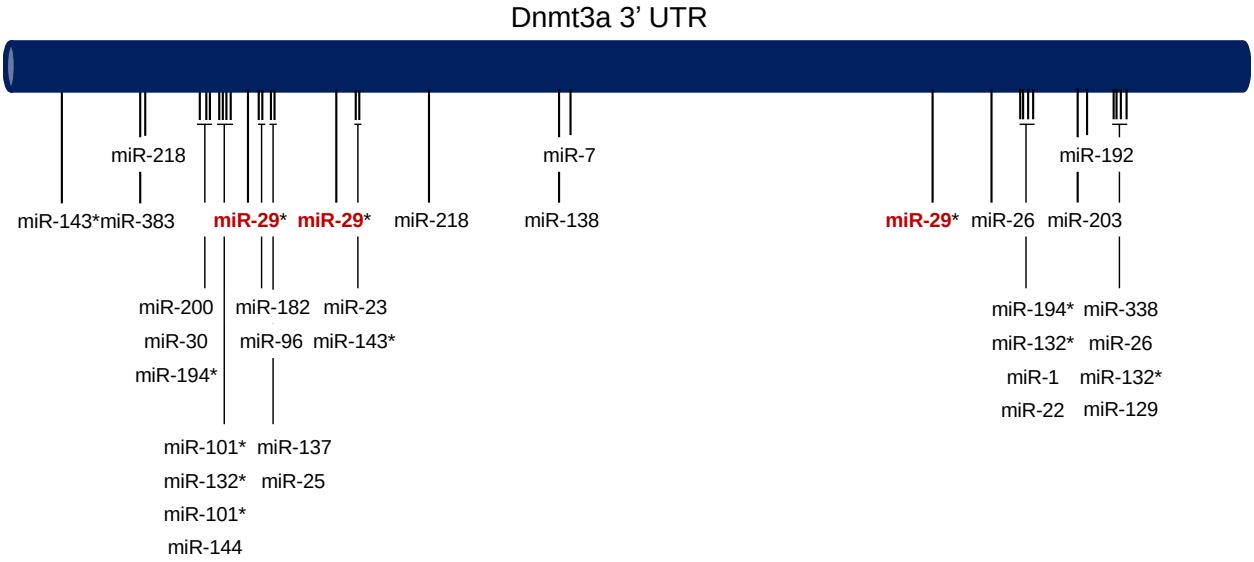
Dnmt3a 3' UTR
miR-143*
miR-218
miR-383
miR-29*
miR-29*
miR-218
miR-7
miR-138
miR-29*
miR-26
miR-203
miR-192
miR-200
miR-30
miR-194*
miR-182
miR-96
miR-23
miR-143*
miR-194*
miR-132*
miR-1
miR-22
miR-338
miR-26
miR-132*
miR-129
miR-101*
miR-132*
miR-101*
miR-144
miR-137
miR-25

Figure 3.2: Cerebellar granule neural precursor cells complete their differentiation into cerebellar granule neurons by P18.

Cerebella from P7 and P18 were co-stained with PCNA (red), a marker of proliferation, and p27 (green), a marker of differentiation. Scale bar denotes 200 μm.

Figure 3.2

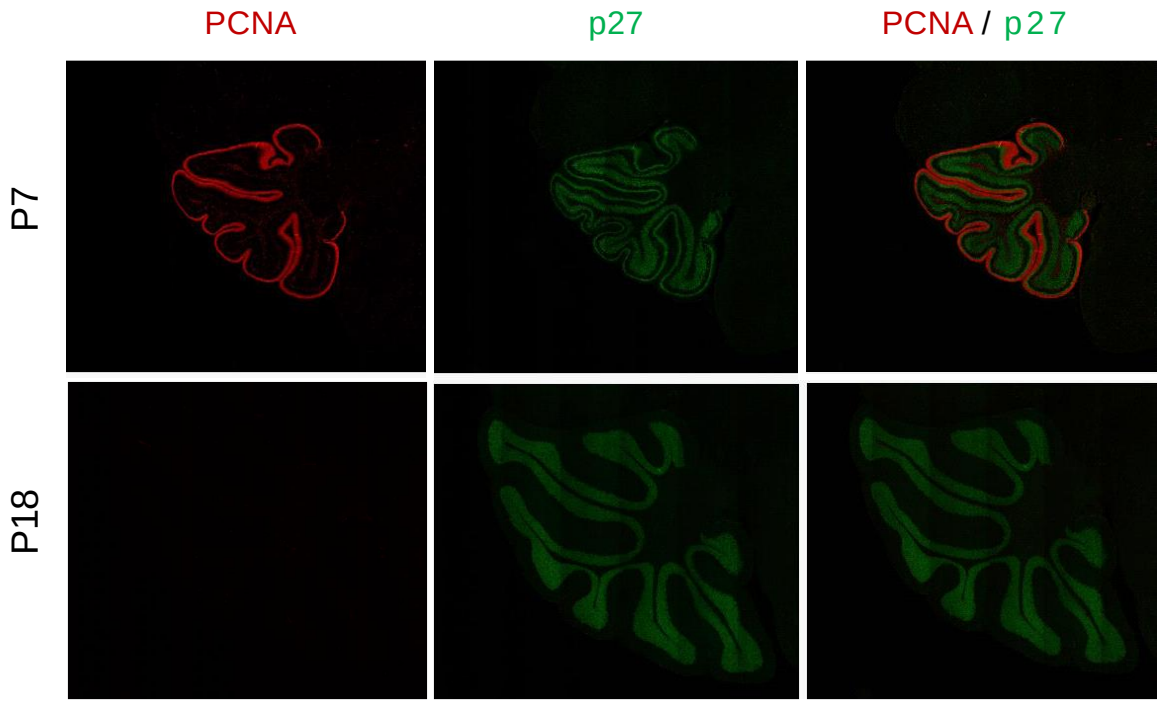

Figure 3.3: miR-29 upregulation is essential for brain maturation.

(**A**) Small RNA-sequencing of young (P18) and adult (P250) differentiated mouse cerebella reveals miR-29 as the most upregulated miRNA family. Quantitative PCR analysis for miR-29b in mouse cerebellum (**B**) and cortex (**C**) at different ages. Data shown are means ± s.e.m. for each group; ** $P < 0.01$. (**D**) WT and miR-29^{CMV} mice at P10 and P28. Body weights (males) (**E**) and Kaplan-Meier survival curve (**F**) for WT and miR-29^{CMV} mice. (**G**) WT and miR-29^{Nestin} mice at P10 and P28. Body weights (males) (**H**) and Kaplan-Meier survival curve (**I**) for WT and miR-29^{Nestin} mice.

Figure 3.3

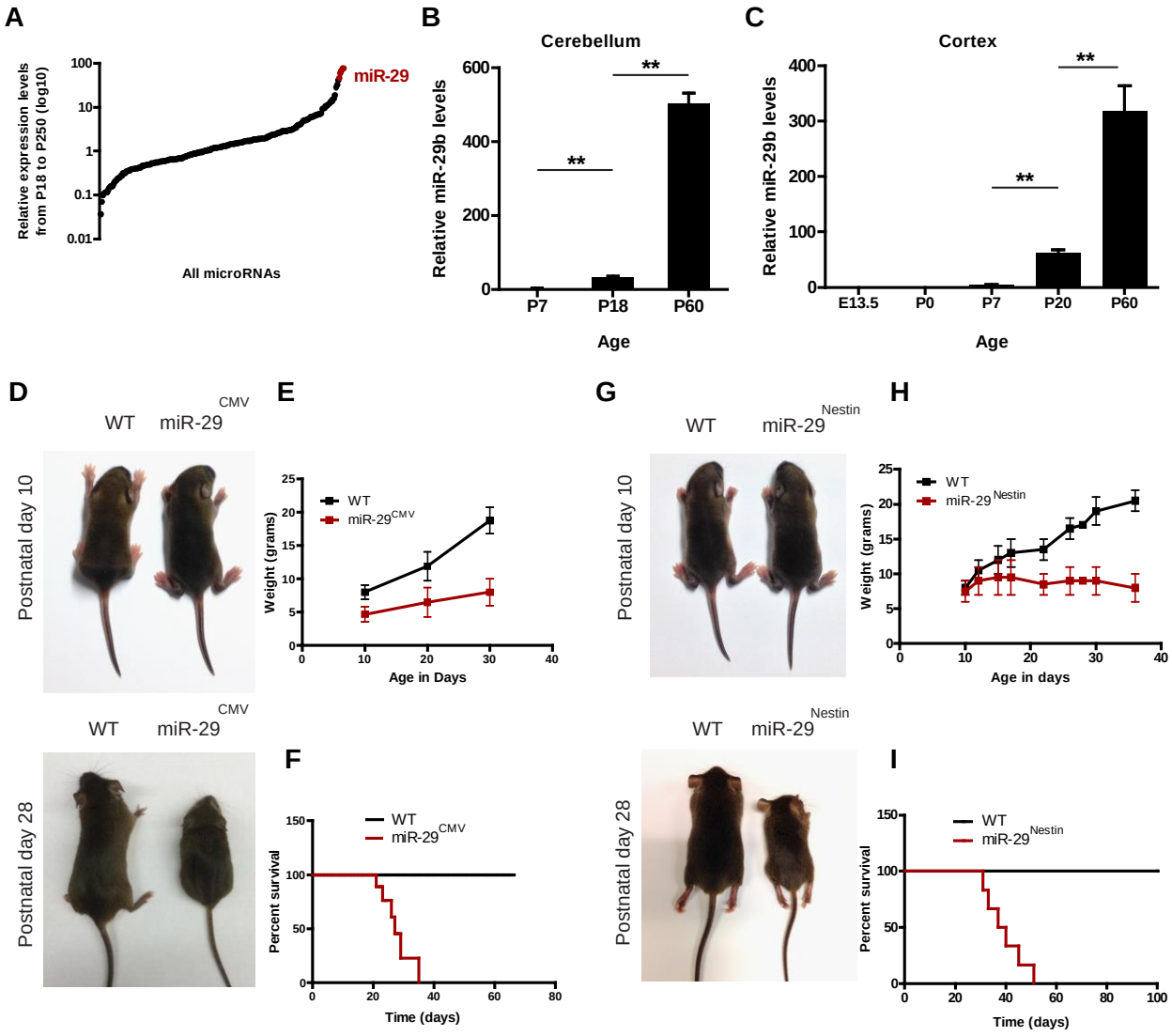
A
Relative expression levels from P18 to P250 (log10)
100
10
1
0.1
0.01
miR-29
All microRNAs
B
Cerebellum
Relative miR-29b levels
600
400
200
0
**
**
P7
P18
P60
Age
C
Cortex
Relative miR-29b levels
400
300
200
100
0
**
**
E13.5
P0
P7
P20
P60
Age
D
WT
miR-29CMV
Postnatal day 10
E
WT
miR-29CMV
Weight (grams)
Age in Days
F
WT
miR-29CMV
Postnatal day 28
Percent survival
Time (days)
G
WT
miR-29Nestin
Postnatal day 10
H
WT
miR-29Nestin
Weight (grams)
Age in days
I
WT
miR-29Nestin
Postnatal day 28
Percent survival
Time (days)

Figure 3.4: Generation of miR-29 mice.

(**A**) PCR genotyping (toe clips) for the floxed (f) and wildtype (w) bands in miR-29ab1$^{f/f}$ CMV-Cre^{-}; miR-29ab1$^{f/+}$ CMV-Cre^{+}; miR-29ab1$^{f/f}$ CMV-Cre^{+} mice. Note the disappearance of the miR-29ab1 band in the miR-29ab1$^{f/f}$ CMV-Cre^{+} sample. (**B**) Quantitative PCR analysis for all three family members of miR-29 from the cortex of WT and miR-29^{CMV} mice at P30. (**C**) PCR genotyping for floxed and wildtype bands in WT, miR-29ab1$^{f/+}$ Nestin-Cre^{+} and miR-29ab1$^{f/f}$ Nestin-Cre^{+} mice. Similar PCR genotyping for miR29b2c loci is shown in (**D**). (**E**) Quantitative PCR analysis for all three family members of miR-29 from the cortex of WT and miR-29^{Nestin} mice at P40. L = ladder; f = floxed; w = wildtype.

Figure 3.4

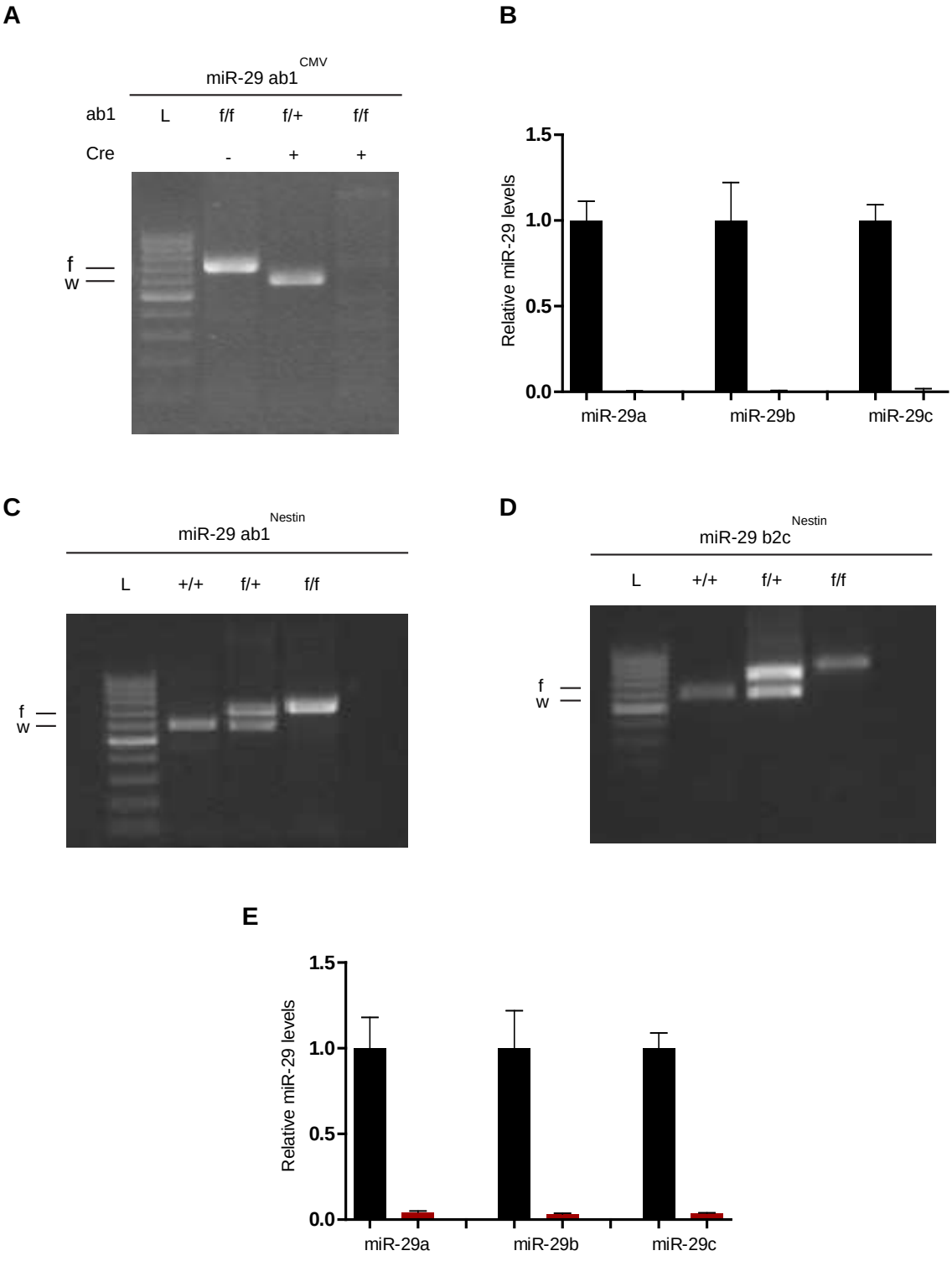
A
CMV
miR-29 ab1
ab1
L
f/f
f/+
f/f
Cre
-
+
+
f
w
B
Relative miR-29 levels
1.5
1.0
0.5
0.0
miR-29a
miR-29b
miR-29c
C
Nestin
miR-29 ab1
L
+/+
f/+
f/f
f
w
D
Nestin
miR-29 b2c
L
+/+
f/+
f/f
f
w
E
Relative miR-29 levels
1.5
1.0
0.5
0.0
miR-29a
miR-29b
miR-29c

Figure 3.5: Kaplan-Meier survival curve of mice partially deleted for miR-29 shows dose-dependent effect.

Kaplan-Meier survival curves of miR-29 WT, miR-29 $ab^{f/+}$ $bc^{f/f}$ and miR-29 $ab^{f/f}$ $bc^{f/+}$ mice.

Figure 3.5

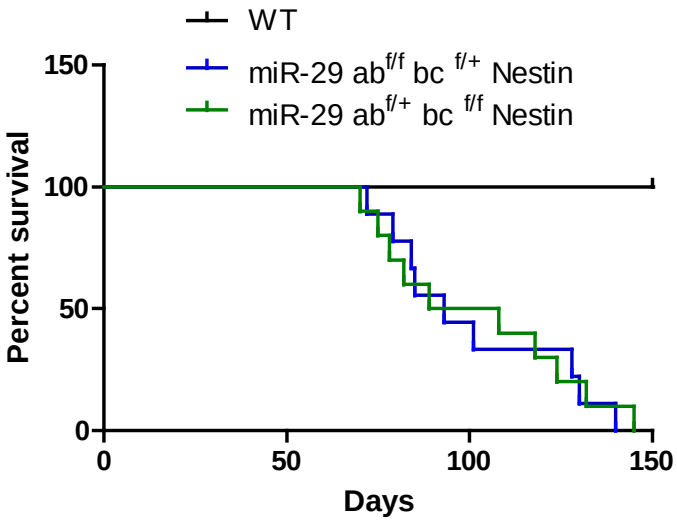
WT
miR-29 ab f/f bc f/+ Nestin
miR-29 ab f/+ bc f/f Nestin
Percent survival
150
100
50
0
0
50
100
150
Days

Figure 3.6: miR-29-deficient mouse brains appear grossly normal.

Hematoxylin and eosin (H/E) stains of representative wildtype, miR-29^{CMV} and miR-29^{Nestin} mouse sagittal brains at P30.

Figure 3.6

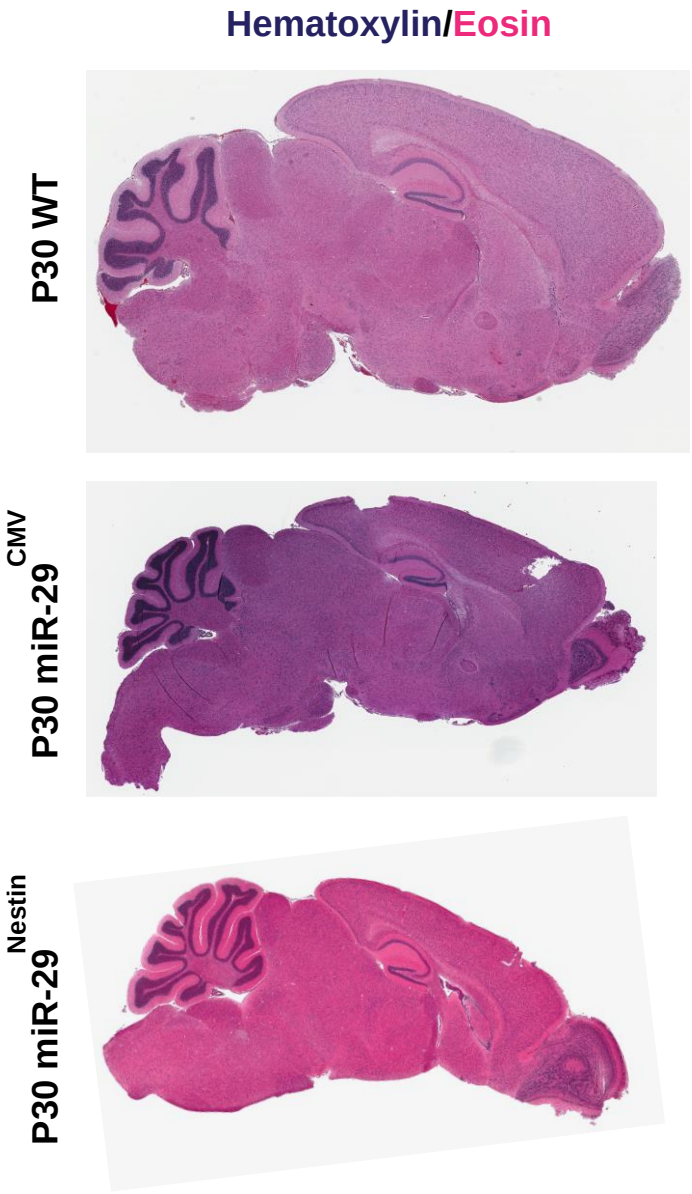

Figure 3.7: miR-29-deficient mouse brains do not exhibit increased apoptosis.

Representative images of wildtype, miR-29^{CMV} and miR-29^{Nestin} mouse cortex (**A**) and hippocampus (**B**) stained with cleaved caspase-3 (green), NeuN (red).

Figure 3.7

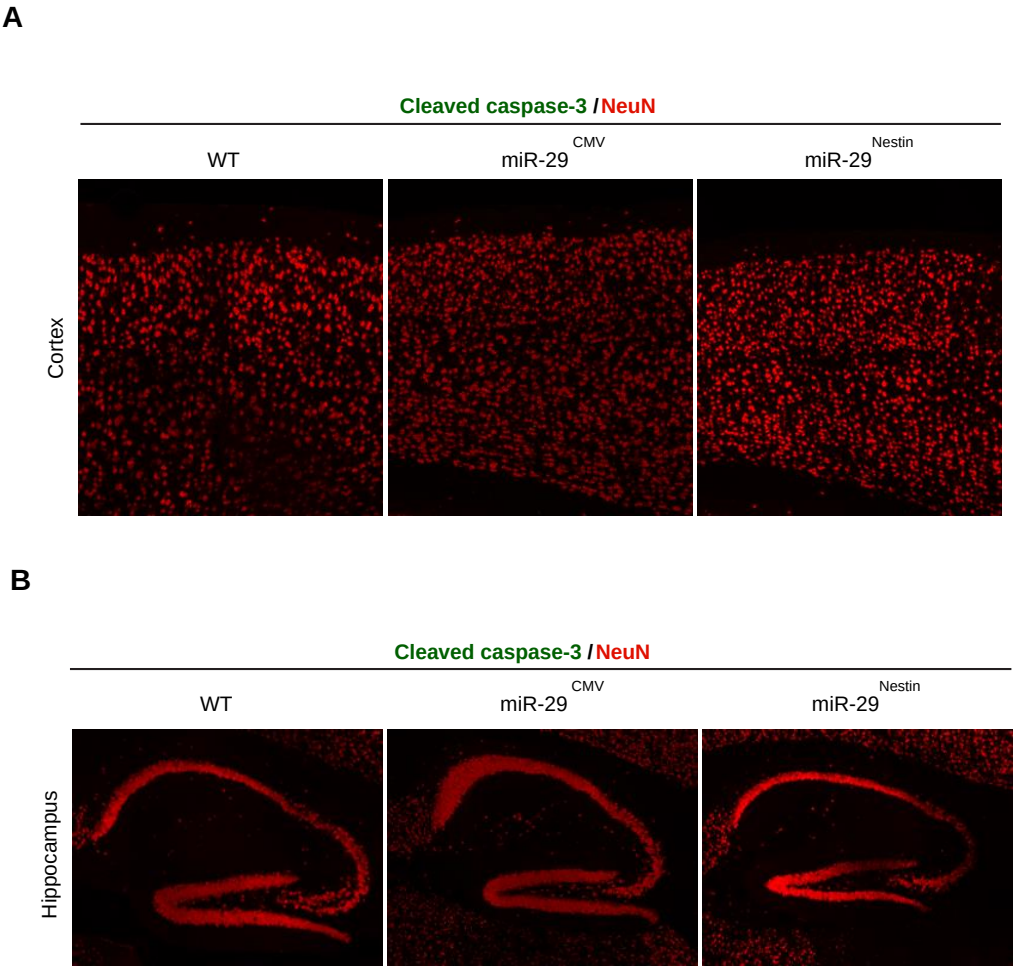
A
Cleaved caspase-3 / NeuN
WT
miR-29 CMV
miR-29 Nestin
Cortex
B
Cleaved caspase-3 / NeuN
WT
miR-29 CMV
miR-29 Nestin
Hippocampus

Figure 3.8: Orbitofrontal cortex (OFC) pyramidal neurons did not differ in basic properties of intrinsic excitability or current-injected firing.

(**A**) WT and miR-29^{Nestin} mice had similar resting membrane potentials (RMPs). (**B**) There were no differences seen in the rheobase, the minimum amount of current required to fire an action potential (AP) at either RMP or -70mV. WT = wildtype; KO = miR-29^{Nestin} mice. (**C**) No differences were observed in the action potential threshold, the membrane potential at which the first action potential fired, at either either RMP or -70mV. The current-injected firing at RMP or -70mV was similar between wildtype and miR-29^{Nestin} mice (**D, E**). n.s. = not significant ($p>0.05$).

Figure 3.8

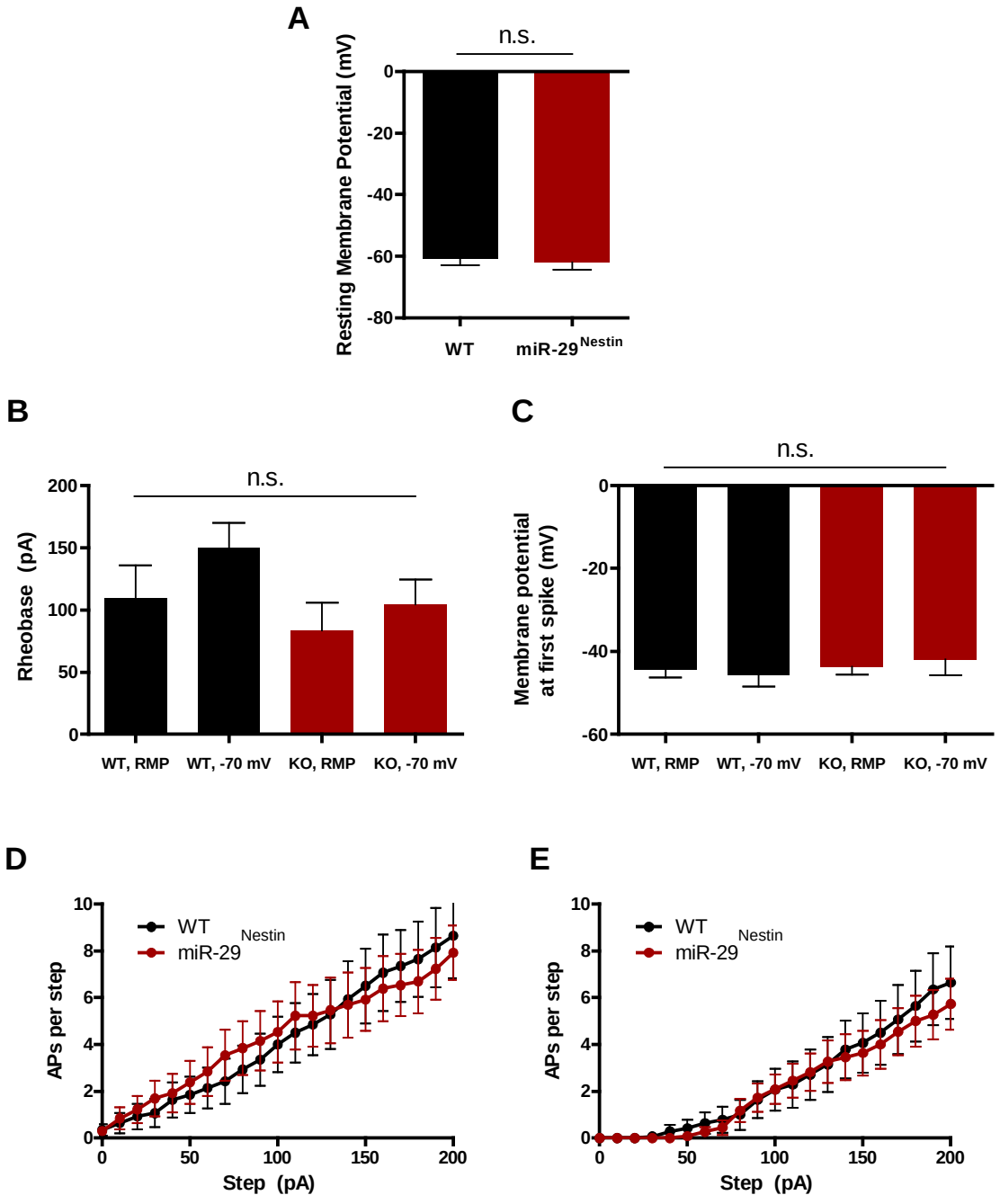
A
n.s.
Resting Membrane Potential (mV)
0
-20
-40
-60
-80
WT
miR-29Nestin
B
n.s.
Rheobase (pA)
200
150
100
50
0
WT, RMP
WT, -70 mV
KO, RMP
KO, -70 mV
C
n.s.
Membrane potential at first spike (mV)
0
-20
-40
-60
WT, RMP
WT, -70 mV
KO, RMP
KO, -70 mV
D
WT
miR-29 Nestin
APs per step
Step (pA)
E
WT
miR-29 Nestin
APs per step
Step (pA)

Figure 3.9: Bisulfite sequencing and gene array analysis reveal non-canonical DNA methylation and dysregulation of synapse-associated pathways in the miR-29^{Nestin} brain.

(**A**) Quantitative PCR analysis for Dnmt3a in the cortex of WT and miR-29^{Nestin} mice at P40. Data shown are means ± s.e.m. for each group; ** P < 0.01. (**B**) Western blot analysis of Dnmt3a levels in cortices from P40 WT and miR-29^{Nestin} mice. (**C**) Genome-wide non-CG methylation levels of cortices from P40 WT and miR-29^{Nestin} mice (n=4 WT and n=4 miR-29^{Nestin} mice). (**D**) mCH increase in miR-29^{Nestin} cortices compared to WT occurs at sites normally CH methylated. mCH levels (of 4 WT and 4 miR-29^{Nestin} mice) were calculated in 5 kb tiles across the genome and ranked by previously reported 6 week frontal cortex mCH levels (x-axis) (Lister et al., 2013). The average mCH levels in WT and miR-29^{Nestin} within 2000 tiles were calculated (y-axis). Tiles with low coverage in the frontal cortex data (Lister et al., 2013) were removed ((#C+#T)<100). (**E**) Gene array analysis from the cortices of P40 WT and miR-29^{Nestin} mice reveal a total of 444 significantly altered genes (226 upregulated genes, 218 downregulated genes) in the miR-29^{Nestin} mice. Analysis was conducted on n=3 WT and n=3 miR-29^{Nestin} mice. (**F**) Statistically significant enrichment of miR-29 target sites among the highly upregulated genes in the miR-29^{Nestin} mice using miRHub analysis. (**G**) Heatmaps for synapse-associated genes between WT and miR-29^{Nestin} mice reveal significant downregulation of these genes in the miR-29-deficient brain. Disease associations for each downregulated gene are listed at right. Red denotes significantly upregulated genes and green denotes significantly downregulated genes. (**H**) mCH levels of the representative repressed neuronal genes in wildtype and miR-29^{Nestin} mice. Data shown are means ± s.e.m. for each group; * P< 0.05, ** P < 0.01.

Figure 3.9

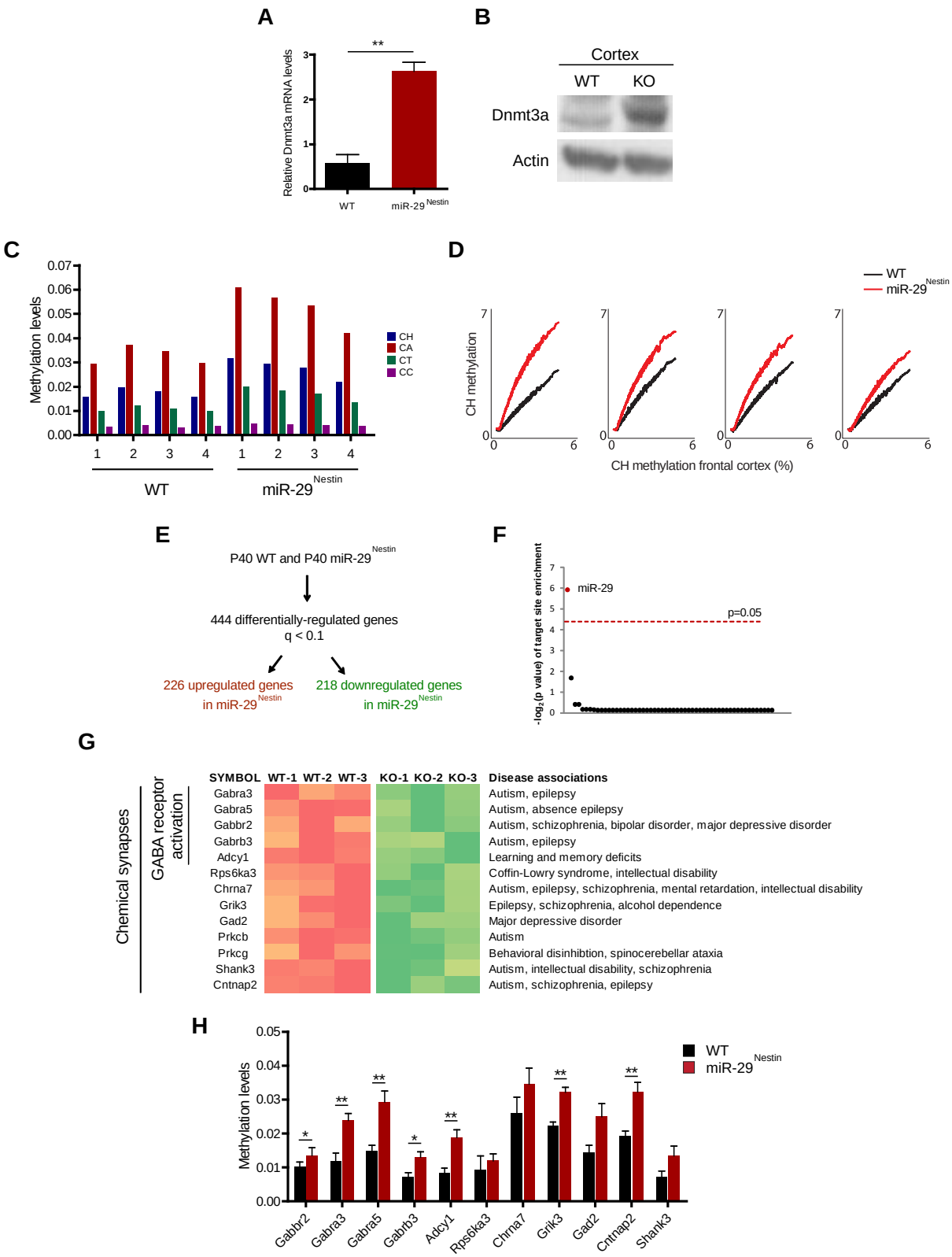
A
Relative Dnmt3a mRNA levels
**
WT
miR-29 Nestin
B
Cortex
WT
KO
Dnmt3a
Actin
C
Methylation levels
CH
CA
CT
CC
WT
miR-29 Nestin
D
WT
miR-29 Nestin
CH methylation
CH methylation frontal cortex (%)
E
P40 WT and P40 miR-29 Nestin
444 differentially-regulated genes
q < 0.1
226 upregulated genes in miR-29 Nestin
218 downregulated genes in miR-29 Nestin
F
-log2(p value) of target site enrichment
miR-29
p=0.05
G
Chemical synapses
GABA receptor activation
SYMBOL WT-1 WT-2 WT-3 KO-1 KO-2 KO-3 Disease associations
Gabra3 Autism, epilepsy
Gabra5 Autism, absence epilepsy
Gabbr2 Autism, schizophrenia, bipolar disorder, major depressive disorder
Gabrb3 Autism, epilepsy
Adcy1 Learning and memory deficits
Rps6ka3 Coffin-Lowry syndrome, intellectual disability
Chrna7 Autism, epilepsy, schizophrenia, mental retardation, intellectual disability
Grik3 Epilepsy, schizophrenia, alcohol dependence
Gad2 Major depressive disorder
Prkcb Autism
Prkcg Behavioral disinhibtion, spinocerebellar ataxia
Shank3 Autism, intellectual disability, schizophrenia
Cntnap2 Autism, schizophrenia, epilepsy
H
Methylation levels
WT
miR-29 Nestin
Gabbr2
Gabra3
Gabra5
Gabrb3
Adcy1
Rps6ka3
Chrna7
Grik3
Gad2
Cntnap2
Shank3

Figure 3.10: miR-29 deficiency in the brain results in upregulation of the Dnmt3a and the Wnt/β-catenin pathway.

(**A**) Gene array heatmap of Dnmt3a in the cortex, hippocampus and striatum of WT and miR-29^{Nestin} mice reveals significant upregulation of Dnmt3a in the miR-29-deficient brain. (**B**) Gene array heatmap of genes in the Wnt/β-catenin pathway between WT and miR-29^{Nestin} mice reveal significant upregulation of these genes in the miR-29-deficient brain.

Figure 3.10

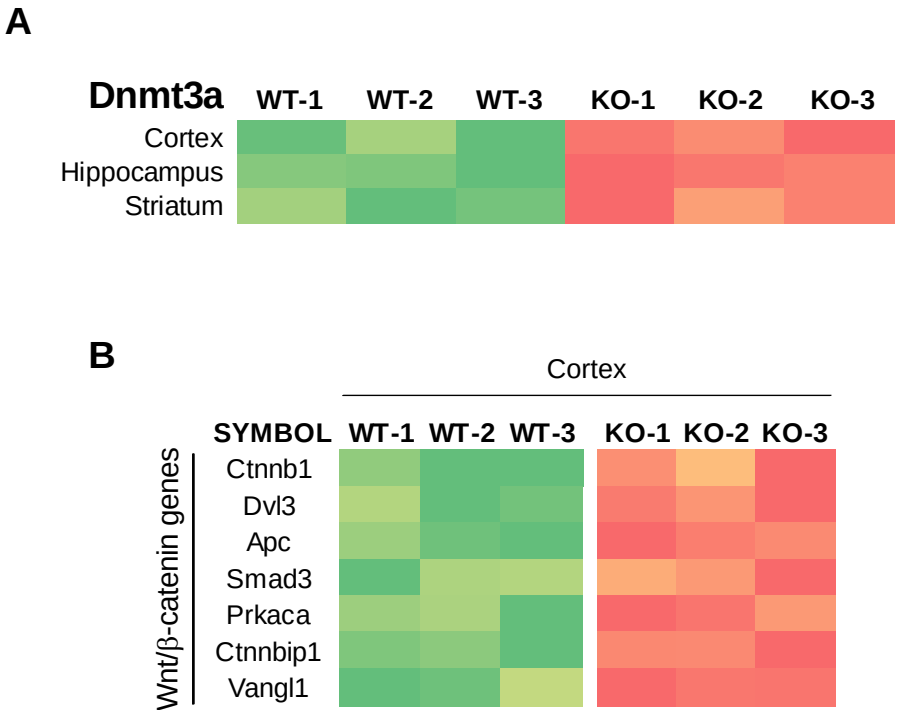
A
Dnmt3a
WT-1
WT-2
WT-3
KO-1
KO-2
KO-3
Cortex
Hippocampus
Striatum
B
Cortex
SYMBOL
WT-1
WT-2
WT-3
KO-1
KO-2
KO-3
Wnt/β-catenin genes
Ctnnb1
Dvl3
Apc
Smad3
Prkaca
Ctnnbip1
Vangl1

Figure 3.11: CG methylation is unaltered in miR-29^{Nestin} mice.

Genome-wide CG methylation levels of cortices from P40 WT and miR-29^{Nestin} mice.

Figure 3.11

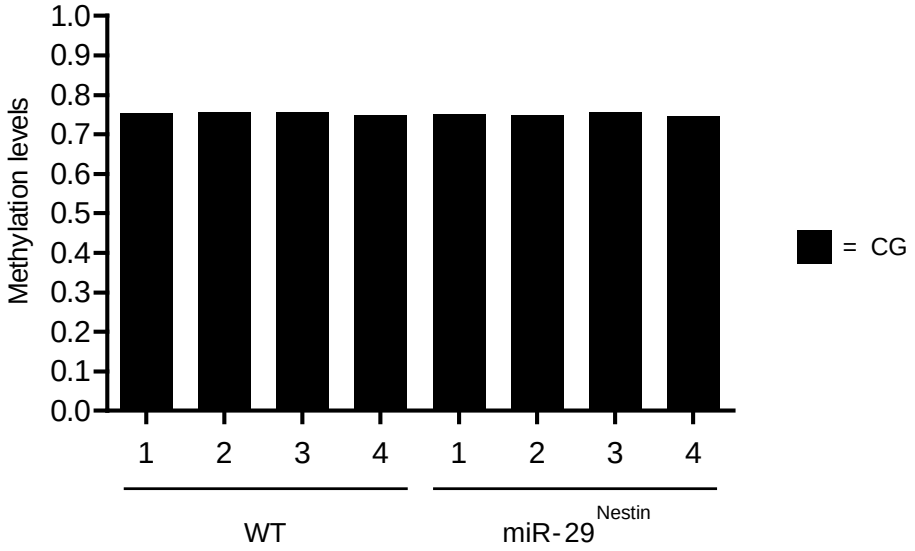
Methylation levels
1.0
0.9
0.8
0.7
0.6
0.5
0.4
0.3
0.2
0.1
0.0
1
2
3
4
1
2
3
4
WT
miR-29Nestin
= CG

Figure 3.12: Altered excitatory/inhibitory balance in miR-29^{Nestin} mice leads to increased susceptibility to tonic-clonic seizures.

(**A-D**) Decreased number of inhibitory interneurons observed throughout the cortex of P40 miR-29^{Nestin} mice. (**E**) miR-29^{Nestin} mice show a significant increase in the number of Cux1-positive neurons in the cortex. Data shown are means ± s.e.m. for each group. * $P < 0.05$ and ** $P < 0.01$. (**F**) miR-29^{Nestin} mice injected with kainic acid display Racine seizure scale characteristics much earlier compared to WT animals. (**G**) miR-29^{Nestin} mice are significantly more susceptible to undergoing tonic-clonic seizures and subsequent death with kainic acid compared to WT. Data shown are from n= 4 WT and n=6 miR-29^{Nestin} mice.

Figure 3.12

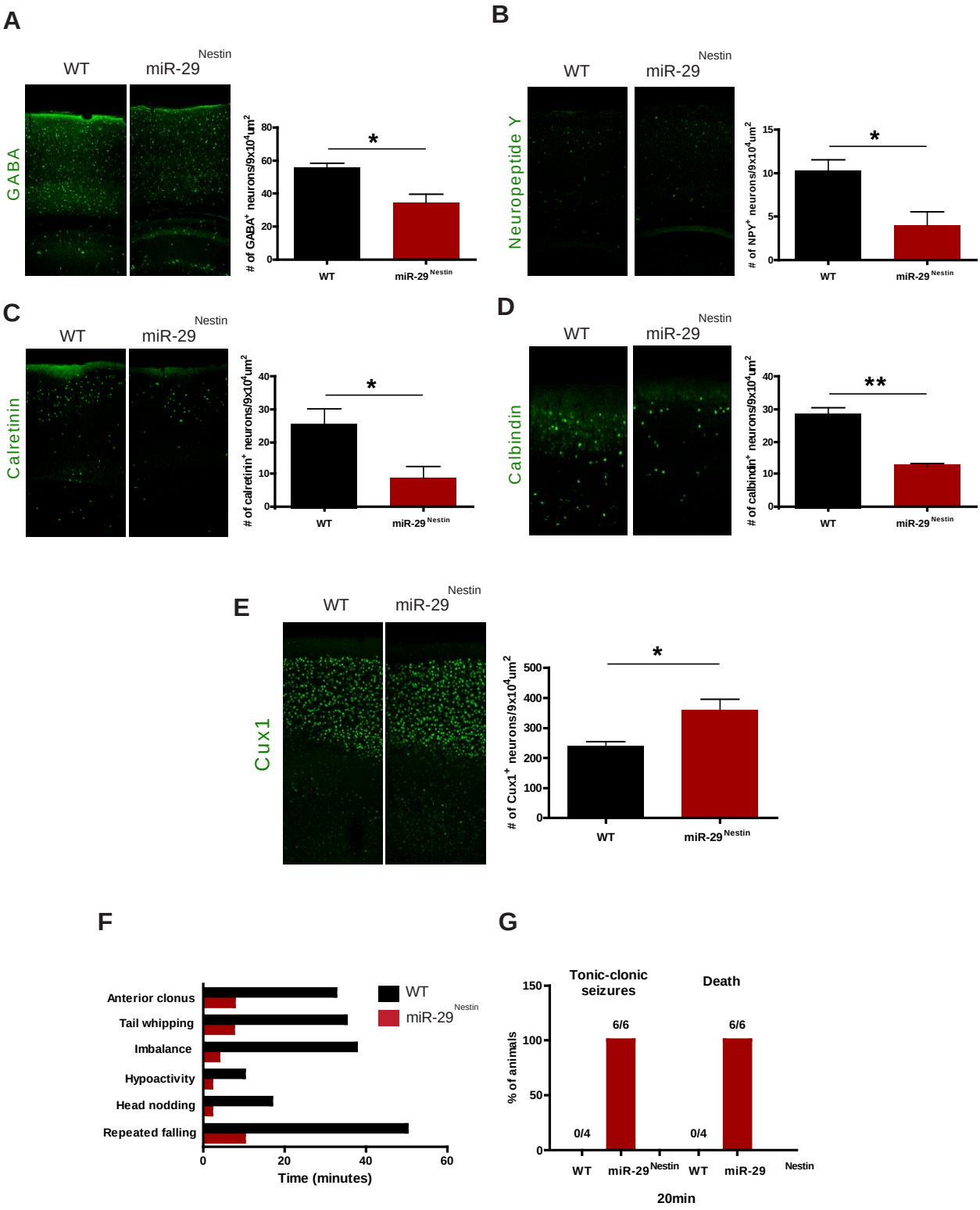
A
WT
miR-29 Nestin
GABA
# of GABA+ neurons/9x10^4um^2
WT
miR-29 Nestin
B
WT
miR-29 Nestin
Neuropeptide Y
# of NPY+ neurons/9x10^4um^2
WT
miR-29 Nestin
C
WT
miR-29 Nestin
Calretinin
# of calretinin+ neurons/9x10^4um^2
WT
miR-29 Nestin
D
WT
miR-29 Nestin
Calbindin
# of calbindin+ neurons/9x10^4um^2
WT
miR-29 Nestin
E
WT
miR-29 Nestin
Cux1
# of Cux1+ neurons/9x10^4um^2
WT
miR-29 Nestin
F
Anterior clonus
Tail whipping
Imbalance
Hypoactivity
Head nodding
Repeated falling
WT
miR-29 Nestin
Time (minutes)
G
Tonic-clonic seizures
Death
% of animals
6/6
6/6
0/4
0/4
WT
miR-29 Nestin
WT
miR-29 Nestin
20min

Figure 3.13: miR-29-deficient mice display excessive self-grooming, facial lesions and neurobehavioral abnormalities.

(**A-B**) miR-29^{Nestin} mice exhibit significantly greater periods of time undergoing hindlimb clasping upon tail suspension. Analyses were conducted on P30 mice. miR-29-deficient mice display severe facial lesions (**C, D**) and spend significantly greater periods of time grooming compared to wildtype (**E**). 60-minute open field analyses reveal that miR-29^{Nestin} mice travel greater distances (**F**), exhibit greater numbers of fine movements (**G**), and spend more time in the center region (**H**) compared to wildtype animals. (**I**) Reduced prepulse inhibition in miR-29^{Nestin} mice. Data shown are means ± s.e.m. miR-29^{Nestin} mice have significantly reduced grip strength (**J**) and reduced latency to fall on the accelerating rotarod (**K**). B,E, ** $P < 0.01$. F-K, * $P < 0.05$, post-hoc test following repeated measures ANOVA.

Figure 3.13

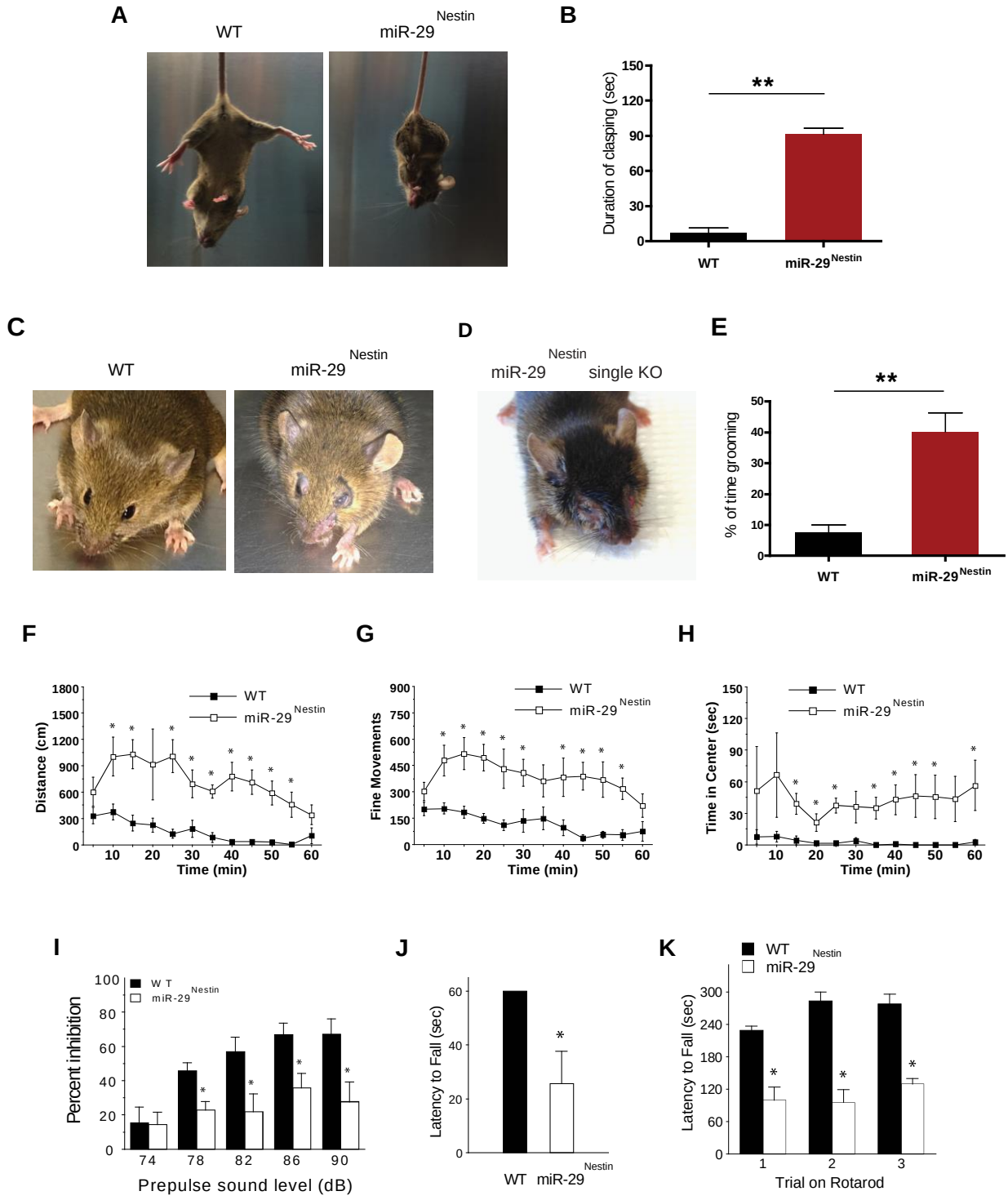
A
WT
miR-29 Nestin
B
Duration of clasping (sec)
150
120
90
60
30
0
**
WT
miR-29 Nestin
C
WT
miR-29 Nestin
D
miR-29 Nestin
single KO
E
% of time grooming
50
40
30
20
10
0
**
WT
miR-29 Nestin
F
Distance (cm)
1800
1500
1200
900
600
300
0
WT
miR-29 Nestin
10 20 30 40 50 60
Time (min)
G
Fine Movements
900
750
600
450
300
150
0
WT
miR-29 Nestin
10 20 30 40 50 60
Time (min)
H
Time in Center (sec)
150
120
90
60
30
0
WT
miR-29 Nestin
10 20 30 40 50 60
Time (min)
I
Percent inhibition
100
80
60
40
20
0
W T
miR-29 Nestin
74 78 82 86 90
Prepulse sound level (dB)
J
Latency to Fall (sec)
60
40
20
0
*
WT miR-29 Nestin
K
WT
miR-29 Nestin
Latency to Fall (sec)
300
240
180
120
60
0
1 2 3
Trial on Rotarod

Figure 3.14: Whole-body deletion of miR-29 leads to facial and dorsal body lesions.

Photos of miR-29^{CMV} double knockout (**A**) and single knockout (**B**) mice showing extensive facial and dorsal body lesions resulting from excessive self-grooming.

Figure 3.14

A

CMV
miR-29 double KO

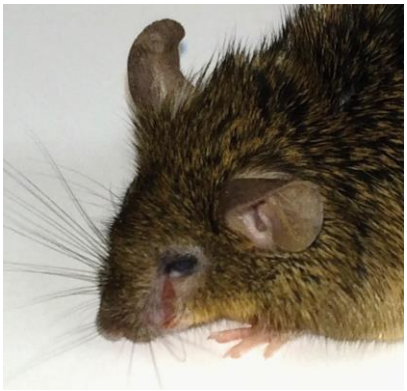

B

CMV
miR-29 single KO

CHAPTER FOUR: DISCUSSION

5.1 Part I: Summary of findings, clinical relevance and future directions

Bcl-xL is essential for the survival and function of differentiated neurons in the cortex that control complex behaviors:

Every neuron in the brain undergoes different phases or stages throughout the life of an organism. The life cycle of a neuron starts with the generation of neuronal progenitors from pluripotent stem cells (Kriegstein et al. 2006). These mitotically active neuronal progenitor cells go on to differentiate into early postmitotic neurons before they migrate to their eventual destinations in the brain (Kriegstein and Alvarez-Buylla 2009; Lui et al. 2011). More importantly, these immature neurons undergo a phenomenon known as maturation in the early postnatal to adolescent period to become mature neurons, during which new synapses are made and the synaptic connections between neurons are scaled back and refined. This stage of brain maturation ensures the development of a properly formed brain which, during old age, undergoes degeneration.

It is widely accepted that the apoptotic machinery is strictly regulated during the period of neurogenesis in the brain. In fact, all of the mice deficient in the apoptotic machinery (*e.g.* Apaf-1, Caspase-3, Caspase-9) display severe consequences during the peak of neurogenesis in which the precursors that normally undergo physiological cell death

continue to persist in these mutant mice (Kuida et al. 1996; Cecconi et al. 1998; Hakem et al. 1998; Kuida et al. 1998; Woo et al. 1998; Yoshida et al. 1998). This persistence of mitotically active precursor cells results in either embryonic or perinatal lethality. These findings highlight the importance of physiological cell death in which the brain generates more precursors than needed in order to kill the extra neuronal precursors and suggest that the cell death pathway is most crucial during the period of embryonic development. Indeed, much of the literature focuses on the requirement of the apoptotic pathway before the period of differentiation. Here, we found that the reliance of the brain on the apoptotic machinery is not restricted to neuronal precursors in the embryonic brain but instead also extends to early postmitotic neurons. In particular, the neurons that are critical for governing certain higher order functions are acutely dependent on Bcl-xL for their survival. The main findings of this work are summarized below:

1. Programmed cell death in the brain during the embryonic as well as early postnatal periods is tightly regulated by the anti-apoptotic protein Bcl-xL.
2. Neural precursor cells in the brain express very low levels of Bcl-xL and are resistant to cell death upon deletion of the gene.
3. In contrast, early differentiated neurons are acutely dependent on Bcl-xL for their survival. Deletion of Bcl-xL in the neural precursor cells results in a marked increase in cell death in the neurons of the brains of early postnatal mice.
4. Upper layer cortical neurons are more vulnerable to Bcl-xL deletion compared to deeper layer neurons, suggesting that Bcl-xL has a role in the survival of specific postmitotic neurons in the developing brain.

5. The cell death induced by loss of Bcl-xL can be rescued by co-deletion of the pro-apoptotic proteins Bax and Bak.
6. Deletion of Bcl-xL exclusively in postmitotic neurons results in a similar pattern of cell death and also has a significant effect on the body size of these mice.
7. Importantly, Bcl-xL deletion in the brain led to severe behavioral and cognitive deficits, implicating the role of Bcl-xL in the survival of neurons that are involved in higher order brain functions.

Clinical relevance:

While physiological cell death is critical for proper brain development, dysregulated apoptosis that occurs after the brain is fully developed could lead to severe defects. Indeed, cell death proteins have been implicated in multiple neurodegenerative disorders including Alzheimer's, Parkinson's and Huntington's disease (Mattson 2000). We recently conducted a gene array analysis of the cortices isolated from wildtype and Bcl-xL-deficient mice to study gene-disease associations. Using GSEA (Gene Set Enrichment Analysis, Broad Institute), we identified the gene sets that are highly upregulated or downregulated upon deletion of Bcl-xL in the brain. Interestingly, the disease pathway that is most significantly associated with Bcl-xL deletion in the brain is the set of genes downregulated in Alzheimer's disease. This finding suggests that Bcl-xL deficiency could play a major role in the pathogenesis of Alzheimer's disease. The data could be used not only for the therapeutic potential of Bcl-xL in neurodegenerative disease but could also reveal the downstream effectors of Bcl-xL in the brain. Another exciting finding of our study is an unexpected role of Bcl-xL in preventing compulsive overgrooming and the resultant self-

inflicted lesions. While the role of Bcl-xL in cell death is well studied and uncontroversial, its function in controlling complex behaviors is surprising but exciting.

Future directions:

While our results on the consequence of Bcl-xL deletion in the brain *in vivo* are striking and somewhat surprising, these findings also pave the path for exciting prospective studies. For example, why are early differentiated neurons more sensitive to loss of Bcl-xL compared to neuronal precursors and mature neurons? While physiological apoptosis is known to be activated in rapidly dividing neuronal precursor cells during embryonic development, these cells do not express high levels of Bcl-xL and thus do not appear to be acutely dependent on Bcl-xL for their survival. In contrast, Bcl-xL becomes highly expressed in the neurons that differentiate from these precursor cells, possibly as a result of increased energetic dependence on the mitochondria in postmitotic neurons. Indeed, Bcl-xL is tightly associated with the mitochondria as discussed below. As neurons become mature, multiple apoptotic brakes are activated, making mature neurons resistant to loss of Bcl-xL. Indeed, we can test this hypothesis by culturing neuronal precursor cells, differentiating these cells into neurons, maturing them in culture, and testing the sensitivity of these cells to apoptosis by inhibiting various cell death genes.

Another possible reason for the dependency on Bcl-xL could be due to a non-apoptotic role of Bcl-xL in early differentiated neurons but not in precursors and late differentiated neurons. Indeed, multiple labs have shown that Bcl-xL plays an important role in mitochondrial respiration and in the F_1F_0 ATPase (Alavian et al. 2011; Chen et al. 2011). Because of our discovery that Bcl-xL is most critical during early differentiation,

future studies showing that mitochondrial respiration is most sensitive during this stage (as compared to neuronal precursors and/or mature neurons) could be very informative for the field of neurodevelopment. Indeed, neurons are generally believed to rely more on glycolysis than on oxidative phosphorylation, and it is possible that, during this shift from oxidative phosphorylation to glycolysis, there is a vulnerable period when neurons are acutely dependent on ox-phos for their survival.

Finally, the unexpected finding of the role of Bcl-xL in governing complex higher order behaviors should be studied in detail in the future. By utilizing the Bcl-xL$^{f/f}$ Bax$^{f/f}$ Bak$^{-/-}$ Nex-Cre triple knockout mice, we can examine whether the behaviors observed the mice deleted for Bcl-xL is mediated *via* its apoptotic or non-apoptotic role. Thus, if the triple knockout mice still exhibit similar neurobehavioral deficits such as hyperactivity and self-injurious and risk-taking behaviors, this points to a non-apoptotic role of Bcl-xL in regulating these behaviors, possibly through its synaptic functions.

5.2 Part II: Summary of findings, clinical relevance and future directions

MicroRNA-29 is an essential regulator of DNA methylation during brain maturation:

After a neuron has differentiated, it undergoes a period of maturation. Surprisingly, this period in the life cycle of a neuron has not been studied in detail, perhaps because of the belief that an early or immature postmitotic neuron has similar physiological properties to a mature differentiated neuron. Recently, however, neuroscientists have taken a keen interest in the period of brain maturation and have recognized that dynamic changes occur during this stage, including processes such as synaptogenesis and

subsequent pruning of the synapses to maintain proper connections between neurons. Here, we found that the period of maturation from a young neuron to a mature neuron is critical for the identity and proper function of a neuron during adulthood. Collectively, this maturation process is essential for homeostatic control in the brain. While many genes and pathways are likely involved in this process, we identified a single microRNA known as miR-29 which, in turn, can modulate multiple pathways during maturation. Nevertheless, it is not surprising that miR-29 also plays other roles during neuronal maturation, such as restricting the apoptotic pathway in mature neurons to maintain their long-term survival. The main findings of this work are summarized below:

1. The microRNA-29 (miR-29) family is induced specifically during the period of brain maturation.
2. Deletion of all the three members of the miR-29 family, both globally or conditionally in the brain, leads to post-natal lethality at approximately P30.
3. miR-29-deficient mice exhibit several neurological deficits including hindlimb clasping, motor deficits, hyperactivity as well as risk-taking behaviors. These mice also exhibit repetitive behaviors including compulsive overgrooming that leads to facial ulcers and bleeding.
4. Mice deleted for miR-29 are hypersociable in the three-chamber sociability test.
5. These mice also show an excitatory/inhibitory (E/I) imbalance that leads to increased susceptibility to seizures and status epilepticus following kainic acid injection.

6. DNA methylation plays an important role during brain maturation, and miR-29 targets a critical protein of the pathway Dnmt3a. Consistently, brain deleted for miR-29 show increased levels of Dnmt3a.
7. Bisulfite sequencing of miR-29-deficient mice shows hypermethylation of genes throughout the brain. Interestingly, this hypermethylation occurs in a non-CG context (also referred to as CH methylation).
8. Gene array and RNAseq analysis of these mice revealed multiple downregulated genes that are critical for neuronal function. Additionally, many of these genes have a direct association with autism spectrum disorders.
9. Indeed, gene association studies showed significant overlap in genes downregulated in miR-29 KO brain and in human ASD brain.
10. Long neuronal genes are specifically downregulated in the miR-29-deleted brain. This phenomenon has also been recently reported to occur in the brains of ASD patients.

Clinical relevance:

According to data in 2014 from the Centers for Disease Control, 1 in every 68 children is currently diagnosed with autism spectrum disorder (ASD) in the United States. Multiple gene association studies have failed to pinpoint a single causative gene for ASD. This led to the consensus that there should be increasing focus be on multiple genes and pathways rather than a single gene (Abrahams and Geschwind 2008). Similarly, there has been considerable attention on the role of epigenetics as the underlying cause of ASD (Schanen 2006; Siniscalco et al. 2013).

The miR-29 family of microRNAs could be critical in the pathogenesis of ASD as it plays an essential role in regulating DNA methylation across the mammalian genome. First, because of its ability to target the 3'UTR of multiple genes, miR-29 can regulate multiple pathways that play a role in ASD. More importantly, we have shown in our study that miR-29 targets the DNA methyltransferase Dnmt3a and decreases gene expression throughout the genome *via* hypermethylation of these genes. This finding is underscored by the fact that most of the genes that are downregulated in the miR-29-deficient brain are associated with neuronal functions that are directly implicated in ASDs and other neurodevelopmental disorders. Therefore, our study lays the foundation for exciting clinically relevant studies whereby miR-29 could be developed as a small molecule therapy for ASDs and related neurodevelopmental disorders. The notion of increasing the levels of an endogenous gene rather than treating a subject with an exogenous chemical is preferable and avoids potential immune reactions or rejections. Further, our gene association study has revealed that ASD brains are similar to the brains of miR-29-deficient brains. Thus, therapies could be aimed at increasing the miR-29 levels in ASD patients to physiological levels rather than to artificial levels that could have potential off-target effects of expressing too high levels of miR-29.

Moreover, one of the reasons our lab initially became interested in miR-29 was our discovery than miR-29 can prevent apoptotic cell death in sympathetic neurons. In fact, our lab has been granted a patent for the role of miR-29 in neuronal protection. In addition, multiple labs have shown miR-29 levels to be decreased in Alzheimer's, Parkinson's and Huntington's disease brains. Therefore, miR-29 could be also tested as a small molecule therapy in patients with neurodegenerative diseases. In fact, GSEA (Gene Set Enrichment

Analysis, Broad Institute) analysis showed a commonality between genes downregulated in miR-29-deleted brains and those downregulated in the brains of Alzheimer's disease patients, thus suggesting a common etiological role.

Future directions:

While the above proposed clinical studies are directly relevant to both ASDs as well as neurodegenerative diseases and could lead to clinical trials testing the therapeutic potential of miR-29, our present study also lays the foundation of exciting research to further our understanding of neurodevelopment, neuronal maturation and neurodegeneration. We expect a subset of the phenotypes of the miR-29-deficient mice to be a result of Dnmt3a overexpression. As a consequence of overexpression of Dnmt3a, we also expect a global hypermethylation of genes in the brain. To accurately define the exact phenotypes that are mediated by Dnmt3a (and hypermethylation) *versus* those that are independent of Dnmt3a, we are currently crossing our miR-29-deficient mice with mice that are conditionally deleted for Dnmt3a. Once these miR-29/Dnmt3a-deficient mice are generated, we plan to characterize the phenotypes of these mice using behavioral tests (*e.g.* open field analysis), three-chamber social interaction tests, RNAseq and bisulfite sequencing analysis to assess which phenotypes are rescued in the miR-29/Dnmt3a double-deficient mice.

To complement this genetic experiment, we are also generating transgenic mice that conditionally overexpress Dnmt3a. Surprisingly, we are not aware of any lab that has generated a mouse model overexpressing Dnmt3a to date. Here, we hypothesize that these mice will phenocopy the mice that are deleted for miR-29 in the brain. In addition to the

neurobehavioral experiments outlined above, we will assess the ASD phenotypes that are directly related to epigenetics (*e.g.* hypermethylation). Finally, to accurately define the relationship between miR-29 and Dnmt3a, we are generating a new mouse model in which the endogenous Dnmt3a is modified such that the miR-29 binding sites along the 3'UTR are abolished. These three novel mouse models will serve as excellent tools in the future to study the relationship between miR-29, Dnmt3a and ASD.

Furthermore, deciphering the neuronal subtypes that are responsible for the neurobehavioral phenotype of the miR-29-deficient mice is also important. Here, we show that deletion of miR-29 leads to an increase in the number of excitatory projection neurons and a reduction in the number of inhibitory interneurons, thus leading to an E/I imbalance and shifting the brain towards an excitatory phenotype. In fact, studies have found that, in the cortex of patients with ASD there is increased neuronal diversity and neuronal numbers as compared to the brains of control subjects (McCaffery and Deutsch 2005; Casanova et al. 2006; Courchesne et al. 2011). In addition, mutations in the Shank3 gene are known to lead to autism and ASD-like phenotypes in mice (Durand et al. 2007; Peca et al. 2011). Mice deficient in Shank3 were shown to exhibit cortical hyperactivity during the early postnatal period (Peixoto et al. 2016), while Takao Hensch's group found a reduction in the number of parvalbumin-expressing neurons in the cortex of these mice (Gogolla et al. 2014). Huda Zoghbi's group has also found a link between Shank3 and abnormal excitatory and inhibitory synapses, where overexpression or duplication of Shank3 was found to result in a hyperkinetic disorder with manic-like behavior and seizures that were attributed to an E/I imbalance in the brain (Han et al. 2013).

Recently, there has also been a push to link the behavior of mice to the specific neuronal subtypes present within the brain. For example, Nancy Ip's group recently found that an *in utero* intraventricular injection of the small molecule XAV939, which increases the intermediate progenitor population in the brain to generate more pyramidal neurons in layers II/III of the cortex, led to an E/I imbalance in the brain and resulted in behaviors that resembled what is observed in patients with autism, including repetitive self-grooming behavior, deficits in social interaction, and repetitive digging behavior on the marble burying test (Fang et al. 2014).

To determine the precise role of excitatory *versus* inhibitory neurons, we crossed the miR-29 floxed mice with a mouse expressing the Nex-Cre transgene (these mice referred to as miR-29^{Nex}), which recombines exclusively in the postmitotic excitatory projection neurons that spares recombination in the inhibitory interneurons. We also generated mice in which miR-29 was recombined in the inhibitory interneurons using the Parvalbumin-Cre line (thus sparing the excitatory projection neurons; these mice are referred to as miR-29^{Parvalbumin}). Interestingly, our preliminary data shows that miR-29^{Nex} mice show similar repetitive grooming and resultant facial ulcers as seen in the miR-29^{Nestin} mice. Further, miR-29^{Nex} mice die by P90, suggesting that many of the miR-29 knockout phenotypes are driven by the loss of miR-29 in the excitatory projection neurons. The miR-29^{Parvalbumin} mice appear grossly normal. However, to specifically probe the role of the excitatory *versus* inhibitory interneurons in the phenotype of the miR-29-deficient mice, a detailed neurobehavioral analysis as described for the miR-29^{Nestin} mice must be conducted.

5.4 Concluding remarks

The mystery behind the brain is slowly unravelling. However, the enigma of the brain continues to surprise us and excite us even after more than 100 years Ramon y Cajal, the father of modern neuroscience, identified multiple neurons and pathways in the brain. For example, the field of optogenetics rapidly emerged in the last five years identifying new pathways and functions of parts of brain challenging previous known knowledge about those pathways. During my time in graduate school, I was fortunate to study two distinct but important phases in neuron life cycle. The work presented here and by others demonstrates that neuronal survival during early embryonic and postnatal development and the maturation of and long-term survival of neurons in the brain are mediated by multiple, complex mechanisms that involve anti-apoptotic proteins and microRNAs. Further investigation of the mechanistic insights into how these players mediate critical events in the brain will drive the generation of targeted therapeutics for patients suffering from many of the neurodevelopmental and psychiatric disorders that are seen today. The coming years in neuroscience will be an exciting field for neuroscientists.

REFERENCES

Abe M, Bonini NM. 2013. MicroRNAs and neurodegeneration: role and impact. *Trends Cell Bio* **23**: 30-36.

Abrahams BS, Geschwind DH. 2008. Advances in autism genetics: on the threshold of a new neurobiology. *Nat Rev Genet* **9**: 341-355.

Alavian KN, Li H, Collis L, Bonanni L, Zeng L, Sacchetti S, Lazrove E, Nabili P, Flaherty B, Graham M et al. 2011. Bcl-xL regulates metabolic efficiency of neurons through interaction with the mitochondrial F1FO ATP synthase. *Nat Cell Biol*.

Bachman M, Uribe-Lewis S, Yang X, Williams M, Murrell A, Balasubramanian S. 2014. 5-Hydroxymethylcytosine is a predominantly stable DNA modification. *Nat Chem* **6**: 1049-1055.

Bandeira F, Lent R, Herculano-Houzel S. 2009. Changing numbers of neuronal and non-neuronal cells underlie postnatal brain growth in the rat. *Proc Natl Acad Sci* **106**: 14108-14113.

Baran-Gale J, Fannin EE, Kurtz CL, Sethupathy P. 2013. Beta Cell 5′ -Shifted isomiRs Are Candidate Regulatory Hubs in Type 2 Diabetes. *PLoS ONE* **8**: e73240.

Bartel DP. 2004. MicroRNAs: genomics, biogenesis, mechanism, and function. *Cell* **116**: 281-297.

Bender A, Weber M. 2013. DNA methylation: an identity card for brain cells. *Genome Biol* **14**: 1-3.

Besirli CG, Deckwerth TL, Crowder RJ, Freeman RS, Johnson EM, Jr. 2003. Cytosine arabinoside rapidly activates Bax-dependent apoptosis and a delayed Bax-independent death pathway in sympathetic neurons. *Cell Death Differ* **10**: 1045-1058.

Blakemore S-J. 2008. The social brain in adolescence. *Nat Rev Neurosci* **9**: 267-277.

Bodda C, Tantra M, Mollajew R, Arunachalam JP, Laccone FA, Can K, Rosenberger A, Mironov SL, Ehrenreich H, Mannan AU. 2013. Mild Overexpression of Mecp2 in Mice Causes a Higher Susceptibility toward Seizures. *Am J Pathol* **183**: 195-210.

Bogner C, Leber B, Andrews DW. 2010. Apoptosis: embedded in membranes. *Curr Opin Cell Biol* **22**: 845-851.

Braat S, Kooy RF. 2015. The GABAA Receptor as a Therapeutic Target for Neurodevelopmental Disorders. *Neuron* **86**: 1119-1130.

Brainard DH. 1997. The Psychophysics Toolbox. *Spat Vis* **10**: 433-436.

Casanova MF, van Kooten IA, Switala AE, van Engeland H, Heinsen H, Steinbusch HW, Hof PR, Trippe J, Stone J, Schmitz C. 2006. Minicolumnar abnormalities in autism. *Acta Neuropathol* **112**: 287-303.

Cecconi F, Alvarez BG, Meyer BI, Roth KA, Gruss P. 1998. Apaf1 (CED-4 homolog) regulates programmed cell death in mammalian development. *Cell* **94**: 727-737.

Chan SWL, Henderson IR, Jacobsen SE. 2005. Gardening the genome: DNA methylation in Arabidopsis thaliana. *Nat Rev Genet* **6**: 351-360.

Chao H-T, Chen H, Samaco RC, Xue M, Chahrour M, Yoo J, Neul JL, Gong S, Lu H-C, Heintz N et al. 2010. Dysfunction in GABA signalling mediates autism-like stereotypies and Rett syndrome phenotypes. *Nature* **468**: 263-269.

Chen L, Chen K, Lavery LA, Baker SA, Shaw CA, Li W, Zoghbi HY. 2015. MeCP2 binds to non-CG methylated DNA as neurons mature, influencing transcription and the timing of onset for Rett syndrome. *Proc Natl Acad Sci* **112**: 5509-5514.

Chen RZ, Akbarian S, Tudor M, Jaenisch R. 2001. Deficiency of methyl-CpG binding protein-2 in CNS neurons results in a Rett-like phenotype in mice. *Nat Genet* **27**: 327-331.

Chen YB, Aon MA, Hsu YT, Soane L, Teng X, McCaffery JM, Cheng WC, Qi B, Li H, Alavian KN et al. 2011. Bcl-xL regulates mitochondrial energetics by stabilizing the inner membrane potential. *J Cell Biol* **195**: 263-276.

Cheng EHYA, Wei MC, Weiler S, Flavell RA, Mak TW, Lindsten T, Korsmeyer SJ. 2001. BCL-2, BCL-XL Sequester BH3 Domain-Only Molecules Preventing BAX- and BAK-Mediated Mitochondrial Apoptosis. *Mol Cell* **8**: 705-711.

Chipuk JE, Bouchier-Hayes L, Green DR. 2006. Mitochondrial outer membrane permeabilization during apoptosis: the innocent bystander scenario. *Cell Death Differ* **13**: 1396-1402.

Chipuk JE, Moldoveanu T, Llambi F, Parsons MJ, Green DR. 2010. The BCL-2 Family Reunion. *Mol Cell* **37**: 299-310.

Chuang LS-H, Ian H-I, Koh T-W, Ng H-H, Xu G, Li BFL. 1997. Human DNA-(Cytosine-5) Methyltransferase-PCNA Complex as a Target for p21WAF1. *Science* **277**: 1996-2000.

Collins AL, Levenson JM, Vilaythong AP, Richman R, Armstrong DL, Noebels JL, David Sweatt J, Zoghbi HY. 2004. Mild overexpression of MeCP2 causes a progressive neurological disorder in mice. *Hum Mol Genet* **13**: 2679-2689.

Courchesne E, Mouton PR, Calhoun ME, et al. 2011. Neuron number and size in prefrontal cortex of children with autism. *JAMA* **306**: 2001-2010.

Danial NN, Korsmeyer SJ. 2004. Cell death: critical control points. *Cell* **116**: 205-219.

De Zio D, Giunta L, Corvaro M, Ferraro E, Cecconi F. 2005. Expanding roles of programmed cell death in mammalian neurodevelopment. *Semin Cell Dev Biol* **16**: 281-294.

Deckwerth TL, Elliott JL, Knudson CM, Johnson EM, Jr., Snider WD, Korsmeyer SJ. 1996. Bax is required for neuronal death after trophic factor deprivation and during development. *Neuron* **17**: 401-411.

Dekkers MPJ, Barde Y-A. 2013. Programmed Cell Death in Neuronal Development. *Science* **340**: 39-41.

Dekkers MPJ, Nikoletopoulou V, Barde Y-A. 2013. Death of developing neurons: New insights and implications for connectivity. *J Cell Biol* **203**: 385-393.

Deng J, Carlson N, Takeyama K, Dal Cin P, Shipp M, Letai A. 2007. BH3 Profiling Identifies Three Distinct Classes of Apoptotic Blocks to Predict Response to ABT-737 and Conventional Chemotherapeutic Agents. *Cancer Cell* **12**: 171-185.

Denis H, Ndlovu MN, Fuks F. 2011. Regulation of mammalian DNA methyltransferases: a route to new mechanisms. *EMBO Rep* **12**: 647-656.

Durand C, Betancur C, Boeckers T, Bockmann J, Chaste P, Fauchereau F, Nygren G, Rastam M, Gillberg I, Anckarsater H et al. 2007. Mutations in the gene encoding the synaptic scaffolding protein SHANK3 are associated with autism spectrum disorders. *Nat Genet* **39**: 25 - 27.

Eckhardt F, Lewin J, Cortese R, Rakyan VK, Attwood J, Burger M, Burton J, Cox TV, Davies R, Down TA et al. 2006. DNA methylation profiling of human chromosomes 6, 20 and 22. *Nat Genet* **38**: 1378-1385.

Elmore S. 2007. Apoptosis: A Review of Programmed Cell Death. *Toxicol Pathol* **35**: 495-516.

Fabbri M, Garzon R, Cimmino A, Liu Z, Zanesi N, Callegari E, Liu S, Alder H, Costinean S, Fernandez-Cymering C et al. 2007. MicroRNA-29 family reverts aberrant methylation in lung cancer by targeting DNA methyltransferases 3A and 3B. *Proc Natl Acad Sci* **104**: 15805-15810.

Fang W-Q, Chen W-W, Jiang L, Liu K, Yung W-H, Fu Amy KY, Ip Nancy Y. 2014. Overproduction of Upper-Layer Neurons in the Neocortex Leads to Autism-like Features in Mice. *Cell Rep* **9**: 1635-1643.

Feng J, Chang H, Li E, Fan G. 2005. Dynamic expression of de novo DNA methyltransferases Dnmt3a and Dnmt3b in the central nervous system. *J Neurosi Res* **79**: 734-746.

Feng S, Cokus SJ, Zhang X, Chen P-Y, Bostick M, Goll MG, Hetzel J, Jain J, Strauss SH, Halpern ME et al. 2010. Conservation and divergence of methylation patterning in plants and animals. *Proc Natl Acad Sci* **107**: 8689-8694.

Friedman AA, Letai A, Fisher DE, Flaherty KT. 2015. Precision medicine for cancer with next-generation functional diagnostics. *Nat Rev Cancer* **15**: 747-756.

Fu Y, Rusznák Z, Herculano-Houzel S, Watson C, Paxinos G. 2013. Cellular composition characterizing postnatal development and maturation of the mouse brain and spinal cord. *Brain Struct Funct* **218**: 1337-1354.

Fuchs Y, Steller H. 2011. Programmed Cell Death in Animal Development and Disease. *Cell* **147**: 742-758.

Gabel HW, Kinde B, Stroud H, Gilbert CS, Harmin DA, Kastan NR, Hemberg M, Ebert DH, Greenberg ME. 2015. Disruption of DNA-methylation-dependent long gene repression in Rett syndrome. *Nature* **522**: 89-93.

Geaghan M, Cairns MJ. 2015. MicroRNA and Posttranscriptional Dysregulation in Psychiatry. *Biol Psychiatry* **78**: 231-239.

Globisch D, Munzel M, Muller M, Michalakis S, Wagner M, Koch S, Bruckl T, Biel M, Carell T. 2010. Tissue distribution of 5-hydroxymethylcytosine and search for active demethylation intermediates. *PLoS One* **5**: e15367.

Goebbels S, Bormuth I, Bode U, Hermanson O, Schwab MH, Nave K-A. 2006. Genetic targeting of principal neurons in neocortex and hippocampus of NEX-Cre mice. *Genesis* **44**: 611-621.

Gogolla N, Takesian Anne E, Feng G, Fagiolini M, Hensch Takao K. 2014. Sensory Integration in Mouse Insular Cortex Reflects GABA Circuit Maturation. *Neuron* **83**: 894-905.

Goll MG, Bestor TH. 2005. EUKARYOTIC CYTOSINE METHYLTRANSFERASES. *Annu Rev Biochem* **74**: 481-514.

Gonzalez-Garcia M, Garcia I, Ding L, O'Shea S, Boise LH, Thompson CB, Nunez G. 1995. bcl-x is expressed in embryonic and postnatal neural tissues and functions to prevent neuronal cell death. *Proc Natl Acad Sci U S A* **92**: 4304-4308.

Gonzalez-Garcia M, Perez-Ballestero R, Ding L, Duan L, Boise LH, Thompson CB, Nunez G. 1994. bcl-XL is the major bcl-x mRNA form expressed during murine development and its product localizes to mitochondria. *Development* **120**: 3033-3042.

Gorski JA, Talley T, Qiu M, Puelles L, Rubenstein JL, Jones KR. 2002. Cortical excitatory neurons and glia, but not GABAergic neurons, are produced in the Emx1-expressing lineage. *J Neurosci* **22**: 6309-6314.

Goto K, Numata M, Komura JI, Ono T, Bestor TH, Kondo H. 1994. Expression of DNA methyltransferase gene in mature and immature neurons as well as proliferating cells in mice. *Differentiation* **56**: 39-44.

Grasshoff U, Bonin M, Goehring I, Ekici A, Dufke A, Cremer K, Wagner N, Rossier E, Jauch A, Walter M et al. 2011. De novo MECP2 duplication in two females with random X-inactivation and moderate mental retardation. *Eur J Hum Genet* **19**: 507-512.

Grimson A, Farh KK-H, Johnston WK, Garrett-Engele P, Lim LP, Bartel DP. 2007. MicroRNA Targeting Specificity in Mammals: Determinants beyond Seed Pairing. *Mol Cell* **27**: 91-105.

Guo H, Ingolia NT, Weissman JS, Bartel DP. 2010. Mammalian microRNAs predominantly act to decrease target mRNA levels. *Nature* **466**: 835-840.

Guo JU, Su Y, Shin JH, Shin J, Li H, Xie B, Zhong C, Hu S, Le T, Fan G et al. 2014. Distribution, recognition and regulation of non-CpG methylation in the adult mammalian brain. *Nat Neurosci* **17**: 215-222.

Guy J, Hendrich B, Holmes M, Martin JE, Bird A. 2001. A mouse Mecp2-null mutation causes neurological symptoms that mimic Rett syndrome. *Nat Genet* **27**: 322-326.

Hagberg B, Aicardi J, Dias K, Ramos O. 1983. A progressive syndrome of autism, dementia, ataxia, and loss of purposeful hand use in girls: Rett's syndrome: report of 35 cases. *Ann Neurol* **14**: 471-479.

Hakem R, Hakem A, Duncan GS, Henderson JT, Woo M, Soengas MS, Elia A, de la Pompa JL, Kagi D, Khoo W et al. 1998. Differential requirement for caspase 9 in apoptotic pathways in vivo. *Cell* **94**: 339-352.

Han K, Holder Jr JL, Schaaf CP, Lu H, Chen H, Kang H, Tang J, Wu Z, Hao S, Cheung SW et al. 2013. SHANK3 overexpression causes manic-like behaviour with unique pharmacogenetic properties. *Nature* **503**: 72-77.

Hatten ME, Roussel MF. 2011. Development and cancer of the cerebellum. *Trends Neurosci* **34**: 134-142.

He Y-F, Li B-Z, Li Z, Liu P, Wang Y, Tang Q, Ding J, Jia Y, Chen Z, Li L et al. 2011. Tet-Mediated Formation of 5-Carboxylcytosine and Its Excision by TDG in Mammalian DNA. *Science* **333**: 1303-1307.

He Y, Ecker JR. 2015. Non-CG Methylation in the Human Genome. *Annu Rev Genom Hu Genet* **16**: 55-77.

Hebert SS, Horre K, Nicolai L, Papadopoulou AS, Mandemakers W, Silahtaroglu AN, Kauppinen S, Delacourte A, De Strooper B. 2008. Loss of microRNA cluster miR-29a/b-1 in sporadic Alzheimer's disease correlates with increased BACE1/beta-secretase expression. *Proc Natl Acad Sci USA* **105**: 6415-6420.

Hellman A, Chess A. 2007. Gene Body-Specific Methylation on the Active X Chromosome. *Science* **315**: 1141-1143.

Henderson IR, Jacobsen SE. 2007. Epigenetic inheritance in plants. *Nature* **447**: 418-424.

Hite KC, Adams VH, Hansen JC. 2009. Recent advances in MeCP2 structure and function. *Biochem Cell Biol* **87**: 219-227.

Hu L, Li Z, Cheng J, Rao Q, Gong W, Liu M, Shi YG, Zhu J, Wang P, Xu Y. 2013. Crystal Structure of TET2-DNA Complex: Insight into TET-Mediated 5mC Oxidation. *Cell* **155**: 1545-1555.

Hu Y, Ding L, Spencer DM, Nunez G. 1998a. WD-40 repeat region regulates Apaf-1 self-association and procaspase-9 activation. *J Biol Chem* **273**: 33489-33494.

Hu YM, Benedict MA, Wu DY, Inohara N, Nunez G. 1998b. Bcl-XL interacts with apaf-1 and inhibits apaf-1-dependent caspase-9 activation. *Proc Natl Acad Sci USA* **95**: 4386-4391.

Hutnick LK, Golshani P, Namihira M, Xue Z, Matynia A, Yang XW, Silva AJ, Schweizer FE, Fan G. 2009. DNA hypomethylation restricted to the murine forebrain induces cortical degeneration and impairs postnatal neuronal maturation. *Hum Mol Genet* **18**: 2875-2888.

Inano K, Suetake I, Ueda T, Miyake Y, Nakamura M, Okada M, Tajima S. 2000. Maintenance-Type DNA Methyltransferase Is Highly Expressed in Post-Mitotic Neurons and Localized in the Cytoplasmic Compartment. *J Biochem* **128**: 315-321.

Jacobson MD, Weil M, Raff MC. 1997. Programmed cell death in animal development. *Cell* **88**: 347-354.

Jiang X, Wang X. 2004. Cytochrome C-Mediated Apoptosis. *Annu Rev Biochem* **73**: 87-106.

Jonas EA, Hoit D, Hickman JA, Brandt TA, Polster BM, Fannjiang Y, McCarthy E, Montanez MK, Hardwick JM, Kaczmarek LK. 2003. Modulation of Synaptic Transmission by the BCL-2 Family Protein BCL-xL. *J Neurosci* **23**: 8423-8431.

Jones PA. 2012. Functions of DNA methylation: islands, start sites, gene bodies and beyond. *Nat Rev Genet* **13**: 484-492.

Jurkowska RZ, Jurkowski TP, Jeltsch A. 2011. Structure and Function of Mammalian DNA Methyltransferases. *ChemBioChem* **12**: 206-222.

Kaas Garrett A, Zhong C, Eason Dawn E, Ross Daniel L, Vachhani Raj V, Ming G-l, King Jennifer R, Song H, Sweatt JD. 2013. TET1 Controls CNS 5-Methylcytosine Hydroxylation, Active DNA Demethylation, Gene Transcription, and Memory Formation. *Neuron* **79**: 1086-1093.

Kalatsky VA, Stryker MP. 2003. New Paradigm for Optical Imaging: Temporally Encoded Maps of Intrinsic Signal. *Neuron* **38**: 529-545.

Kim H, Rafiuddin-Shah M, Tu H-C, Jeffers JR, Zambetti GP, Hsieh JJD, Cheng EHY. 2006. Hierarchical regulation of mitochondrion-dependent apoptosis by BCL-2 subfamilies. *Nat Cell Biol* **8**: 1348-1358.

Kinde B, Gabel HW, Gilbert CS, Griffith EC, Greenberg ME. 2015. Reading the unique DNA methylation landscape of the brain: Non-CpG methylation, hydroxymethylation, and MeCP2. *Proc Natl Acad Sci* **112**: 6800-6806.

Klein CJ, Botuyan M-V, Wu Y, Ward CJ, Nicholson GA, Hammans S, Hojo K, Yamanishi H, Karpf AR, Wallace DC et al. 2011. Mutations in DNMT1 cause hereditary sensory neuropathy with dementia and hearing loss. *Nat Genet* **43**: 595-600.

Klose RJ, Bird AP. 2006. Genomic DNA methylation: the mark and its mediators. *Trends Biochem Sci* **31**: 89-97.

Kole AJ, Swahari V, Hammond SM, Deshmukh M. 2011. miR-29b is activated during neuronal maturation and targets BH3-only genes to restrict apoptosis. *Genes Dev* **25**: 125-130.

Krajewski S, Krajewska M, Reed JC. 1996. Immunohistochemical analysis of in vivo patterns of Bak expression, a proapoptotic member of the Bcl-2 protein family. *Cancer Res* **56**: 2849-2855.

Kretz A, Kügler S, Happold C, Bähr M, Isenmann S. 2004. Excess Bcl-XL increases the intrinsic growth potential of adult CNS neurons in vitro. *Mol Cell Neurosci* **26**: 63-74.

Kriaucionis S, Heintz N. 2009. The Nuclear DNA Base 5-Hydroxymethylcytosine Is Present in Purkinje Neurons and the Brain. *Science* **324**: 929-930.

Kriegel AJ, Liu Y, Fang Y, Ding X, Liang M. 2012. The miR-29 family: genomics, cell biology, and relevance to renal and cardiovascular injury. *Physiol Genomics* **44**: 237-244.

Kriegstein A, Alvarez-Buylla A. 2009. The Glial Nature of Embryonic and Adult Neural Stem Cells. *Annu Rev Neurosci* **32**: 149-184.

Kriegstein A, Noctor S, Martinez-Cerdeno V. 2006. Patterns of neural stem and progenitor cell division may underlie evolutionary cortical expansion. *Nat Rev Neurosci* **7**: 883-890.

Kroemer G. 1997. The proto-oncogene Bcl-2 and its role in regulating apoptosis. *Nat Med* **3**: 614-620.

Kuida K, Haydar TF, Kuan CY, Gu Y, Taya C, Karasuyama H, Su MS, Rakic P, Flavell RA. 1998. Reduced apoptosis and cytochrome c-mediated caspase activation in mice lacking caspase 9. *Cell* **94**: 325-337.

Kuida K, Zheng TS, Na S, Kuan C, Yang D, Karasuyama H, Rakic P, Flavell RA. 1996. Decreased apoptosis in the brain and premature lethality in CPP32-deficient mice. *Nature* **384**: 368-372.

Laurent L, Wong E, Li G, Huynh T, Tsirigos A, Ong CT, Low HM, Kin Sung KW, Rigoutsos I, Loring J et al. 2010. Dynamic changes in the human methylome during differentiation. *Genome Res* **20**: 320-331.

Lee RC, Feinbaum RL, Ambros V. 1993. The C. elegans heterochronic gene lin-4 encodes small RNAs with antisense complementarity to lin-14. *Cell* **75**: 843-854.

Leonhardt H, Page AW, Weier H-U, Bestor TH. 1992. A targeting sequence directs DNA methyltransferase to sites of DNA replication in mammalian nuclei. *Cell* **71**: 865-873.

Letai A, Bassik MC, Walensky LD, Sorcinelli MD, Weiler S, Korsmeyer SJ. 2002. Distinct BH3 domains either sensitize or activate mitochondrial apoptosis, serving as prototype cancer therapeutics. *Cancer Cell* **2**: 183-192.

Ley TJ, Ding L, Walter MJ, McLellan MD, Lamprecht T, Larson DE, Kandoth C, Payton JE, Baty J, Welch J et al. 2010. DNMT3A Mutations in Acute Myeloid Leukemia. *N Engl J Med* **363**: 2424-2433.

Li H, Alavian KN, Lazrove E, Mehta N, Jones A, Zhang P, Licznerski P, Graham M, Uo T, Guo J et al. 2013. A Bcl-xL–Drp1 complex regulates synaptic vesicle membrane dynamics during endocytosis. *Nat Cell Biol* **15**: 773-785.

Li H, Chen Y, Jones AF, Sanger RH, Collis LP, Flannery R, McNay EC, Yu T, Schwarzenbacher R, Bossy B et al. 2008. Bcl-xL induces Drp1-dependent synapse formation in cultured hippocampal neurons. *Proc Natl Acad Sci* **105**: 2169-2174.

Li H, Mao S, Wang H, Zen K, Zhang C, Li L. 2014a. MicroRNA-29a modulates axon branching by targeting doublecortin in primary neurons. *Protein Cell* **5**: 160-169.

Li X, Wei W, Zhao Q-Y, Widagdo J, Baker-Andresen D, Flavell CR, D'Alessio A, Zhang Y, Bredy TW. 2014b. Neocortical Tet3-mediated accumulation of 5-hydroxymethylcytosine promotes rapid behavioral adaptation. *Proc Natl Acad Sci* **111**: 7120-7125.

Li Y, Tollefsbol TO. 2011. DNA methylation detection: Bisulfite genomic sequencing analysis. *Methods Mol Biol* **791**: 11-21.

Lim DHK, Maher ER. 2010. DNA methylation: a form of epigenetic control of gene expression. *The Obstetrician & Gynaecologist* **12**: 37-42.

Lister R, Mukamel EA, Nery JR, Urich M, Puddifoot CA, Johnson ND, Lucero J, Huang Y, Dwork AJ, Schultz MD et al. 2013a. Global Epigenomic Reconfiguration During Mammalian Brain Development. *Science* **341**: 10.1126/science.1237905.

Lister R, Mukamel EA, Nery JR, Urich M, Puddifoot CA, Johnson ND, Lucero J, Huang Y, Dwork AJ, Schultz MD et al. 2013b. Global epigenomic reconfiguration during mammalian brain development. in *Science*.

Lister R, Pelizzola M, Dowen RH, Hawkins RD, Hon G, Tonti-Filippini J, Nery JR, Lee L, Ye Z, Ngo Q-M et al. 2009. Human DNA methylomes at base resolution show widespread epigenomic differences. *Nature* **462**: 315-322.

Liu X, Kim CN, Yang J, Jemmerson R, Wang X. 1996. Induction of apoptotic program in cell-free extracts: requirement for dATP and cytochrome c. *Cell* **86**: 147-157.

Liu Z, Li X, Zhang J-T, Cai Y-J, Cheng T-L, Cheng C, Wang Y, Zhang C-C, Nie Y-H, Chen Z-F et al. 2016. Autism-like behaviours and germline transmission in transgenic monkeys overexpressing MeCP2. *Nature* **530**: 98-102.

Lombardi LM, Baker SA, Zoghbi HY. 2015. MECP2 disorders: from the clinic to mice and back. *J Clin Invest* **125**: 2914-2923.

Lomonosova E, Chinnadurai G. 2008. BH3-only proteins in apoptosis and beyond: an overview. *Oncogene* **27 Suppl 1**: S2-19.

Lugtenberg D, Kleefstra T, Oudakker AR, Nillesen WM, Yntema HG, Tzschach A, Raynaud M, Rating D, Journel H, Chelly J et al. 2008. Structural variation in Xq28: MECP2 duplications in 1% of patients with unexplained XLMR and in 2% of male patients with severe encephalopathy. *Eur J Hum Genet* **17**: 444-453.

Lui Jan H, Hansen David V, Kriegstein Arnold R. 2011. Development and Evolution of the Human Neocortex. *Cell* **146**: 18-36.

Martinou JC, Youle RJ. 2011. Mitochondria in apoptosis: Bcl-2 family members and mitochondrial dynamics. *Dev Cell* **21**: 92-101.

Mattson MP. 2000. Apoptosis in neurodegenerative disorders. *Nat Rev Mol Cell Biol* **1**: 120-129.

McCaffery P, Deutsch CK. 2005. Macrocephaly and the control of brain growth in autistic disorders. *Prog Neurobiol* **77**: 38-56.

Mo A, Mukamel Eran A, Davis Fred P, Luo C, Henry Gilbert L, Picard S, Urich Mark A, Nery Joseph R, Sejnowski Terrence J, Lister R et al. 2015. Epigenomic Signatures of Neuronal Diversity in the Mammalian Brain. *Neuron* **86**: 1369-1384.

Morimoto K, Fahnestock M, Racine RJ. 2004. Kindling and status epilepticus models of epilepsy: rewiring the brain. *Prog Neurobiol* **73**: 1-60.

Motoyama N, Wang F, Roth KA, Sawa H, Nakayama K, Nakayama K, Negishi I, Senju S, Zhang Q, Fujii S et al. 1995. Massive cell death of immature hematopoietic cells and neurons in Bcl-x-deficient mice. *Science* **267**: 1506-1510.

Mott JL, Kobayashi S, Bronk SF, Gores GJ. 2007. mir-29 regulates Mcl-1 protein expression and apoptosis. *Oncogene* **26**: 6133-6140.

Nan X, Meehan RR, Bird A. 1993. Dissection of the methyl-CpG binding domain from the chromosomal protein MeCP2. *Nucleic Acids Res* **21**: 4886-4892.

Nan X, Ng H-H, Johnson CA, Laherty CD, Turner BM, Eisenman RN, Bird A. 1998. Transcriptional repression by the methyl-CpG-binding protein MeCP2 involves a histone deacetylase complex. *Nature* **393**: 386-389.

Nguyen S, Meletis K, Fu D, Jhaveri S, Jaenisch R. 2007. Ablation of de novo DNA methyltransferase Dnmt3a in the nervous system leads to neuromuscular defects and shortened lifespan. *Dev Dyn* **236**: 1663-1676.

Okano M, Bell DW, Haber DA, Li E. 1999. DNA Methyltransferases Dnmt3a and Dnmt3b Are Essential for De Novo Methylation and Mammalian Development. *Cell* **99**: 247-257.

Oppenheim RW. 1991. Cell death during development of the nervous system. *Annu Rev Neurosci* **14**: 453-501.

Ow Y-LP, Green DR, Hao Z, Mak TW. 2008. Cytochrome c: functions beyond respiration. *Nat Rev Mol Cell Biol* **9**: 532-542.

Pandi G, Nakka VP, Dharap A, Roopra A, Vemuganti R. 2013. MicroRNA miR-29c Down-Regulation Leading to De-Repression of Its Target DNA Methyltransferase 3a Promotes Ischemic Brain Damage. *PLoS ONE* **8**: e58039.

Papadopoulou AS, Serneels L, Achsel T, Mandemakers W, Callaerts-Vegh Z, Dooley J, Lau P, Ayoubi T, Radaelli E, Spinazzi M et al. 2015. Deficiency of the miR-29a/b-1 cluster

leads to ataxic features and cerebellar alterations in mice. *Neurobiol Dis* **73**: 275-288.

Park HA, Licznerski P, Alavian KN, Shanabrough M, Jonas EA. 2015. Bcl-xL is necessary for neurite outgrowth in hippocampal neurons. *Antioxid Redox Signal* **22**: 93-108.

Peca J, Feliciano C, Ting JT, Wang W, Wells MF, Venkatraman TN, Lascola CD, Fu Z, Feng G. 2011. Shank3 mutant mice display autistic-like behaviours and striatal dysfunction. *Nature* **472**: 437-442.

Peixoto RT, Wang W, Croney DM, Kozorovitskiy Y, Sabatini BL. 2016. Early hyperactivity and precocious maturation of corticostriatal circuits in Shank3B-/- mice. *Nat Neurosci* **19**: 716-724.

Pelli DG. 1997. The VideoToolbox software for visual psychophysics: transforming numbers into movies. *Spat Vis* **10**: 437-442.

Penagarikano O, Abrahams BS, Herman EI, Winden KD, Gdalyahu A, Dong H, Sonnenblick LI, Gruver R, Almajano J, Bragin A et al. 2011. Absence of CNTNAP2 leads to epilepsy, neuronal migration abnormalities, and core autism-related deficits. *Cell* **147**: 235-246.

Penn NW, Suwalski R, O'Riley C, Bojanowski K, Yura R. 1972. The presence of 5-hydroxymethylcytosine in animal deoxyribonucleic acid. *The Biochemical journal* **126**: 781-790.

Perry W, Minassian A, Lopez B, Maron L, Lincoln A. 2007. Sensorimotor Gating Deficits in Adults with Autism. *Biol Psychiatry* **61**: 482-486.

Petri R, Malmevik J, Fasching L, Åkerblom M, Jakobsson J. 2014. miRNAs in brain development. *Exp Cell Res* **321**: 84-89.

Pleil KE, Lowery-Gionta EG, Crowley NA, Li C, Marcinkiewcz CA, Rose JH, McCall NM, Maldonado-Devincci AM, Morrow AL, Jones SR et al. Effects of chronic ethanol exposure on neuronal function in the prefrontal cortex and extended amygdala. *Neuropharmacology*.

Rabinowicz PD, Palmer LE, May BP, Hemann MT, Lowe SW, McCombie WR, Martienssen RA. 2003. Genes and Transposons Are Differentially Methylated in Plants, but Not in Mammals. *Genome Res* **13**: 2658-2664.

Raff M, Barres B, Burne J, Coles H, Ishizaki Y, Jacobson M. 1993. Programmed cell death and the control of cell survival: lessons from the nervous system. *Science* **262**: 695-700.

Ramocki MB, Tavyev YJ, Peters SU. 2010. The MECP2 duplication syndrome. *Am J Med Genet A* **152A**: 1079-1088.

Ramsahoye BH, Biniszkiewicz D, Lyko F, Clark V, Bird AP, Jaenisch R. 2000. Non-CpG methylation is prevalent in embryonic stem cells and may be mediated by DNA methyltransferase 3a. *Proc Natl Acad Sci* **97**: 5237-5242.

Rett A. 1966. [On a unusual brain atrophy syndrome in hyperammonemia in childhood]. *Wiener medizinische Wochenschrift* **116**: 723-726.

Riedl SJ, Salvesen GS. 2007. The apoptosome: signalling platform of cell death. *Nat Rev Mol Cell Biol* **8**: 405-413.

Rinkenberger JL, Horning S, Klocke B, Roth K, Korsmeyer SJ. 2000. Mcl-1 deficiency results in peri-implantation embryonic lethality. *Genes Dev* **14**: 23-27.

Roshan R, Shridhar S, Sarangdhar MA, Banik A, Chawla M, Garg M, Singh VP, Pillai B. 2014. Brain-specific knockdown of miR-29 results in neuronal cell death and ataxia in mice. *RNA* **20**: 1287-1297.

Roth K, Motoyama N, Loh D. 1996. Apoptosis of bcl-x-deficient telencephalic cells in vitro. *J Neurosci* **16**: 1753-1758.

Rubenstein JLR, Merzenich MM. 2003. Model of autism: increased ratio of excitation/inhibition in key neural systems. *Genes Brain Behav* **2**: 255-267.

Saelens X, Festjens N, Walle LV, Gurp Mv, Loo Gv, Vandenabeele P. 2004. Toxic proteins released from mitochondria in cell death. *Oncogene* **23**: 2861-2874.

Schanen NC. 2006. Epigenetics of autism spectrum disorders. *Hum Mol Genet* **15**: R138-R150.

Schindelin J, Arganda-Carreras I, Frise E, Kaynig V, Longair M, Pietzsch T, Preibisch S, Rueden C, Saalfeld S, Schmid B et al. 2012. Fiji: an open-source platform for biological-image analysis. *Nat Meth* **9**: 676-682.

Schubeler D. 2015. Function and information content of DNA methylation. *Nature* **517**: 321-326.

Schultz MD, He Y, Whitaker JW, Hariharan M, Mukamel EA, Leung D, Rajagopal N, Nery JR, Urich MA, Chen H et al. 2015. Human body epigenome maps reveal noncanonical DNA methylation variation. *Nature* **523**: 212-216.

Scott Schwoerer J, Laffin J, Haun J, Raca G, Friez MJ, Giampietro PF. 2014. MECP2 duplication: Possible cause of severe phenotype in females. *Am J Med Genet A* **164**: 1029-1034.

Shahbazian MD, Antalffy B, Armstrong DL, Zoghbi HY. 2002a. Insight into Rett syndrome: MeCP2 levels display tissue- and cell-specific differences and correlate with neuronal maturation. *Human Molecular Genetics* **11**: 115-124.

Shahbazian MD, Young JI, Yuva-Paylor LA, Spencer CM, Antalffy BA, Noebels JL, Armstrong DL, Paylor R, Zoghbi HY. 2002b. Mice with Truncated MeCP2 Recapitulate Many Rett Syndrome Features and Display Hyperacetylation of Histone H3. *Neuron* **35**: 243-254.

Sharif J, Muto M, Takebayashi S-i, Suetake I, Iwamatsu A, Endo TA, Shinga J, Mizutani-Koseki Y, Toyoda T, Okamura K et al. 2007. The SRA protein Np95 mediates epigenetic inheritance by recruiting Dnmt1 to methylated DNA. *Nature* **450**: 908-912.

Shin J, Ming G-l, Song H. 2014a. DNA modifications in the mammalian brain. *Phil Trans R Soc B* **369**: 10.1098/rstb.2013.0512.

Shin J, Shin Y, Oh SM, Yang H, Yu WJ, Lee JP, Huh SO, Lee SH, Suh YH, Chung S et al. 2014b. MiR-29b controls fetal mouse neurogenesis by regulating ICAT-mediated Wnt/beta-catenin signaling. *Cell Death Dis* **5**: e1473.

Siniscalco D, Cirillo A, Bradstreet J, Antonucci N. 2013. Epigenetic Findings in Autism: New Perspectives for Therapy. *Int J Environ Res Public Health* **10**: 4261.

Smith SL, Trachtenberg JT. 2007. Experience-dependent binocular competition in the visual cortex begins at eye opening. *Nat Neurosci* **10**: 370-375.

Smith ZD, Meissner A. 2013. DNA methylation: roles in mammalian development. *Nat Rev Genet* **14**: 204-220.

Song CX, Szulwach KE, Fu Y, Dai Q, Yi C, Li X, Li Y, Chen CH, Zhang W, Jian X et al. 2011. Selective chemical labeling reveals the genome-wide distribution of 5-hydroxymethylcytosine. *Nat Biotechnol* **29**.

Southwell DG, Paredes MF, Galvao RP, Jones DL, Froemke RC, Sebe JY, Alfaro-Cervello C, Tang Y, Garcia-Verdugo JM, Rubenstein JL et al. 2012. Intrinsically determined cell death of developing cortical interneurons. *Nature* **491**: 109-113.

Sparrow AM, Lowery-Gionta EG, Pleil KE, Li C, Sprow GM, Cox BR, Rinker JA, Jijon AM, Pena J, Navarro M et al. 2012. Central Neuropeptide Y Modulates Binge-Like Ethanol Drinking in C57BL/6J Mice via Y1 and Y2 Receptors. *Neuropsychopharmacol* **37**: 1409-1421.

Stiles J, Jernigan T. 2010. The Basics of Brain Development. *Neuropsychol Rev* **20**: 327-348.

Strasser A, Jost PJ, Nagata S. 2009. The Many Roles of FAS Receptor Signaling in the Immune System. *Immunity* **30**: 180-192.

Subramaniam D, Thombre R, Dhar A, Anant S. 2014. DNA Methyl Transferases: A novel target for Prevention and Therapy. *Front Oncol* **4**.

Sulston JE, Horvitz HR. 1977. Post-embryonic cell lineages of the nematode, Caenorhabditis elegans. *Dev Biol* **56**: 110-156.

Sulston JE, Schierenberg E, White JG, Thomson JN. 1983. The embryonic cell lineage of the nematode Caenorhabditis elegans. *Dev Biol* **100**: 64-119.

Suzuki MM, Bird A. 2008. DNA methylation landscapes: provocative insights from epigenomics. *Nat Rev Genet* **9**: 465-476.

Szklarczyk D, Franceschini A, Kuhn M, Simonovic M, Roth A, Minguez P, Doerks T, Stark M, Muller J, Bork P et al. 2011. The STRING database in 2011: functional interaction networks of proteins, globally integrated and scored. *Nuc Acids Res* **39**: D561-D568.

Sztainberg Y, Chen H-m, Swann JW, Hao S, Tang B, Wu Z, Tang J, Wan Y-W, Liu Z, Rigo F et al. 2015. Reversal of phenotypes in MECP2 duplication mice using genetic rescue or antisense oligonucleotides. *Nature* **528**: 123-126.

Tait SW, Green DR. 2010. Mitochondria and cell death: outer membrane permeabilization and beyond. *Nat Rev Mol Cell Biol* **11**: 621-632.

Tatton-Brown K, Seal S, Ruark E, Harmer J, Ramsay E, del Vecchio Duarte S, Zachariou A, Hanks S, O'Brien E, Aksglaede L et al. 2014. Mutations in the DNA methyltransferase gene DNMT3A cause an overgrowth syndrome with intellectual disability. *Nat Genet* **46**: 385-388.

Trasler JM, Trasler DG, Bestor TH, Li E, Ghibu F. 1996. DNA methyltransferase in normal and Dnmtn/Dnmtn mouse embryos. *Dev Dyn* **206**: 239-247.

Trivier E, De Cesare D, Jacquot S, Pannetier S, Zackai E, Young I, Mandel J-L, Sassone-Corsi P, Hanauer A. 1996. Mutations in the kinase Rsk-2 associated with Coffin-Lowry syndrome. *Nature* **384**: 567-570.

Ugalde AP, Ramsay AJ, de la Rosa J, Varela I, Marino G, Cadinanos J, Lu J, Freije JM, Lopez-Otin C. 2011. Aging and chronic DNA damage response activate a regulatory pathway involving miR-29 and p53. *EMBO J* **30**: 2219-2232.

Van Esch H. 1993. MECP2 Duplication Syndrome. in *GeneReviews* (eds. RA Pagon, MP Adam, HH Ardinger, SE Wallace, A Amemiya, LJH Bean, TD Bird, CT Fong, HC Mefford, RJH Smith, et al.), Seattle (WA).

-. 2012. MECP2 Duplication Syndrome. *Mol Syndromol* **2**: 128-136.

Vander Heiden MG, Li XX, Gottleib E, Hill RB, Thompson CB, Colombini M. 2001. Bcl-xl Promotes the Open Configuration of the Voltage-dependent Anion Channel and Metabolite Passage through the Outer Mitochondrial Membrane. *J Biol Chem* **276**: 19414-19419.

Villard L. 2007. MECP2 mutations in males. *J Med Genet* **44**: 417-423.

Walensky LD, Gavathiotis E. 2011. BAX unleashed: the biochemical transformation of an inactive cytosolic monomer into a toxic mitochondrial pore. *Trends Biochem Sci* **36**: 642-652.

Wei MC, Zong W-X, Cheng EH-Y, Lindsten T, Panoutsakopoulou V, Ross AJ, Roth KA, MacGregor GR, Thompson CB, Korsmeyer SJ. 2001. Proapoptotic BAX and BAK: A Requisite Gateway to Mitochondrial Dysfunction and Death. *Science* **292**: 727-730.

Westphal D, Kluck RM, Dewson G. 2014. Building blocks of the apoptotic pore: how Bax and Bak are activated and oligomerize during apoptosis. *Cell Death Differ* **21**: 196-205.

Woo M, Hakem R, Soengas MS, Duncan GS, Shahinian A, Kagi D, Hakem A, McCurrach M, Khoo W, Kaufman SA et al. 1998. Essential contribution of caspase 3/CPP32 to apoptosis and its associated nuclear changes. *Genes Dev* **12**: 806-819.

Wu H, Zhang Y. 2011. Mechanisms and functions of Tet protein-mediated 5-methylcytosine oxidation. *Genes Dev* **25**: 2436-2452.

Xi Y, Li W. 2009. BSMAP: whole genome bisulfite sequence MAPping program. *BMC bioinformatics* **10**: 232.

Xie W, Barr Cathy L, Kim A, Yue F, Lee Ah Y, Eubanks J, Dempster Emma L, Ren B. 2012. Base-Resolution Analyses of Sequence and Parent-of-Origin Dependent DNA Methylation in the Mouse Genome. *Cell* **148**: 816-831.

Xu H, Sun J, Shi C, Sun C, Yu L, Wen Y, Zhao S, Liu J, Xu J, Li H et al. 2015. miR-29s inhibit the malignant behavior of U87MG glioblastoma cell line by targeting DNMT3A and 3B. *Neurosci Lett* **590**: 40-46.

Yan X-J, Xu J, Gu Z-H, Pan C-M, Lu G, Shen Y, Shi J-Y, Zhu Y-M, Tang L, Zhang X-W et al. 2011. Exome sequencing identifies somatic mutations of DNA methyltransferase gene DNMT3A in acute monocytic leukemia. *Nat Genet* **43**: 309-315.

Yoshida H, Kong YY, Yoshida R, Elia AJ, Hakem A, Hakem R, Penninger JM, Mak TW. 1998. Apaf1 is required for mitochondrial pathways of apoptosis and brain development. *Cell* **94**: 739-750.

Youle RJ, Strasser A. 2008. The BCL-2 protein family: opposing activities that mediate cell death. *Nat Rev Mol Cell Biol* **9**: 47-59.

Young JI, Zoghbi HY. 2004. X-Chromosome Inactivation Patterns Are Unbalanced and Affect the Phenotypic Outcome in a Mouse Model of Rett Syndrome. *Am J Hum Genet* **74**: 511-520.

Yuan J, Yankner BA. 2000. Apoptosis in the nervous system. *Nature* **407**: 802-809.

Zeng J, Konopka G, Hunt Brendan G, Preuss Todd M, Geschwind D, Yi Soojin V. 2012. Divergent Whole-Genome Methylation Maps of Human and Chimpanzee Brains Reveal Epigenetic Basis of Human Regulatory Evolution. *Am J Hum Genet* **91**: 455-465.